Understanding Protein Adsorption Phenomena on Solid Surfaces

Dissertation

zur

Erlangung der naturwissenschaftlichen Doktorwürde (Dr. sc. nat.)

vorgelegt der

Mathematisch-naturwissenschaftlichen Fakultät

der

Universität Zürich

von

Michael Rabe

aus

Deutschland

Promotionskomitee

Prof. Dr. Stefan Seeger (Vorsitz)

Prof. Dr. Peter Hamm

Prof. Dr. John A. Robinson

Zürich, 2009

To my family

Contents

Abstract

Protein adsorption at solid surfaces plays a key role in many natural processes and has therefore promoted a widespread interest in many research areas. Despite considerable progress in this field there are still widely differing and even contradictive opinions on how to explain the phenomena that are frequently observed. The present dissertation aims to advance the understanding of protein adsorption and to systematically unravel the underlying molecular mechanism. This is achieved by acquiring and evaluating comprehensive experimental data sets using fluorescence sensing and imaging methods. Experiments are conducted on model systems comprising the proteins BSA, Fibrinogen, β-Lactoglobulin, and α-Synuclein, hydrophilic and hydrophobic surfaces and varying pH and ionic strength conditions.

One of the comprehensively studied adsorption phenomena is cooperativity which refers to the effect that the adsorption of proteins is enhanced by the presence of pre-adsorbed proteins. Contradicting a widespread opinion it is shown that cooperativity is not necessarily associated with the growth of tight surface aggregates. Instead, a macroscopic model description is suggested that simply assumes the overlap of two parallel adsorption pathways, one for the adsorption at isolated surface positions and one for the adsorption near other surface-bound proteins. The proposed mechanism implies increasing adsorption rates plus a specific distribution of proteins over the surface. Both properties are experimentally confirmed. Further, a microscopic treatment of the mechanism behind cooperativity is realized through Monte-Carlo simulations which reproduce the experimental data accurately and thereby confirm the suggestion that approaching proteins can be tracked to favorable binding sites near other pre-adsorbed proteins.

In addition, phenomena related to protein adsorption include exchange mechanisms between adsorbing and pre-adsorbed proteins, conformational and orientational rearrangements, as well as overshooting adsorption kinetics. Another model combining these effects is developed and tested with a strong fundament of experimental data. The primary

accomplishment related to this model is a consistent and comprehensible explanation of the overshooting effect.

Finally, the behavior of protein aggregates or clusters on surfaces is explored. Protein clusters can form spontaneously in the solution and subsequently deposit onto the surface. For the first time it was shown that induced by protein-surface interactions freshly deposited protein clusters start to spread in order to maximize the contact area between proteins and surface. The spreading rate is considerably faster on hydrophobic surfaces as compared to hydrophilic surfaces which correlates with the lateral mobility of the protein monomers on theses surfaces. Interestingly, on a hydrophobic surface a spreading protein cluster can even rupture a pre-adsorbed protein monolayer by displacing the monomers from the area that it is about to occupy. Inversely to protein aggregation in solution, the direct growth of aggregates on the surface can also be observed using the protein α-Synuclein which is the pathological component of Parkinson's disease. Whereas the on-surface growth mechanism is the typically proposed one when protein aggregates are detected on a surface, the discovery that protein aggregates can also come from the solution and spread on the surface opens a completely new perspective on this topic. Experimental strategies to distinguish between these two different mechanisms are comprehensively discussed.

The significance of this work results from the successful combination of substantial experimental investigations with efficient theoretical methods giving access to a clear and illustrative view on some exciting adsorption phenomena. Novel ideas shed light on the diversely discussed topics of cooperative adsorption, overshooting adsorption kinetics, and protein aggregation.

Zusammenfassung

Die Adsorption von Proteinen an Oberflächen spielt eine zentrale Rolle in vielen natürlichen Prozessen und ist daher in vielen Forschungsbereichen von Interesse. Trotz beachtlicher Fortschritte in diesem Gebiet gibt es noch immer verschiedene mithin widersprüchliche Ansichten über einige der fundamentalen Phänomene. Das Ziel der vorliegenden Dissertation ist es, Proteinadsorptionsprozesse besser zu verstehen und die zugrunde liegenden molekularen Mechanismen zu entschlüsseln. Erreicht wird dies, indem mittels verschiedener Fluoreszenztechniken grosse Datenmengen gewonnen und entsprechend ausgewertet werden. Die Experimente werden in Modellsystemen durchgeführt, die aus einem der vier Proteine BSA, Fibrinogen, β-Lactoglobulin oder α-Synuclein sowie einer hydrophilen oder hydrophoben Oberfläche bestehen. Zudem werden die pH-Werte und Ionenstärken des Puffers variiert.

Eines der ausführlich untersuchten Adsorptionsphänomene ist Kooperativität, was bedeutet, dass bereits adsorbierte Proteine die Adsorption weiterer Proteine erleichtern. Entgegen einer weit verbreitenden Ansicht kann gezeigt werden, dass Kooperativität nicht zwangsläufig mit der Aggregation von Proteinen auf der Oberfläche einhergeht. Stattdessen wird ein Modell entwickelt, das auf zwei parallelen Adsorptionswegen beruht. Während der erste Weg die Adsorption an einer beliebigen freien Stelle genügend weit entfernt von einem benachbarten Protein beschreibt, behandelt der zweite Weg die Adsorption in unmittelbarer Nähe zu einem benachbarten Protein. Der vorgeschlagene Mechanismus hat zur Folge, dass die Adsorptionsraten einen ansteigenden Verlauf aufweisen und die Verteilung der Proteine auf der Oberfläche einer gewissen Systematik folgt. Beide Eigenschaften findet man auch experimentell. Mit Hilfe von Monte-Carlo-Simulationen wird eine mikroskopische Herangehensweise an den vorgeschlagenen Mechanismus erreicht. Die Simulation bestätigt in eindrücklicher Weise die experimentellen Beobachtungen. Dies untermauert den vorgeschlagenen Standpunkt, nach dem ankommende Proteine auf eine bevorzugte Bindungsstelle in der Nähe anderer zuvor adsorbierter Proteine gelenkt werden.

Weitere Phänomene im Zusammenhang mit der Adsorption von Proteinen sind Austauschprozesse zwischen adsorbierenden und bereits adsorbierten Proteinen, Neuordnung der Konformation und Orientierung sowie das Überschwingen der Adsorptionskinetiken. Auch für diese Effekte wird ein gemeinsames Modell entwickelt, welches anhand umfangreicher experimenteller Daten überprüft wird. Dieses Modell beinhaltet eine widerspruchsfreie Erklärung des Effekts der überschwingenden Adsorptionskinetiken.

Schliesslich wird noch das Verhalten von Proteinaggregaten bzw. Proteinclustern auf Oberflächen untersucht. Unter bestimmten Bedingungen können sich spontan Proteincluster in einer Proteinlösung ausbilden, die sich anschliessend auf der Oberfläche ablagern. Aufgrund der Protein-Oberflächen-Wechselwirkungen beginnen abgelagerte Cluster sich auszudehnen, um die Kontaktfläche zwischen Proteinen und Oberfläche zu maximieren. Die Geschwindigkeit, mit der das Auseinanderdriften der Proteine eines Clusters abläuft, ist auf hydrophoben Oberflächen deutlich höher als auf hydrophilen Oberflächen. Diese Beobachtung steht in Einklang mit der besseren bzw. schlechteren Beweglichkeit der Proteinmonomere auf der jeweiligen Oberfläche. Auf einer hydrophoben Oberfläche kann ein sich ausbreitender Proteincluster sogar eine Proteinmonolage aufreissen und die im Wege befindlichen Proteinmonomere verdrängen. Im Gegensatz zur Proteinaggregation in Lösung kann in einem weiteren Modellsystem gleichfalls die direkte Aggregation auf der Oberfläche beobachtet werden. Dies wird am Beispiel des Proteins α-Synuclein gezeigt, welches die pathologische Komponente in der Parkinson'schen Krankheit ausmacht. Das Wachsen auf der Oberfläche wird in den meisten Fällen zur Erklärung der Entstehung von Protein-Aggregaten auf Oberflächen herangezogen. Währendessen eröffnet die Erkenntnis, dass Proteinaggregate auch in der Lösung heranwachsen können, sich dann auf der Oberfläche ablagern und dort auseinanderdriften, eine völlig neue Perspektive auf dieses Gebiet. Experimentelle Ansätze zur Unterscheidung dieser beiden verschiedenen Mechanismen werden ausführlich diskutiert.

Die hervorzuhebende Bedeutung der vorliegenden Arbeit liegt in der erfolgreichen Kombination ausführlicher experimenteller Untersuchungen mit effizienten theoretischen Methoden, die zu einer klaren und anschaulichen Ansicht einiger interessanter Adsorptions-Phänomene führt. Neue Ideen helfen insbesondere, die Begriffe kooperative Adsorption, überschiessende Kinetiken und Proteinaggregation zu erklären.

List of Publications

Publications related to this dissertation

Chapter 5

Rabe, M., Verdes, D., Zimmermann, J. and Seeger, S.
Surface organization and cooperativity during nonspecific protein adsorption events
J. Phys. Chem. B 2008 (112): 13971-13980.

Chapter 6

Rabe, M., Verdes, D., Seeger, S.
Understanding cooperative protein adsorption events at the microscopic scale
submitted for publication.

Chapter 7

Rabe, M., Verdes, D., Rankl, M., Artus, G. R. J. and Seeger, S.
A comprehensive study of concepts and phenomena of the nonspecific adsorption of β-Lactoglobulin
ChemPhysChem 2007 (8): 862-872.

Chapter 8

Rabe, M., Verdes, D., Seeger, S.
Surface-induced spreading phenomenon of protein clusters
Soft Matter 2009 (5): 1039-1047.

Publications partially related to this dissertation

Rankl, M., Ruckstuhl, T., Rabe, M., Artus, G. R. J., Walser, A. and Seeger, S.
Conformational reorientation of Immunoglobulin G during nonspecific interaction with surfaces
ChemPhysChem 2006 (7): 837-846.

Zimmermann, J., Rabe, M., Verdes, D. and Seeger, S.
Functionalized silicone nanofilaments: A novel material for selective protein enrichment
Langmuir 2008 (24): 1053-1057.

Zimmermann, J., Rabe, M., Artus, G. R. J. and Seeger, S.
Patterned superfunctional surfaces based on a silicone nanofilament coating
Soft Matter 2008 (4): 450-452.

Contributions to conferences

Rabe, M., Verdes, D., Seeger, S.
Supercritical angle fluorescence (SAF) microscopy: An experimental approach to detect surface generated fluorescence.
Poster at the '12th International Workshop on Single Molecule Spectroscopy and Ultra Sensitive Analysis in the Life Sciences'.
Berlin (Germany), 19.09. – 22.09.2006.

Rabe, M., Seeger, S.
A comprehensive model for the non-specific adsorption behavior of β-Lactoglobulin.
Poster at the '5. Deutsches Biosensor Symposium'.
Bochum (Germany), 18.03. – 21.03.2007.

Rabe, M., Zimmermann, J., Verdes, D., Seeger, S.
Specific and non-specific adsorption of proteins on solid interfaces.
Poster and Proceedings at the '2007 NSTI Nanotechnology and Trade Show -Nanotech 2007'.
Santa Clara (California, USA) 20.05. – 24.05.2007.

Rabe, M., Verdes, D., Seeger, S.
Monitoring and modeling of protein adsorption kinetics.
Poster at the 'Methods and Applications of Fluorescence –MAF 10'.
Salzburg (Austria), 09.09. – 12.09.2007.

Rabe, M., Verdes, D., Seeger, S.,
Organization of surface adsorbed proteins.
Poster at 'The Tenth World Congress on Biosensors'.
Shanghai (China), 14.05. – 16.05.2008.

Rabe, M., Verdes, D., Seeger, S.
Understanding protein adsorption phenomena.
Poster at the 'Swiss Chemical Society (SCS) Fall meeting 2008'.
Zurich (Switzerland), 11.09.2008.

Rabe, M., Verdes, D., Seeger, S.
Understanding the formation and adsorption of 2-dimensional and 3-dimensional protein aggregates on a solid surface.
Talk and Proceedings at the '2009 NSTI Nanotech and Expo -Nanotech 2009'.
Houston (Texas, USA) 03.05. – 07.05.2009.

Rabe, M., Verdes, D., Seeger, S.
Suface-induced spreading of protein aggregates.
Poster at the '8th European Symposium of The Protein Society, ESPS'.
Zurich (Switzerland), 14.06. – 18.06.2009.

Rabe, M., Verdes, D., Seeger, S.
Observing protein aggregates on surfaces.
Poster at the 'EBSA 2009; European Biophysics Congress Genoa'.
Genoa (Italy), 11.07. - 15.07.2009.

1 Introduction

In the title of his widely recognized review paper Nakanishi finds very simple and plausible words to express what is the motivation for so many researchers to dedicate their work to study the adsorption of proteins on solid surfaces: it is "[…] a common but very complicated phenomenon".[1] Remarkably, this statement precisely hits the two most important aspects of this field. Protein adsorption to surfaces is indeed a common event as it happens in countless systems. In living individuals most biological processes take place at interfaces, for instance trans membrane signaling events or the blood coagulation cascade, which are often initiated by the adsorption of proteins.[2-5] Protein adsorption is a desired event on artificial tissue scaffolds ensuring a proper vascularization in the human body.[6] By contrast, protein adsorption is risky when it occurs at biomedical implants that are in contact with the blood stream as it can lead to thrombosis.[7, 8] A similar situation is found in the case of the adsorption of the protein lysozyme to contact lenses which can trigger eye inflammation.[9] In the food processing industry protein adsorption at container walls is the primary reason of biofouling.[10, 11] A further example is the specific adsorption of analyte proteins to protein chips and assay platforms which are essential elements of analytical devices. Whereas a strong adhesion of target proteins is desired, the contamination through unspecific binding of untargeted proteins degrades the analytical performance.[12] Although this brief list is incomplete it should sufficiently clearly underline that protein adsorption is undoubtedly a fundamental issue in many research fields including medicine, pharmaceutical and analytical sciences, biotechnology, biology, etc.[13-18] To this end protein adsorption is a common phenomenon; however, why is it also termed complicated? Probably the major part of researchers working in this field would understand Nakanishi's words in the sense of 'complicated to avoid'. In fact there is a huge community seeking for efficient protein resistant materials applicable to biomedical implants or analytical platforms. There are considerable advances in this subject, in particular due to the introduction of poly(ethylene glycol) grafted polymers or self-assembled monolayers (SAM). However, the principles that

are responsible for protein rejection are still not fully understood and the long term stability of theses surfaces still needs to be clarified.[19-22]

Alternatively, one can also focus on the complicated behavior of proteins from an opposite perspective, namely when they do adsorb to a solid surface. In contrast to small molecules that behave like rigid particles most proteins do not simply attach to or detach from an interface with certain adsorption and desorption probabilities determining their adsorption equilibrium. Instead, the complex composition and structure of proteins causes by far more exciting processes. To name an example, it is nowadays a generally accepted phenomenon that a protein relaxes into an energetically favored state after it has come into contact with a surface.[23-26] This usually involves a rearrangement of the protein's secondary and tertiary structure leading to an increase of the protein-surface contact area. The driving force for this process is a complex combination of enthalpic contributions resulting from attractive protein-surface interactions and entropic contributions due to the loss of structural order within the protein and the release of surface bound water. Further astonishing phenomena include lateral interactions or overshooting adsorption kinetics which are only rarely observed at artificial polymers but frequently reported in the case of proteins. Additionally, the behavior of an isolated protein upon adsorption can be substantially different to the behavior of proteins in an ensemble. Such ensemble phenomena are, for instance, cooperativity which means that adsorbed proteins enhance the adsorption of further proteins, or protein aggregation. The latter aspect is of outstanding interest in the research field of neurodegenerative diseases including Parkinson's or Alzheimer's disease since protein aggregation is associated with the plaque formation processes related to neuron degeneration.[27, 28]

The superior objective of researchers working in this field is to understand how protein adsorption regulates biological processes in living organisms, how protein adsorption to surfaces can be avoided or enhanced, how proteins can be forced to adapt the desired conformation or orientation on the surface, or what can be done to hinder protein aggregation. Advances of our knowledge of protein adsorption were mainly achieved through experimental approaches. Since the first systematic works in this field which approximately date back to the 1970s, a continuous progress in the development of methods and techniques has remarkably increased the precision of experimental data. Starting from crude measurements of adsorption kinetics at high bulk protein concentrations in the past it is nowadays possible to detect even single molecules at the surface, to measure orientational and structural properties of adsorbed proteins, or to image protein covered surfaces with high resolution, to name a few of the most important achievements. However, the broad spectrum of different adsorption phenomena

requires intelligent combinations of complementary experimental methods as so far any technique is restricted to a specific application area.

Naturally, experimental observations need to be carefully analyzed to avoid misinterpretations. This is preferably realized by comparing them to theoretical model descriptions whose advantage consists of a very illustrative access to complex processes and mechanisms. A newly emerging approach to protein adsorption is opened by computational methods aspiring to simulate the behavior of proteins at interfaces. Unfortunately, at the present, even strong computer systems can only treat small systems accurately at rather limited time scales. Thus, computational methods are restricted to a small number of very specific aspects of protein adsorption. However, their enormous potential is obvious considering that technical or physical constraints such as the diffraction limit in optical methods do not exist in simulations.

The primary aim of the present dissertation is to advance the understanding of protein adsorption phenomena at solid surfaces. To achieve this, comprehensive experimental data sets serve as an input to suggest consistent mechanistic details which then have to be translated into mathematical concepts. In the end, these concepts may be combined into a model whose validity is tested again with the experiment. To this end the consistent model is the envisaged output of all effort and preferably constitutes an aid to understand complex adsorption processes in an illustrative manner. Suitable experimental techniques for this work include fluorescence sensing which gives rise to protein adsorption kinetics and fluorescence imaging providing information about the protein distribution on the surface as well as about protein aggregation.

The results of this work are presented as follows: First, the validity and the limits of the used experimental methods are outlined in Chapter 4. Thereafter, in Chapter 5, the cooperative effect observable during the adsorption of BSA is explored based on experimental data and on a macroscopic model. Subsequently, in Chapter 6, the experimental results of Chapter 5 are revisited with a microscopic approach. In Chapter 7 different adsorption phenomena including cooperative effects, overshooting adsorption kinetics, and lateral interactions are studied using the model protein β-Lactoglobulin. Finally the topic of protein aggregation, with a particular emphasis on the spreading behavior of surface deposited protein clusters is addressed in Chapter 8.

2 Theory of Protein Adsorption

The following chapter is conceived as an overview and a discussion of the theoretical concepts in the field of protein adsorption which have been discussed in the literature until today. The presented topics were selected according to their relevance for the present dissertation and can not be considered as complete. Important issues, which were selected since they inspired parts of this work, include thermodynamic aspects of the driving forces, kinetic aspects revealing mechanistic phenomena, as well as computational and experimental approaches that are commonly used to study protein adsorption.

2.1 Driving forces

Protein adsorption is an event that happens almost immediately when a surface comes into contact with a protein solution. As already mentioned above, it is a non-trivial challenge to design surfaces that resist protein adsorption. The reason why proteins adsorb so easily to many surfaces is found in a complex composition of factors that constitute the driving forces for this process.[17] The term driving force refers to the gain of free energy when dissolved proteins adsorb on a surface which divides into enthalpic and entropic contributions. Enthalpic contributions to the total free energy include electrostatic or coulomb interactions, van der Waals (VDW) interactions, and hydrogen bonds. Entropic contributions result from the release of counter ions and solvation molecules as well as the loss of structural order when proteins unfold upon adsorption to maximize the protein-surface contact area. Further, there are hydrophobic forces which are strong and long-range forces between hydrophobic surfaces in aqueous media and also play an important role. Although the exact origin of these interactions is still not fully explained they are expected to be mainly an entropic effect resulting from the restructuring and the release of surface water molecules.[29] Also the

formation of hydrogen bonds between surface and protein may imply entropic effects since it can coincide with the destruction of other hydrogen bonds within the protein leading to a loss of structural order and hence to an increase of the entropy.[18]

Proteins are very versatile and complex molecules. On hydrophobic surfaces they adsorb with their non-polar patches directed towards the surface mediated by hydrophobic interactions. On hydrophilic or charged surfaces, by contrast, proteins direct their polar or charged regions towards the surface and bind predominantly through VDW or coulomb interactions to the surface. The entropic contributions also depend on the protein's structural stability, its ability to form new hydrogen bonds, and on the surface affinity of the solvent molecules. Coulomb interactions which are important when surface and proteins are charged strongly depend on the buffer pH and on the concentration of dissolved ions which have a screening effect. Thus, an exact formalism that quantifies all contributions to the driving force for protein adsorption is practically impossible and suitable simplifications to allow approximate solutions need to be found.

A possibility to describe the electrostatic interactions of a particle with a charged surface is given by the screened coulomb potential which considers the screening effect of the electrolyte solution above the surface.[30]

$$U_{el} = \sum_{i,j} \frac{q_i q_j}{4\pi\varepsilon_0\varepsilon_r} \cdot \frac{1}{r_{ij}} \cdot e^{-\kappa r_{ij}} \tag{2.1}$$

$$\kappa^{-1} = \sqrt{\frac{\varepsilon_0\varepsilon_r \cdot k_b T}{2N_A \cdot e^2 \cdot I}} \tag{2.2}$$

q: electric charge of particles; ε_0: dielectric constant; ε_r: relative static permittivity; r: distance; κ^{-1}: Debye length; N_A: Avogadro's number; e: elementary charge; I: ionic strength; k_b: Boltzmann's constant; T: temperature

In principle the total coulomb energy acting on a protein close to the surface is a sum of all interactions of each charge inside the protein with the charged surface and with the charges of other proteins nearby. However, in most studies mean field approximations are implemented describing proteins as spheres whose charges are arbitrarily distributed within the sphere or simply centered in the middle.[30-34] The classical description of the VDW interactions is given by:

$$U_{VDW} = -\sum_{i,j} \frac{\varepsilon}{r_{ij}^6} \tag{2.3}$$

ε: constant accounting for the strength of VDW interactions

Again, instead of summing up the VDW interactions between individual atoms a suitable value for epsilon is used to describe the interaction between the surface and the protein as one entity. Additionally, it was argued that protein-protein VDW interactions can be omitted since their distances on the surface are mostly large compared to the short range of VDW interactions.[30] For completeness, a hard-sphere potential that prevents proteins from penetrating into the sorbent surface has to be formulated. This can be achieved, for instance, by setting the inner energy to infinity as soon as the protein touches the surface or, as is implemented in the Lennard-Jones potential, by adding a repulsive term of the form $1/r^n$. The combined enthalpic contributions can be used to approximate the inner energy* of a specific system which is for instance needed to evaluate the Metropolis criterion of a Monte-Carlo (MC) simulation.[30, 35] Such a MC simulation will end up in the equilibrium state of the system which is also the state of free energy minimum provided the simulation time is long enough or the simulated system is large enough, i.e., contains enough proteins.

A mathematical approach that not only provides a formalism for the inner energy but directly accounts for the free energy of an ensemble of adsorbing proteins is given by the DLVO theory developed independently by Derjaguin/Landau and Verwey/Overbeek. This theory combines VDW interactions and the so called double layer forces which are actually coulomb forces near a charged surface on which an electric double layer of counter ions has been established. Additionally, the shapes of the interacting partners are taken into consideration. As an example, the free energy of two interacting spherical particles is given by:[29]

$$W_{DLVO}(D) = \frac{\alpha \cdot c \cdot R}{\kappa^2} \cdot e^{-\kappa D} - \frac{A \cdot R}{6D} \tag{2.4}$$

α: constant dependent on temperature and surface potential; c: electrolyte concentration; R: radius of spherical particles; D: distance between particles; A: Hamaker constant

* As protein adsorption processes in aqueous media typically proceed without changes in volume and pressure the change of inner energy is equivalent to the change of enthalpy.

The first term of this equation describes the coulomb interactions, the second term describes the VDW interaction. Although the DLVO theory was originally designed to describe the stability of colloidal systems, further extensions of this theory have been used in protein adsorption studies, for instance to investigate the relevance of VDW and electrostatic interactions during protein adsorption at varying pH conditions.[32] As the equilibrium state follows directly from the mathematical expressions, a simulation is not necessary.

The DLVO theory is only one approach among others to express the free energy of a system that describes protein adsorption.[31, 36] Likewise the number of mathematical expressions accounting for the change of the inner energy upon adsorption of a single protein is also huge as can be inferred from the vast number of different force fields used in more accurate computer simulations of small systems. The conclusion of such a versatile repertoire of mathematical expressions is that a unique theory for the driving forces of protein adsorption is yet non-existent. Thus, the choice of the most suitable formalism and hence the relevance of each of the contributing factors depends on the questions that one is trying to answer.

2.2 Mechanistic concepts and phenomena

As mentioned before, the adsorption of proteins to solid interfaces is a non-trivial topic. Proteins typically do not behave like symmetric rigid particles that can either adsorb on or desorb from a surface. These two processes were the only ones that Irving Langmuir considered when he developed a theory for the adsorption of gas molecules to surfaces, nowadays widely known as the *Langmuir adsorption isotherm*. Although this theory is still a kind of starting point serving for the development of theoretical descriptions of protein adsorption events, it is obviously too simplistic to match the complex behavior of proteins. Remarkably, Langmuir himself was absolutely aware of the limits of his equation. He commented: “Considering the nature of the simplifying assumptions made in its derivation it should, of course, not be looked upon as a general equation of the adsorption isotherm” (Langmuir, 1932).[37] Unlike small and rigid gas molecules proteins exist in a large variety of structural properties, size, and shape. Due to a defined folding into their secondary and tertiary structure proteins contain a specific distribution of hydrophobic, hydrophilic, positively charged and negatively charged side chains which has a major impact on their

adsorption characteristics. Things become even more complex considering that many properties like the folding state or the number of positive and negative charges inside proteins can vary in different environmental conditions depending on pH, ionic strength, or temperature. In the following the most frequently reported mechanistic effects occurring during protein adsorption to solid interfaces are outlined (Fig. 2.1).

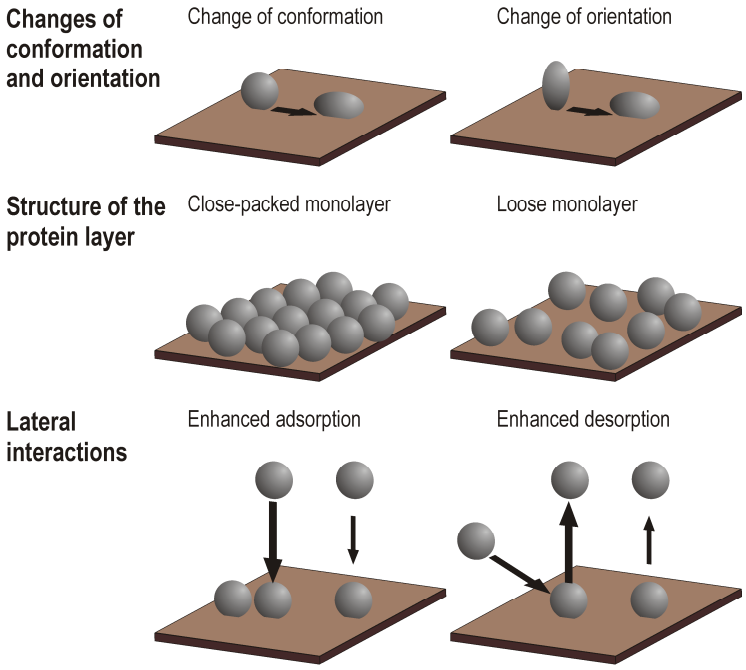

Fig. 2.1. Schematic illustration of various mechanistic effects frequently reported in the literature.

Changes of conformation and orientation

According to a protein's flexibility to undergo structural changes it can be classified as 'hard' or 'soft' protein.[18] When a protein comes in contact with a surface its native folding state may not be the most favorable one any more because additional protein-surface interactions start to play a role. In fact, numerous experimental studies have provided evidence that in particular structural flexible, i.e., soft proteins, undergo conformational changes upon adsorption which typically proceeds towards an augmentation of the protein-surface contact area.[23-26] Favorable protein-surface interactions and an entropy gain due to a loss of ordered secondary structure inside the molecule plus the release of counter ions or solvation molecules are the most dominant driving forces for this process. To this end the conformational changes upon

adsorption corresponds to a relaxation process leading to macroscopically observable effects such as a flattened protein layer structure, an altered secondary structure, and an increased resistance to elution. Closely related to structural changes is the concept of re-orientation upon adsorption which implies little or no unfolding but a change of the protein's orientation as a whole entity. Such a behavior is mainly restricted to structurally stable, i.e., hard proteins.[38-41] As most globular proteins are not of ideal spherical shape the orientation of adsorbed proteins, for instance 'side-on' or 'end-on', determines the protein layer thickness.[40, 42] Not surprisingly, conformational or orientational changes upon adsorption may affect the protein's biological activity. It is known that many proteins exhibit their function only after adsorption.[16, 39] By contrast, adsorption can also lead to the irreversible alteration of proteins that do not refold into their native structure after desorption. It is assumed that such events potentially inactivate certain species such as receptors or enzymes.[43, 44] In some cases it was even noticed that surface adsorption stabilizes the structure of proteins and hence improves their resistance to thermal denaturation as compared to dissolved proteins.[45, 46]

Structure of the protein layer

If a surface is sufficiently long equilibrated in the presence of a protein solution a saturation coverage will establish. The protein layer structure at this point can be a densely or loosely packed monolayer or even a multilayer. Multilayers are found under specific conditions that promote protein aggregation or repress inter protein repulsion.[47, 48] Monolayers establish when protein-protein interactions are only weak or repulsive which is often the case for proteins bearing charges of equal sign.[49, 50] A general observation is that the packing density of monolayers depends on the strength of the electrostatic repulsions between surface-adsorbed proteins. If proteins bear a relatively high net charge ($pH \neq pI$ and low ionic strength conditions) they assemble into a loose layer whereas proteins that are net neutral ($pH = pI$ or high ionic strength conditions) assemble in a more densely packed layer.[14, 32, 48, 50] The highest possible monolayer density, i.e., a close-packed monolayer implies the formation of two-dimensional surface aggregates. Interestingly, the surface density has also been found to be dependent on the bulk protein concentrations even in the case of irreversible adsorption.[50-52] The following explanation for such a behavior was suggested by Ramsden.[53] Induced by an increased 'pressure' of proteins approaching the surface, the proteins that are already adsorbed undergo structural changes such that the binding area per protein decreases leading

to a more compact packing. Further, it was proposed that surface aggregation processes take place above a certain critical bulk concentration. Below that concentration only a loose protein layer may establish.[52]

In the absence of significant protein-protein interactions except short range repulsions proteins populate the surface in a pure randomized arrangement which is described by the 'random sequential adsorption' (RSA) theory. According to this framework proteins do only adsorb to the surface if they approach an area which does not overlap with any other pre-adsorbed protein. Otherwise, if a protein were to hit an adsorbed protein on its way towards the surface it is rejected back into the bulk volume. This results in a very inefficiently packed protein layer leaving undefined gaps between adsorbed proteins which are not large enough to accommodate another protein. The probability by which an incoming protein finds an available adsorption site decreases faster with increasing surface coverage as is the case in the simple Langmuir adsorption theory. So far, an exact description for the 'probability function' or more commonly termed the 'available surface function' $\Phi(\theta)$ exists only for the one-dimensional problem which is also known as 'random parking'.[54] Concerning the more relevant two-dimensional problem an approximate function was proposed by Schaaf and Talbot (1989)[55] which satisfactorily matched the results of a Monte-Carlo simulation.*

$$\Phi^{RSA}(\theta) = \frac{\left(1-\frac{\theta}{\theta_j}\right)^3}{1-0.812\cdot\left(\frac{\theta}{\theta_j}\right)+0.2336\cdot\left(\frac{\theta}{\theta_j}\right)^2+0.0845\cdot\left(\frac{\theta}{\theta_j}\right)^3} \qquad (2.5)$$

Using hard discs as model particles a simulation of the RSA mechanism yielded a saturation coverage or 'jamming limit' of $\theta_j = 54.7\%$ implying a minute degree of surface order.[56] Considering that the RSA theory allows an adsorption of particles at any free position it is certainly the more realistic model compared to the Langmuir adsorption theory which restricts the adsorption to discrete binding sites. Experimental evidence that proteins under certain conditions follow the RSA mechanism was found through analyzing adsorption kinetics.[54, 57] However, the RSA model was also suggested to be insufficient as additional effects may contribute to the adsorption process.[58] Following the first treatments of the RSA

* Ever since this function was published no better solution for the reference RSA probability function was proposed. Up to the year 2009 this work was cited more than 200 times.

problem, formalisms that allow a generalization were developed including processes like bulk diffusion, conformational and orientational changes, protein desorption, multilayer formation and even gravitational effects in the case of large polymer particles.[57, 59, 60]

Lateral interactions

Lateral interactions refer to the possibility that proteins not only interact with the sorbent surface but also with one another. As mentioned above, proteins of the same species usually bear a net charge of equal sign that causes long-range inter protein repulsions and hence leads to a non close-packed protein layer structure. To this end the adsorption process can be easily described by assigning an effective size to the proteins that is larger then their real size. However, it is often observed that adsorbing proteins accelerate the adsorption of further proteins which is manifested by increasing adsorption rates as a result of increasing surface coverages.[52, 61-63] This phenomenon is generally expressed by the term cooperative protein adsorption and is most commonly described by surface aggregation mechanisms.[64-69] That means, proteins are assumed to preferably adsorb to the surface in the immediate vicinity of one or more proteins. However, protein aggregation is not an indispensible explanation for cooperative protein adsorption events. It is also suggested that the complex electrostatic field in the circumference of adsorbed proteins induces a kind of electrostatic self-assembly which in turn enhances the protein uptake rate.[70-72] Clearly, mechanistic aspects of cooperative adsorption are still under debate. Although the effect is frequently observed during kinetic studies there are widely differing concepts how to mathematically express the coverage dependence of the adsorption rate constant including square-root,[73] linear, [74] or exponential[75] functions.*

Apart from an accelerated adsorption of proteins in the presence of pre-adsorbed proteins the inverse, namely the enhanced desorption of adsorbed proteins is also discussed in the literature. Experimentally, it has been shown that in some conditions proteins approaching the surface may hit other pre-adsorbed proteins which, as a result, are released from the surface.[74, 76] In the case of protein mixtures it was concluded from theoretical considerations that larger proteins tend to repel smaller ones from the sorbent surface.[31]

* In Chapters 5 and 6 of the present dissertation a comprehensive model for cooperative protein adsorption is proposed which supports the idea that a tight surface aggregation is not essential. Nevertheless, there is a certain self-organization of proteins due to locally encountered lateral interactions between adsorbed and approaching proteins.

Finally, interactions between proteins which are already adsorbed onto the surface are found as well. Conformational and orientational changes have been observed to be triggered when a certain coverage level is exceeded, i.e., when the average protein-protein distance has become small.[72, 77]

Overshootings

Under the continuous supply of protein solution to a sorbent surface the adsorbed amount of protein, i.e., the protein coverage, monotonically increases in time approaching a saturation level at which the number of adsorbing proteins equals the number of desorbing proteins. In the case of irreversible adsorption the saturation is reached as soon as the surface is fully occupied. An overshoot during the adsorption occurs when the surface is temporarily oversaturated and equilibration is reached through a net desorption of proteins despite a further supply of protein solution. In a number of colloid and polymer adsorption studies overshoots and even oscillations of adsorption kinetics are reported and mechanistically explained by the so-called *time delay model*.[78-80] It states that polymer adsorption begins when desorption from the surface is not allowed. After a certain time delay, however, desorption starts due to conformational rearrangements which may cause the overshoot provided the surface is fairly covered and consequently oversaturated. Several experimental data were found to match this model.[80]

Considering that proteins are in fact biopolymers consisting of up to several thousands of amino acids as monomeric units it can be inferred that protein adsorption kinetics could also include overshoots. However, the properties and shapes of these overshoots differ broadly which has led to a variety of concepts seeking to explain this peculiar behavior (Fig. 2.2). The most prominent work on this issue was conducted by Vroman et al.[81-83] who investigated the adsorption of proteins from blood plasma to a solid interface. It turned out that the protein Fibrinogen rapidly adsorbs to the surface but after a short time passes through a coverage maximum and finally covers the surface in smaller amounts at the equilibrium state than in the intermediate state. Experiments with differing protein compositions revealed that this behavior is actually a displacement effect due to which Fibrinogen is replaced by other proteins of higher surface affinity, predominantly by the protein High molecular weight kininogen (HMWK). Numerous subsequent studies confirmed this mechanism which was hence concluded to be of general validity.[31, 84] In recognition to his initial studies this effect is

now called 'Vroman effect'.[85, 86] Interestingly, displacement events are not necessarily restricted to the adsorption from protein mixtures. Elofsson et al. observed an overshoot during the adsorption of β-Lactoglobulin which was attributed to an initial adsorption of metastable octamers that were subsequently replaced by the more stable monomers and dimers.[11]

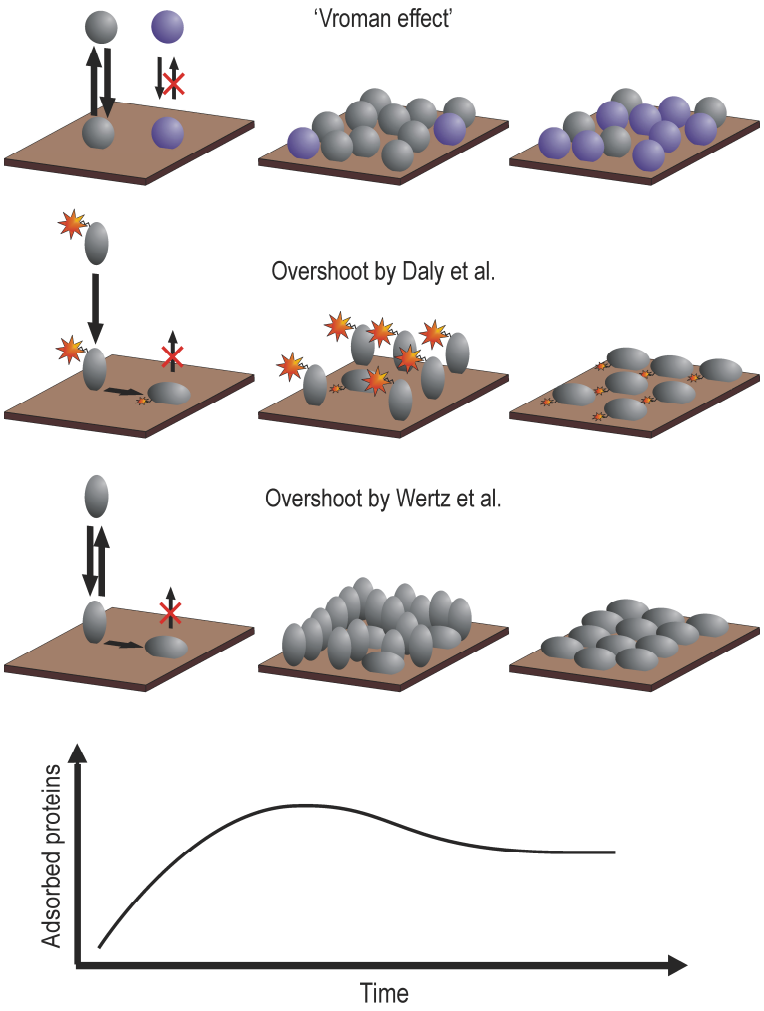

Fig. 2.2. Three different explanations for overshooting adsorption kinetics: The Vroman effect (upper row) describes the competitive adsorption of a fast adsorbing species of relative low surface affinity and a slowly adsorbing species of high surface affinity. The explanation by Daly et al. (middle row) is based on a change of the protein's orientation after adsorption which results in a decrease of fluorescence emission intensity of the dye.[77] Wertz et al. (lower row) argues that the initial end-on orientation allows more species to adsorb on the surface as the final and energetically preferred side-on orientation.[41]

However, studies on Lysozyme (Lys) in its monomeric form have revealed that other mechanisms than described by the Vroman effect must also be taken into consideration. In

two separate studies, Daly et al.[77] and Wertz et al.[41] found overshooting adsorption kinetics when fluorescently labeled Lys was adsorbed at neutral pH (7.4) on hydrophilic or hydrophobic surfaces, respectively. On the hydrophilic surface the adsorption from relatively small bulk protein concentrations ranging from ~0.07 µM to ~0.7 µM resulted in an overshoot whose peak width turned out to be the broader the lower the bulk concentration was. The authors argued that an orientational rearrangement from an initial end-on to a final side-on orientation takes place which is accelerated at a high flux of incoming proteins. As a result of the orientational change the fluorescent label fluorescein isothiocyanate (FITC) is moved closer to the negatively charged surface where the pH is practically increased leading to a preferred protonation of the fluorophore. Since FITC is a pH-dependent fluorophore its protonation in turn reduces the fluorescence emission intensity.[87] In this sense, the overshoot is believed to be only a signal loss caused by the characteristics of the experimental method and hence does not reflect a reduction of the surface coverage.[77] On the hydrophobic surface, by contrast, Wertz et al. observed the overshoot only at bulk concentrations as high as ~700 µM or higher.[41] The overshoot in this case was described as a displacement of the more loosely bound proteins in the end-on orientation by the more strongly bound proteins in the side-on orientation. When the adsorbed proteins change their orientation they require 1.5 times more space on the surface than before such that the equilibrium coverage is lower than the intermediate maximum. The authors concluded that overshoots occur when the adsorption rate is high compared to the transition rate of the orientational change. No dependence of the peak shape on the bulk concentration was considered. The comparison of these two works highlights the complexity of protein adsorption phenomena. Both research groups work under almost identical experimental conditions including the same technique, the same fluorophore (FITC), and the same buffer pH (7.4). The most important difference is the used sorbent surface which is either net negatively charged and hydrophilic[77] or neutral and hydrophobic.[41] In agreement with each other they both consider the overshoot of the adsorption kinetics to be a consequence of an orientational rearrangement of surface adsorbed Lys molecules from the reversibly bound end-on to the tightly bound side-on orientation. From this point on, however, the overshoot is explained in completely different ways, namely by a loss of fluorescence intensity, on the one hand, and by a displacement of the species that require less surface area, on the other hand. Unfortunately, desorption experiments through rinsing the surface with protein free buffer at different stages before and after the overshoot are lacking in both

studies. Therefore, the assumed difference of the binding affinities of the end-on and side-on oriented proteins is not supported experimentally.*

Protein aggregation

A highly important aspect connected with protein adsorption is the aggregation of proteins into oligomers of a few monomers or into clusters of up to several hundreds of protein monomers. This process can accommodate protein adsorption at solid interfaces and influence the adsorption kinetics as well as the resulting layer structure. To this end the term protein cluster refers to a two-dimensional assembly of protein monomers on a surface. The formation mechanisms of protein clusters may include either the diffusion of surface bound molecules towards precursor aggregates or the direct adsorption of bulk proteins adjacent to other surface bound proteins or protein aggregates.[65, 67] Regardless of the pathway, these two-dimensional protein clusters are assumed to evolve directly on the surface.[88, 89] In the case of a high degree of internal order these surface assemblies are even termed two dimensional surface crystal.[68] As mentioned before, surface-induced aggregation is often considered as a result of cooperative adsorption.[64-68] Note however, that cooperativity is a more general term which includes other mechanisms than a tight aggregation. In particular the use of atomic force microscopy (AFM) has confirmed the existence of two-dimensional protein aggregates on surfaces.[64, 68, 88, 89] However, AFM potentially affects the protein arrangements during the measurement as it is an invasive technique. Of course the growth of surface aggregates is not restricted to two dimensions as three-dimensional surface-induced aggregation has also been observed.[47, 90]

Apart from a surface-induced process protein aggregation can also be a solution process and the resulting protein clusters may adsorb to the surface in addition to monomer adsorption. In this sense the term protein clusters is used for stable, ordered or amorphous aggregates that grow in a protein solution.[91] Their morphology ranges from linear, fibril-like to spherical and display diameters of up to a few hundreds of nanometers.[92, 93] Many different protein species were found to form such soluble clusters as proven by a broad spectrum of different analytical techniques.[91, 92, 94-98] The generally accepted formation mechanism of this kind of protein cluster includes a nucleation step resulting in a seed of one or a few

* In Chapter 7 various desorption experiments are of central importance to suggest a consistent explanation for the overshooting effect.

aggregated monomers followed by the cluster polymerization through monomer addition.[94, 99] However, universal detailed mechanistic models for protein cluster formation and growth are subjects of current research.[94, 99-104] Dissolved protein clusters can behave like large particles that compete with protein monomers for adsorption on the surface. Moreover, their behavior on the surface may differ from that inside the solution.[*] The considerable attention brought to the field of protein clusters or aggregates results from the awareness that there is a link between their precursors and a number of neurodegenerative diseases including Alzheimer's disease, Parkinson's disease, and Type II diabetes to name a few.[27, 105] Investigations of the mechanisms and the conditions that lead to protein clusters or aggregates are hence of great interest.

2.3 Mathematical models

A mathematical model is a theoretical construct that serves as a simplified substitute of a real system. The degree of simplification depends on the specific scientific question in mind, and researchers asking different questions will come up with all legitimacy with distinct model designs. In this sense the validation of a model is not that is 'true' or 'false' but that it generates verifiable hypotheses in the context in which it was developed.

Kinetic models

In the field of protein adsorption studies the primary objective is to understand the behavior of proteins in close proximity to or deposited onto the surface. This includes their behavior as individual species and as a component in an ensemble. Given the considerable albeit not unlimited technical opportunities to date, large amounts of experimental data are available. However, techniques allowing a direct observation of the undisturbed adsorption of proteins in molecular dimensions are still far from being mature. Thus, experimental data typically contain macroscopic information resulting from the individual behaviors of one or an ensemble of several proteins. At this point the design of a model that mathematically

[*] In Chapter 8 of this dissertation the behavior of protein clusters that adsorb from the solution to the surface will be investigated in detail.

describes the experimental data is an efficient way to unravel or confirm mechanistic details of the adsorption process. A model always opens the opportunity to 'play' with different ideas or to test different sets of parameters which in the end helps to argue what is possible and what is not. However, models are typically restricted to the experimental limits in which their hypotheses can be tested and generalization to other systems must be done with care.

As the mechanisms behind protein adsorption events strongly affect the adsorption kinetics, the majority of models developed in this field are 'kinetic models' which are usually expressed through rate equations. In general it is rather uncomplicated to construct a kinetic model by using terms that represent the mathematical translation of the adsorption phenomena discussed before. The easiest way is to start with a reference model, for instance the Langmuir adsorption model, which is successively modified or extended.

$$\frac{\mathrm{d}\theta}{\mathrm{d}t} = k^{on} \cdot c_s \cdot \left(1 - \frac{\theta}{\theta_{max}}\right) - k^{off} \cdot \theta \tag{2.6}$$

In equation (2.6) θ refers to the protein coverage, θ_{max} is the maximum coverage level at which no more binding site is available, k^{on} and k^{off} are, respectively, the on-rate and off-rate constants and c_s is the protein concentration directly above the surface. The adsorption of proteins from the bulk solution causes a depletion of the surface concentration c_s which in turn leads to a protein transport from the bulk solution to the region above the surface. As a consequence, the surface concentration varies during the adsorption process which is often taken into consideration in the model design.[41, 70, 74, 75, 106] A straight-forward possibility to implement the transport of proteins towards the surface was proposed by Corsel et al.[106] who argued that the surface concentration changes very slowly in time throughout the adsorption and is hence approximately constant ($\mathrm{d}c_s / \mathrm{d}t \approx 0$). Consequently, the protein flux to the surface equals the protein adsorption rate leading to the following expression of the surface concentration which has been implemented in some works.[41, 74, 106]

$$c_s(t) = c_b - \frac{1}{k^{transport}} \cdot \frac{\mathrm{d}\theta}{\mathrm{d}t} \tag{2.7}$$

The transport rate constant $k^{transport}$ has to be calculated according to some further models accounting for the used measuring cell system. However, a number of researchers judges the

influence of transport to the surface less important to the resulting adsorption kinetics and leaves the surface concentration as a constant that is equal or at least directly proportional to the bulk concentration.[61, 77, 107]

The term $\left(1-\theta/\theta_{max}\right)$ in equation (2.6) which accounts for the continuous reduction of available surface sites is often replaced by the available surface function $\Phi(\theta)$ as defined by equation (2.5).[54, 57, 71] In this way a more realistic depletion of surface sites considering the random sequential adsorption of proteins is achieved.

Lateral interactions between surface bound proteins are implemented into kinetic models by expressing the corresponding rate constants as functions of the surface coverage.[73-75]

$$k^{on,off,trans} = f(\theta) \tag{2.8}$$

This concept was in particular useful to include cooperative effects. By defining the on-rate constant being proportional to the surface coverage, increasing adsorption kinetics expressing the acceleration of the adsorption rate due to pre-adsorbed proteins were described.[71]

$$k^{on} = \alpha \cdot \theta \tag{2.9}$$

In most published models proteins can adopt different states on the surface, for instance compact and expanded, monomer and dimer or end-on and site-on. If their adsorption characteristics differ from one another each state needs to be expressed with a specific rate equation. Transition or exchange mechanisms between them require a coupling of these equations. It is however highly desirable to keep the number of different species and likewise the number of adjustable parameters at a minimum as a higher complexity of the model degrades its validity. Models comprising two,[25, 77, 108] three,[74] or even six[109] different species are common.

A somewhat special model has been proposed by Minton to describe the growth of two-dimensional protein clusters on the surface.[67] In this model each surface bound i-mer, that means monomer, dimer, trimer, etc., has a specific tendency to attract a further incoming protein that increases the cluster by one unit. As a consequence the number of coupled rate equations is expanded to infinity, at least in theory. In practice the formalism has to be cut at an upper limit of cluster species to allow the computation of adsorption kinetics with

reasonable effort.* Apart from the simplest models, such as the Langmuir model (equation (2.6)) or a two-state transition model,[108] the rate equations require numerical integration which is typically achieved with standard algorithms, such as the fourth-order Runge-Kutta method.

Equilibrium models

A few models found in the literature are focusing on thermodynamics rather than on kinetic aspects and can be classified as 'equilibrium models'. The first step is to develop a suitable expression for the free energy of the particular states of a chosen system which is, in a simplified view, composed of protein-protein interactions and protein-surface interactions as well as the entropy of the corresponding state. Finding the free energy minimum among a selected choice of systems gives access to adsorption isotherms or other specific information that are experimentally testable. Minton, who has already been mentioned before in the context of kinetic models also developed an equilibrium model to comprehensively explore cooperative and surface clustering effects.[65] Apart from adsorption isotherms he calculated the coverage-dependant average cluster size and the *Hill n* which describes to which extend the aggregation of an incoming protein to a pre-adsorbed protein is favored over adsorption to a separate binding site. Szölősi et al. formulated an equilibrium model that allows a forward and backward transition between adsorbed states of differing footprints.[110] Using arbitrary parameters for the internal energies of the particular states and for the energy barriers between them, MC simulations were performed that gave rise to calculated adsorption kinetics. In this way the authors predicted exchange effects between adsorbing and pre-adsorbed proteins as well as the overshooting effect. Fang and Szleifer proposed expressions for calculating the free energy of systems containing proteins of different size that are either neutral or arbitrarily charged.[31, 36] The equilibrium surface compositions and densities as a function of bulk composition and ionic strength of the buffer solution were obtained. Additionally, dynamic simulations were performed that gave rise to the adsorption kinetics resulting from mixtures of large and small proteins under varying input parameters.

* In Chapter 5 Minton's formalism is used up to a 15-mer to test its validity for experimental data acquired in this work.

2.4 Computational approaches

An increasingly important access to molecular-scale studies of protein adsorption events has been opened by computational methods. The adsorption of one or several proteins to a selected surface is simulated with differing degrees of exactness based on physical laws. Although, at the present, computer simulations are far from being suitable to replace experimental works they provide a growing amount of useful information about some details of adsorption mechanisms. Without the technical and physical constraints ruling experimental methods, computational approaches to protein adsorption practically allow to 'see' the movement of every protein or even of its atoms. Limitation, however, results from the computational costs which rise rapidly with increasing structural detail and precision.

Starting at the highest level of precision molecular dynamics (MD) simulations were applied to study which atoms are involved in protein-surface interactions,[111] to determine the preferred orientations of surface bound proteins,[112, 113] to visualize conformational rearrangements,[114-116] or to explore solvent effects.[112, 117] The common procedure consists of defining a system composed of an artificial surface, for instance gold, graphite, or quartz, typically one protein or protein fraction, and solvent molecules. A critical point in every MD simulation is the choice of a valid force field which is always designed for a specific problem. Again, the more exactly all contributing forces are treated the higher are the computational costs. Compromises are for instance made by treating solvent molecules implicitly in an effective dielectric medium or by using force fields that have no extra term for H-bonds.[113-116] At the present the study of protein adsorption using MD simulations is limited to small systems comprising mostly no more than one protein and surface areas that are a bit larger than the size of the protein. Given that simulated times scale around a few nanoseconds one can easily infer that an MD simulation of a realistic system with several proteins on time scales of at least seconds is out of question.

A promising step forward to larger systems are simulations based on coarse-grained models in which structural information is maintained in a strongly simplified manner.[118] In the simulation performed by Carlsson et al. the protein Lysozyme was represented by a hard sphere with embedded positive and negative charges.[30] Using an ensemble of 64 proteins information about preferred orientations, surface density, and the effect of pH and ionic strength was obtained. Skepö studied the influence of electrostatic and short-range

interactions on the adsorption of the protein Statherin on charged and uncharged surfaces.[35] The protein was represented by a chain of charged spheres each one representing one amino acid. Thus, coarse graining enables simulations of larger systems or on longer time scales but referring to the adsorption phenomena that result from the interplay of a large ensemble, such as cooperative effects, this method is still inappropriate.

The only practical solution to exploring large ensembles of adsorbed proteins on reasonable time scales is to abandon any detail of structural information.[33, 34] This is done by defining proteins as single particles, mostly spherically shaped, with a selected charge located in its center.[33, 34, 119] The adsorption process is then simulated with a Metropolis Monte-Carlo simulation according to appropriate algorithms. To evaluate the Metropolis criterion after each MC step, the potential energy has to be calculated using valid pair-potential models which is the critical point in this method. Most models are again based on crude approximations such as a uniform, coverage-independent protein-surface potential which may be inappropriate for some specific problems. An exact description of the potential energy near the surface would be a non-trivial high dimensional function considering the short- and long range interactions between the adsorbing protein and all pre-adsorbed proteins plus the surface at least in a local environment. In other words, the loss of structural information hinders an accurate evaluation of the energy difference resulting from each MC step. One solution is to invent arbitrary interaction energies for the adsorption of a protein, its transition into another state, or its aggregation with other pre-adsorbed proteins.[120, 121] Another possibility consists of replacing the parameters of the approximate models with empirical values.[120-123] In particular the qualitative conclusions from such approaches are justified as they should remain unaffected from the chosen values.

2.5 Experimental approaches

The experiment in the field of protein adsorption is indispensible. Adsorption phenomena are observations made during experimental investigations which are interpreted in terms of adsorption mechanisms and eventually translated into mathematical concepts that are preferably combined into a model. This model can be used to formulate further hypotheses which again have to be tested through the experiment. Thus, a cyclic procedure that puts the

experiment before and after the formulation or refinement of the model is the best way to achieve a reliant and consistent description of the adsorption process.

Of course, there are always constrains resulting from technical and physical principles, such as a limited sensitivity or selectivity, temporal or spatial resolution limits, interferences of the measurement process to the adsorption behavior, and many more. Hence, the used technique has to be chosen according to the category of asked questions, and a combination of complementary techniques is highly recommended to acquire information from different perspectives. Subjects on which experimental investigations focus include adsorption kinetics or isotherms, the protein layer thickness or density, the secondary or tertiary structure of adsorbed proteins, protein-surface or protein-protein interactions, etc. Additionally, the effect of the adsorption of proteins on their biological behavior is a further field of interest. In the following, an overview of the most important experimental techniques and their fields of application is given.

Label-free techniques

There are several widely applied optical techniques that allow for the detection or analysis of unlabeled proteins adsorbed to an interface. Ideally suited for recording adsorption kinetics and isotherms are the following techniques: Ellipsometry (ELM), surface plasmon resonance (SPR), and optical waveguide lightmode spectroscopy (OWLS). Ellipsometry is based on the change of the polarization state of light after reflection from a surface. The measured ellipsometric angles Ψ and Δ refer respectively to the ratio of the amplitudes of parallel and perpendicular light vectors and to the phase shift. With the help of a model analysis these angles can be transformed into layer thickness and refractive index information. In this way the mass of the adsorbed protein layer can be obtained. ELM was used by a considerable number of researchers to measure adsorption kinetics.[11, 25, 63, 75, 124, 125] The technique requires planar, reflecting substrates, preferably quartz, silicon, or silica, and a sufficiently strong change of the refractive index upon protein adsorption.

Surface Plasmon resonance makes use of the light excitation of surface plasmons in thin metal layers. The resonance frequency and the angle of reflection minimum depend on the boundary conditions of the interface. Thus, by measuring these parameters the layer thickness, the adsorbed amount, and density fluctuations can be determined which also allows to record

protein adsorption kinetics.[39, 126] However, SPR necessarily requires substrates coated with a metal layer which constrains its versatility.

Optical waveguide lightmode spectroscopy is based on coupling a light beam into a waveguide through a specific incident angle. Because of the interaction of the evanescent field of the light with the molecules of the adsorbed layer, the incident angle is very sensitive to the refractive index change and to the layer thickness. Again, the adsorbed mass of a protein layer is amenable through the use of appropriate models. OWLS requires planar, optically transparent substrates such as quartz or $Si(Ti)O_2$ but no metal layer coating. Probably due to its high sensitivity and easy handling this technique has been used for numerous studies of protein adsorption kinetics.[62, 70, 71, 127-129]

Techniques that specifically focus on the secondary structure of adsorbed proteins such as attenuated total internal reflectance – infrared spectroscopy (ATR-IR) and circular dichroism (CD) spectroscopy are valuable tools to study conformational changes. Using ATR-IR frequency and amplitude shifts of the amide I and amide II band of surface bound proteins were measured in time and interpreted in terms of changes of the secondary structure.[26, 130] CD spectroscopy exploits the interaction of circular polarized light in the near UV range with the secondary structure of proteins. In contrast to most other techniques presented here, CD spectra are measured in the solution. Therefore proteins are adsorbed to colloidal silica particles in solution which do not interfere with the resulting spectra. Several studies report the use of this technique for direct observations of structural rearrangements of adsorbed proteins.[23, 38, 44]

In contrast to optical methods the working principle of the quartz crystal microbalance (QCM) technique is a change of the oscillating frequency of the substrate upon mass load. In protein adsorption studies the mass includes also the water coupled to or trapped within the layer which is an important difference to the afore described techniques ELM, SPR, and OWLS that actually measure the adsorbed dry mass. To this end the QCM is inappropriate to determine the absolute mass whereas it is sensitive for water rich and extended layers. The technique was used to record protein adsorption and desorption kinetics, mostly in combination with other techniques.[64, 68] Modern QCM instruments are extended to allow energy dissipation measurements within the adlayer upon off-switching the driving voltage (QCM-D). Slow and fast dissipation thereby refer to rigid and flexible layers, respectively. Höök et al. made use of the combination of frequency shift and energy dissipation

measurements to reveal a biphasic adsorption of the protein hemoglobin.[48, 131] First, a monolayer is formed that reaches strong adhesion and rigidity due to conformational relaxations. On the top of this layer a second protein layer establishes which constitutes more flexible proteins that were suggested to stay in their native state. Concerning the required substrate the QCM technique can be considered as flexible since the electrodes embedding the piezoelectric crystal can be coated with practically any desired thin film whereas special properties like transparency or reflectivity do not need to be considered.

The most powerful technique to measure the layer thickness of adsorbed protein films is neutron reflectometry. A collimated neutron beam at wavelengths ranging between 0.1 nm and 1 nm is exposed to and reflected from a protein covered surface. The reflectivity, i.e., the intensity of the reflected beam, is recorded as a function of the momentum transfer which depends on the chosen wavelength and the angle of incidence. In comparison to UV or visible light the wavelength of the neutron beam is considerably smaller, up to three orders in magnitude. Thus, film thickness information with sub nanometer resolution can be measured. Data analysis is performed via appropriate models in which values for the film thickness and the composition-dependent scattering length densities are fitted to the measured reflectivity profiles. In a series of publications Su et al. could provide detailed information about the preferred orientations and the mass of surface adsorbed protein layers using neutron reflectometry.[40, 42, 50] As an example, even minute differences in the layer thickness between side-on (30 Å) and end-on orientation (35 Å) of surface adsorbed Lysozyme were noticed precisely.[40] However, the technique is very cost-intensive as it requires a neutron source which noticeably limits the number of instruments around the world.

Whilst neutron reflectometry has a strong resolution in direction normal to the surface it lacks a powerful resolution in lateral directions. At this point the surface imaging techniques atomic force microscopy (AFM), scanning tunneling microscopy (STM) and electron microscopy (EM) with a lateral resolution down to atomic levels are of great value. In AFM a sharp tip positioned at the end of a cantilever scans over the surface either in contact mode or in tapping mode. At close distances surface-tip interactions increase the force acting on the cantilever in the case of contact mode or reduce the amplitude of the oscillating cantilever in the case of tapping mode. A feed-back loop moves the tip up and down to keep the strength of these interactions at a constant level which directly yields height information. In the field of protein adsorption AFM is often applied to image the distribution of proteins within a layer

with a special regard to cooperative effects and surface aggregation.[58, 89, 120, 122, 132] Even protein adsorption kinetics albeit at very poor temporal resolution and conformational changes of individual proteins were measured.[133, 134] The limiting factor of most AFM studies is that imaging is performed after drying the surface which potentially affects the folding state of the individual proteins or the structure of the protein layer. Furthermore, tip-induced movement of adsorbed proteins is a potential source of error. However, in addition to surface imaging AFM is a valuable tool to measure force-distance curves that give rise to the strength of protein-surface interactions. A single protein is immobilized at the end of the AFM tip and brought into contact with the surface. By slowly retracting the tip adhesive forces between protein and surface can be quantified. Due to this method it could be shown that most proteins adhere stronger to hydrophobic than to hydrophilic surfaces and stronger to charged than to uncharged surfaces.[135, 136]

As a comparable technique, STM is based on a constant tunneling current between tip and surface to obtain topographic information. This naturally requires an electrically conducting layer which is reached by coating the sample with a thin layer of metal or graphite. As a consequence, STM has minor importance in the field of protein adsorption. Publications reporting the use of this technique are often proof-of-principle studies.[61, 137, 138] A similar problem is encountered in EM where imaging is achieved through an electron beam. Again, a conductive layer on top of the sample has to be established which hinders in-situ imaging. Nevertheless, EM was applied to study protein aggregation on surfaces.[92, 139, 140]

Techniques with labels

Over the past decades techniques based on fluorescence have become highly sophisticated tools in life sciences. In particular the astonishing sensitivity down to the single molecule, the versatility, and the easy handling are strengths that lead to the wide use of fluorescence methods in the field of protein adsorption. Fluorescence takes place when a fluorophore is excited into a higher electronic state by the energy of a photon from the excitation light. Part of the energy is dissipated into heat through internal conversion before the fluorophore returns in its ground state through emitting a photon whose wavelength is shifted to higher values (Stoke's shift). Due to efficient optical elements and sophisticated detectors with single photon sensitivity the fluorescence light can be efficiently separated from the excitation light and accurately be detected and even quantified. The use of pulsed light sources allows to

additionally measure the average time that a fluorophore remains in its excited state which gives rise to a further source of information through life time measurements.

Fluorescence methods can be used as 'sensing devices' focusing on a fixed position and as 'imaging devices' visualizing the state of a given surface area with highest possible spatial resolution. In protein adsorption studies there is a demand for selectively detecting proteins bound to the surface and thereby excluding all proteins which diffuse in the solution close to the surface. Comparable to the working principle of OWLS, total internal reflection fluorescence (TIRF) detection exploits the evanescent field upon total reflection to exclusively excite fluorophores in proximity (100 ~ 200 nm) to the surface. Thus the excitation light hits the substrate at an incident angle above the critical angle and the fluorescence emission is collected perpendicularly to the surface. Measurements can be performed in aqueous media on transparent substrates including simple glass cover slides* which renders the technique to a low cost and versatile tool. Glass substrates are usually subject to a specific pre-coating to obtain the desired surface characteristics. TIRF sensing has been frequently applied to record protein adsorption kinetics at high sensitivity.[41, 47, 61, 77, 134] TIRF imaging was for instance applied to observe enzymatic reactions of single surface immobilized proteins or to visualize the mobility of myosin on actin.[141-143]

An alternative method to TIRF is supercritical angle fluorescence (SAF) detection which exploits the effect that fluorophores positioned at the glass/water interface emit a considerable fraction of the fluorescence light into the substrate above the critical angle. The optical set-up is inverse to that of TIRF with an excitation beam illuminating the sample perpendicularly and a collection of fluorescence light emitted into the supercritical angle of the substrate using a parabolic mirror objective. The SAF technology itself (2000),[144, 145] a SAF sensing instrument (2003),[146] and also a SAF imaging instrument (2007)[147] was developed in our group (group Prof. Seeger, Institute of Physical Chemistry, University of Zurich, Switzerland). First SAF sensing experiments related to protein adsorption were performed by Rankl et al. in 2006.[148] SAF imaging experiments are subject of the present dissertation (see Chapters 5 and 8).

Apart from protein detection and imaging there are at least two further important techniques related to fluorescence methods, namely fluorescence correlation spectroscopy (FCS) and Förster resonance energy transfer (FRET). In FCS fluorescence fluctuations are monitored as a function of time and statistically evaluated. The resulting autocorrelation

* In the very special case that fluorescence techniques are used in the UV range, substrates naturally are restricted to quartz.

function describes the probability to find a molecule within the detection volume a certain time after a molecule was detected. A curve fit of appropriate models to the autocorrelation function can provide physical parameters such as the diffusion coefficient of particles, aggregation states or molecular interactions. In terms of instrumentation FCS is routinely combined with confocal or TIRF set-ups and, more recently, also with the SAF optics.[149] In relation to protein adsorption the applicability of FCS to reveal the aggregation of proteins in the solution or on the surface has been demonstrated.[150, 151]

FRET is the non-radiative transfer of the excited state energy from a donor fluorophore to an acceptor fluorophore via long range dipole-dipole interactions. This process requires an overlap of the donor emission spectrum with the acceptor absorption spectrum, a favorable relative orientation of the two involved transition dipole moments, and a donor-acceptor distance in the range of the Förster radius (3 ~ 7 nm). Since the energy transfer efficiency is inversely proportional to the sixth power of the spacing between donor and acceptor fluorophore it can be used as a 'spectroscopic ruler' which is highly sensitive to small distance changes. To realize FRET experiments most optical set-ups can be readily equipped with a further dichroic mirror to split the fluorescence light into its donor and acceptor part which both have to be detected separately. The FRET technique has been successfully applied in the solution to map protein folding processes at the single molecule level or to understand the relation between protein unfolding and aggregation.[152, 153] Further, FRET imaging of surface adsorbed proteins was performed to study protein-protein interactions and aggregation.[51, 154, 155] The combination of FRET with SAF imaging is subject of the present dissertation (Chapter 8).

A limiting factor of fluorescence imaging methods as well as of optical methods in general is that only those details can be separately detected that are at least half a wavelength apart. However, even this paradigm formulated by Ernst Abbé is being overcome by some remarkable recent developments in fluorescence microscopy. Probably the best known technique, albeit not the only one, is called stimulated emission depletion (STED) microscopy. A second drawback is the need of a fluorophore attached to the analyte molecule that is studied unless it is a fluorophore itself. Comfortably, a large number of fluorescent dyes is commercially available including coupling groups for a covalent attachment to biomolecules. However, the potential interference of the additional tag to the experimental result needs to be clarified prior to any scientific conclusion.[156]

In principle a very efficient solution to the problems connected with the attachment of a fluorescent tag to a protein is radiolabeling. Typically, the gamma emitter ^{125}I is attached to Tyrosine residues within a protein which increases the total molecular mass approximately five times less than in the case of dye labeling. The method was applied to record adsorption and desorption kinetics and could reveal exchange mechanisms and cooperative effects.[72, 76, 157] However, the use of radioactive materials may not always be appreciated.

3 Materials and Methods

3.1 Buffer preparation

All adsorption experiments presented in Chapters 4 - 7 were conducted in citrate buffer which can be readily adjusted to any required pH value in the range of pH 3 to pH 7 since the three pKa values (3.13, 4.76, 6.40) differ by less than two units. 10.5 g or 1.05 g of citric acid (Riedel de Haen, Switzerland) was dissolved in 1.0 L of water to obtain a 50 mM and 5 mM buffer solution, respectively. Subsequent titration with NaOH (5N) (Fluka, Switzerland) led to the desired pH-value. The ionic strength is given by:

$$I = \frac{1}{2} \cdot \sum c_i \cdot z_i^2 \qquad (3.1)$$

(I: ionic strength; c_i: molar concentration of the i^{th} ion; z_i charge)

Citric acid predominantly forms a monovalent anion at pH 3 such that the ionic strength is considered equal to the used citric acid concentration. At higher pH values this approximation naturally becomes invalid. Carbonate buffer (50 mM) was prepared by dissolving 4.2 g of $NaHCO_3$ (Fluka, Switzerland) in 1.0 L of water and adjusting the pH to 9.3 with HCl (1N) (Acros, Switzerland). The buffer used for lipid vesicles composed of NaCl (100 mM), $CaCl_2 \cdot H_2O$ (3 mM), and Tris (10 mM) was prepared by dissolving 5.85 g of NaCl, 0.441 g of $CaCl_2$, and 1.576 g of Tris in 1.0 L of water and adjusting the pH to 7.5. Before use, all buffer solutions were filtrated using a 0.22 µm pore size membrane filter (Millipore, Switzerland). Double distilled water was used throughout the preparation procedures.

3.2 Model proteins: selection and labeling

Four different proteins were used as model in this work: bovine serum albumin (BSA), Fibrinogen (Fib), bovine β-Lactoglobulin (β-Lg), and human α-Synuclein (α-Syn). The proteins were selected to provide diversity in size, shape, and physiological importance. As all model proteins have been studied comprehensively by other research groups details on some crucial issues including surface saturation densities or the protein's structural flexibility were easily amenable. The adsorption characteristics of BSA, Fib, and β-Lg were found to be of particular relevance in the fields of assay technologies,[124, 158, 159] biocompatible materials,[5, 82] or food processing.[10, 11, 160] The protein α-Syn is the pathological component of Lewy bodies in patients suffering from Parkinson's disease and is therefore highly important in the field of protein aggregation. Table 3.1 lists some properties and the physiological importance of the model proteins.

Table 3.1. Properties and physiological relevance of the selected model proteins.

Protein	Bovine serum albumin	Fibrinogen	β-Lactoglobulin	α-Synuclein
structure	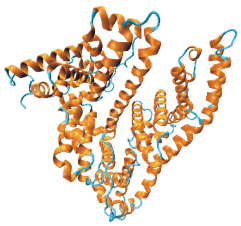 crystal structure of human serum albumin	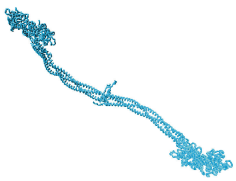 crystal structure of chicken Fibrinogen	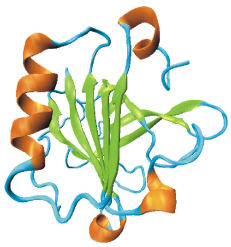 crystal structure of bovine β-Lactoglobulin	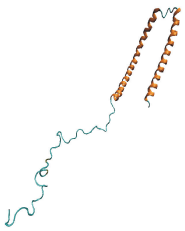 NMR-structure of lipid vesicle bound α-Synuclein
PDB-ID	1E7H[161]	3BLG[162]	1EI3[163]	1XQ8[164]
mol. weight	67 kDa	340 kDa	18.4 kDa	14.5 kDa
pI	4.85	5.2	5.5	4.67
source	blood plasma (~50 mg/mL)	blood plasma (~3 mg/mL)	whey (~3.0 mg/mL in cow's milk)	neural tissue
shape / dimension (nm × nm)	prolate ellipsoid (14 × 4)[42, 165]	rod-like (45 × 6)[166]	globular (3.6 × 3.6)[167]	elongated / hook (14 nm long when vesicle bound)
physiological importance	transport of fatty acids, amino acids, metabolites, etc.; maintains pH and osmotic pressure	precursor in blood clotting process	probably transport of fatty acids, retinol, nonpolar molecules	largely unknown; probably protection against injury of nerve terminals

The proteins bovine serum albumin (BSA, A-4378, >97% protein), bovine Fibrinogen (Fib, F-4753, >61% protein), and bovine β-Lactoglobulin A+B (β-Lg, L-2506-16, > 80% protein) were purchased from Sigma (Switzerland) and used as received. For recording protein adsorption kinetics (Chapter 5 and 7) the fluorophore DY-647-monofunctional N-hydroxysuccinimide ester (DY-647-NHS, Dyomics, Germany) was used. The coupling of the dye to the proteins was conducted by adding 0.5 mL (BSA, β-Lg) or 1.0 mL (Fib) of protein dissolved in carbonate buffer, pH 9.3, at high concentrations (BSA: 20 mg/mL; Fib: 5 mg/mL, β-Lg: 10 mg/mL) to 0.2 mg of lyophilized DY-647-NHS. The mixture was kept in the dark at room temperature for about one hour under slight agitation. Since hydrolysis of the NHS-ester is a concurrence reaction the final solution contains labeled protein and unbound dye. The unbound dye was removed via size exclusion chromatography using a Superdex^{TM} 200 10/300 GL column (Amersham Biosciences, UK) run with PBS buffer (Invitrogen, Switzerland) at 1.0 mL/min flow rate. Dye-to-protein label ratios (p*/p - ratios) of the purified fractions were determined via UV/Vis spectroscopy using the following extinction coefficients: λ_{max}(Dy-647)/nm 653 (ε/M^{-1} cm^{-1} 250000); λ_{max}(BSA)/nm 280 (ε/M^{-1} cm^{-1} 39000); λ_{max}(Fib)/nm 280 (ε/M^{-1} cm^{-1} 513000);[168] λ_{max}(β-Lg)/nm 280 (ε/M^{-1} cm^{-1} 17700).[169] The label-ratios were 1.05 (BSA), 5.1 (Fib), and 0.67 (β-Lg). To reach lower label ratios ranging between 0.5% / 1.0% (β-Lg) and 12.5% / 25% (BSA, Fib) dye-labeled proteins were diluted with unlabeled proteins.

During the FRET study (Chapter 8) the fluorophores Cy5 and Cy7 (Amersham Biosciences, UK) were used as donor/acceptor pair in the case of BSA. The fluorophores modified as NHS-ester were coupled to BSA by individually adding 0.2 ml of protein solution (20 mg/mL) to 0.2 mg of lyophilized Cy5 and Cy7 dye. After reaction for one hour at room temperature the final label-ratios of 3.5 (Cy5-BSA) and 2.7 (Cy7-BSA) were determined using the following extinction coefficients: λ_{max}(Cy5)/nm 649 (ε/M^{-1} cm^{-1} 250000); λ_{max}(Cy7)/nm 747 (ε/M^{-1} cm^{-1} 200000). Relatively high protein label ratios of approximately three fluorophores per protein molecule are necessary to ensure a high initial energy transfer rate within protein clusters. However, it was noticed that the fluorescence intensity decreases at label-ratios above three due to self quenching effects.[170]

The protein α-Synuclein (α-Syn) was produced by Alice Soragni of our collaborating group (Prof. Dr. Roland Riek, ETH Zürich) and provided as aqueous solution (~3mg/mL). The donor fluorophore (DY-647-NHS) was attached by adding 250µL of α-Syn solution to 0.2 mg of lyophilized dye and the acceptor fluorophore (Cy7) was attached by adding 100µL of α-Syn to 0.2 mg of dye. Subsequent steps were done as described above leading to final

label-ratios of 1.2 (DY-647-α-Syn) and 0.61 (Cy7-α-Syn) using an extinction coefficient of λ_{max}(α-Syn)/nm 275 (ε/M^{-1} cm^{-1} 5600) for α-Syn.[171] All solutions were stored at 4°C in the dark.

3.3 Hydrophilic and hydrophobic surfaces

Hydrophilic surfaces were produced by thoroughly rinsing common glass coverslips (Menzel, Germany) with ethanol and subsequent immersion in a 0.2% aqueous Deconex solution (Borer Chemie, Switzerland) for at least 14 days. After this procedure the contact angle of the coverslip has decreased from ~30° down to almost 0° indicating a high hydrophilicity. Hydrophobic model surfaces were obtained by immersion of clean coverslips into a 1 mM octadecyltrichlorosilane (OTS, ABCR, Germany) solution in dry toluene (< 50 ppm water content) for one night under nitrogen atmosphere. With this procedure the coverslip was coated with a C18–chain silane monolayer.[172] The water contact angle amounted to ~105° indicating high hydrophobicity of the substrate.

3.4 Model membranes

The experiments on α-Syn aggregation presented in Chapter 8 were partially performed on an artificial model membrane which is mimicked by a planar supported phospholipid bilayer (SLB). A SLB forms spontaneously when a solution containing unilamellar vesicles (ULV) in appropriate buffer is exposed to a hydrophilic surface. During this process the spherical phospholipid vesicles adhere to the surface, rupture, and spread which in the end leads to a planar bilayer.[173] In this work the protocol for SLB formation was taken from Reviakine and Brisson (1999) and was slightly modified.[174] A frequently used model membrane composition consist of 1,2-dioleoyl-*sn*-glycero-3-phosphocholine (DOPC) and 1,2-dioleoyl-*sn*-glycero-3-phospho-L-serine (DOPS) at a ratio of 9:1. Firstly, multilamellar vesicles (MLV) were obtained by mixing the desired amounts of the two artificial phospholipids in chloroform (Sigma), followed by removing the solvent under vacuum overnight, and rehydrating the lipids at 30°C – 40°C in the described buffer. Secondly, ULVs were obtained by extrusion of

the MLVs through a 100 nm pore-size polycarbonate filter. In this step the MLV solution was subjected to at least 15 passes through the filter using a mini-extruder. The resulting ULV solution was further diluted in the same buffer to a final concentration of 0.1 mg/mL and exposed to the 'deconex' cleaned hydrophilic glass surface for at least two hours. The equipment including lipids, filters, and mini-extruder were purchased from Avanti Polar Lipids, Inc. (USA). To test the successful formation of the SLB, the membrane intercalating fluorophore *CellMask™ deep red plasma membrane stain* (Invitrogen, Switzerland) diluted in water was applied to the lipid bilayer. A strong increase of the fluorescence emission as response indicated the presence of the model membrane whereas a control experiment on a hydrophilic glass surface showed no response.

3.5 Recording protein adsorption kinetics: SAF biosensor

All protein adsorption kinetics presented in this work were recorded using the supercritical angle fluorescence (SAF) biosensor. The set-up and the working principle are comprehensively described in recent publications.[144-146] In brief, a HeNe laser (635 nm) illuminates the glass/water interface orthogonally from below using a 400 mm focal distance achromatic lens. The surface emission fluorescence is collected with a parabolic mirror objective which transforms the near field emission of dipoles located near the interface to far field parallel rays. Thus, the fluorescence emission above the critical angle undergoes total internal reflection at the parabolic glass/air interface. Consequently, a plan-convex lens (f = 300 mm) was used to focus the emission through a detection aperture of 1 mm diameter, onto the sensitive area of a photomultiplier tube (PMT, R928 07, Hamamatsu, Japan) running in single photon counting mode. By detecting only the supercritical angle emission (i.e. ~61° for a glass/water interface), the detection volume is restricted to a surface distance well below 100 nm whereas bulk fluorescence is efficiently rejected. Fig. 3.1 depicts a schematic representation of the SAF biosensor.

The adsorption of fluorophore labeled proteins was measured on a circular area with a diameter of roughly 60 µm. In this way the fluorescence intensity of a rather large area that can accommodate huge amounts of adsorbed proteins is collected which ensures that local density fluctuations or defects are balanced out. To minimize photodestruction processes the laser intensity was reduced to approximately 5 µW through grey filters (New Focus, USA). A

shutter across the laser beam allowed for the collection of the total fluorescence in distinct time intervals. Practically all adsorption experiments were conducted by exciting the sample every 60 s over a long period of up to several hours. Unless otherwise stated adsorption kinetics presented in this work are average curves from duplicate measurements. In the case of long-term adsorption kinetics data points were partially omitted for the sake of clarity.

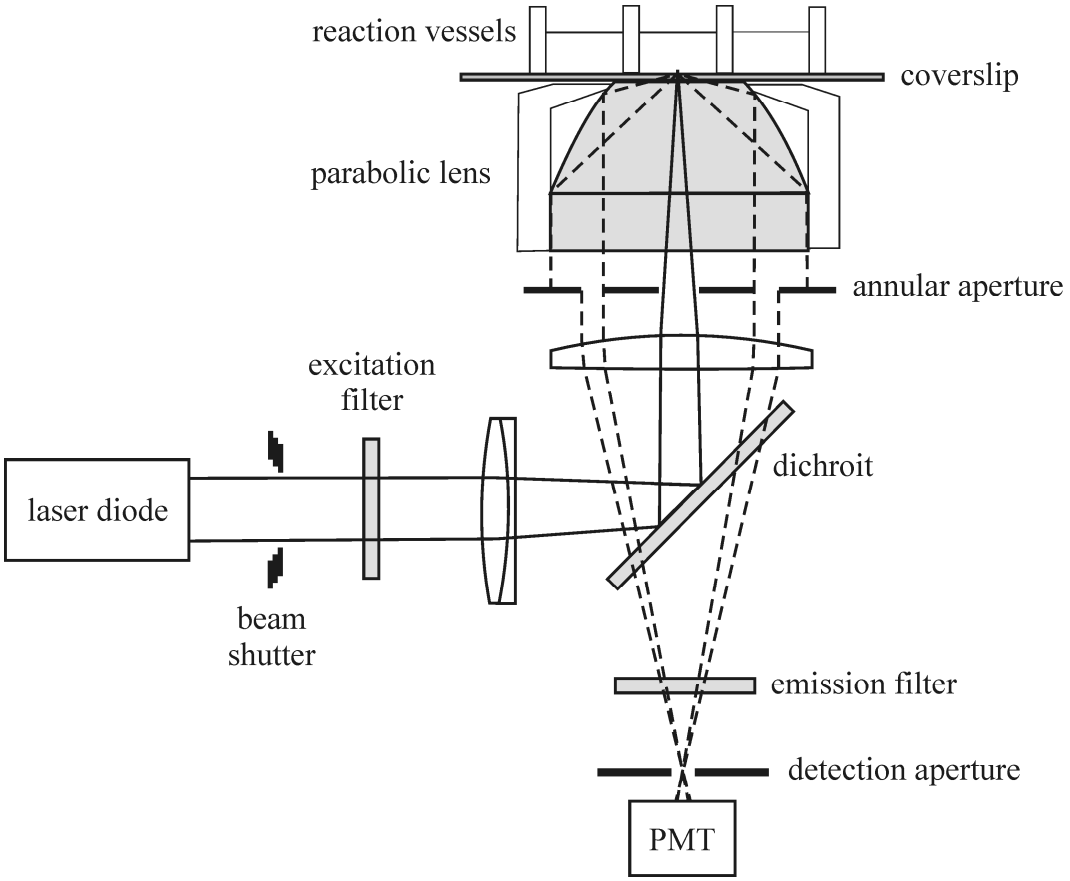

Fig. 3.1. Scheme of the SAF biosensor (taken from ref.[146]).

The measuring cell was designed as a flow cell consisting of an aluminum support with half-cylindrical chambers of a volume of 0.2 mL (Fig. 3.2). During monitoring the adsorption the protein solution was pumped through the cell at 0.25 mL/min using a peristaltic pump (Ismatec, Switzerland). Two methods were applied to fix the glass substrate on the top of the flow cell. In the case of BSA and Fib adsorption the coverslip was simply glued on the support using UV curing adhesive. For adsorption studies on β-Lg the glue appeared to influence the reproducibility of the measurements. In this case it has proven suitable to keep

the coverslip with some pressure on the top of the flow cell using Teflon tape as a seal. The complete measuring cell was mounted on the objective via immersion microscope oil and fixed in a holder.

Fig. 3.2. Photographs of the aluminum flow cell top and down view.

3.6 Recording scan images: SAF microscope

In recent years the SAF technique was implemented into a scanning microscope that allows to record surface images at diffraction limited resolution. The microscope combines two detection channels as schematically depicted in Fig. 3.3.[147, 175] The SAF-channel exclusively collects the fluorescence emitted into the super critical angle of the glass interface which corresponds to fluorophores located in close proximity to the surface. The inner channel corresponds to a typical confocal channel with a detection volume that reaches a few micrometers inside the solution. Thus the instrument allows for the detection of surface bound fluorophores and of fluorophores diffusing in the solution simultaneously. A scanning microscope table moves the measuring cell over the objective of the microscope and hence an area of up to 75 µm × 75 µm can be imaged with a scanning time of 8 min. To increase the time resolution, a smaller area of 15 µm × 15 µm can be imaged with a scanning time of 45 s. The highest possible time resolution of 0.9 s is obtained by repeatedly scanning a single line (75 µm). FRET imaging was realized by splitting the fluorescence emission collected with the SAF channel of the microscope into donor and acceptor emission via a dichroic mirror at 730 nm. Thus, donor and acceptor fluorescence were detected in two separated detectors. In this work all presented scan images were solely recorded with the SAF channel. At low bulk

protein concentration the inner confocal channel typically showed identical images apart from lower signal intensities.

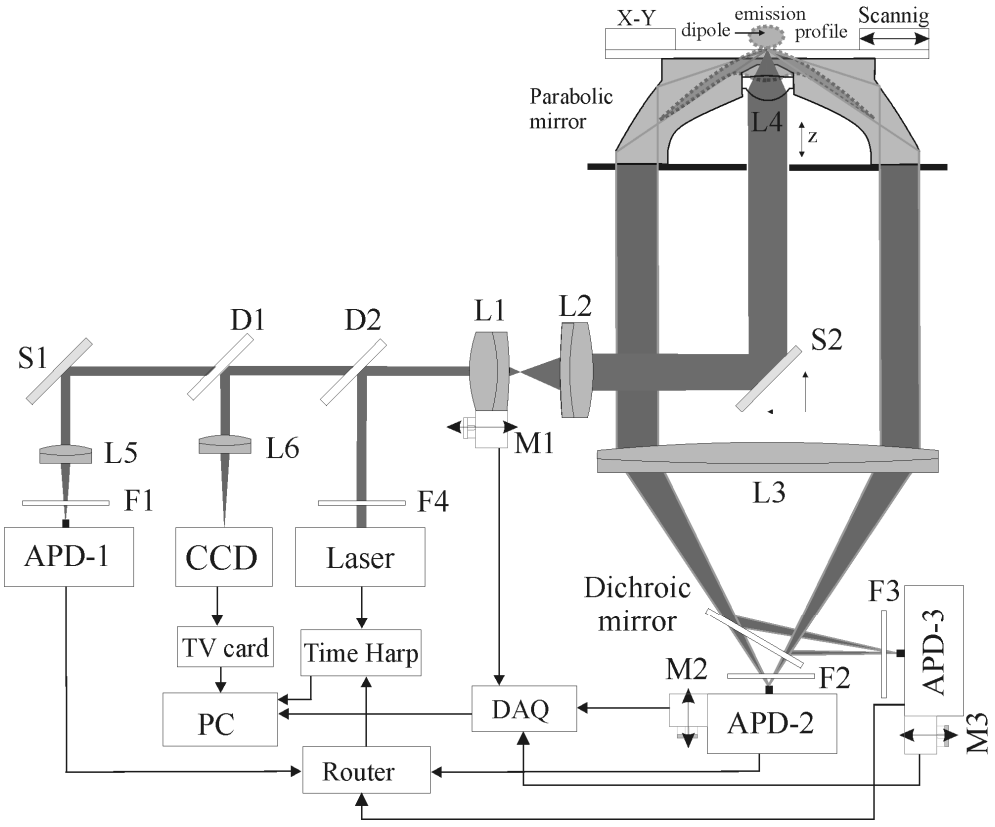

Fig. 3.3. Schematic representation of the SAF microscope (adapted from ref.[147]).

3.7 Mathematical and computational methods

Rate equations and curve fitting

Protein adsorption kinetics were used to model the mechanisms of adsorption phenomena. In a first step the behavior was described with rate equations which by their nature are first order ordinary differential equations (1st order ODEs). Protein adsorption models typically require several coupled rate equations to describe for instance different adsorption states or pathways. Apart from a few exceptions the resulting system of ODEs has to be integrated numerically. In this work numerical integration was performed using standard simulation software (*AQUASIM 2.0*) in which the *backward differentiation formula* is implemented.[176] To decide

if a proposed model is a valid representation of the real adsorption behavior an acceptable overlap between model and experimentally acquired kinetics was crucial. Thus, the main issue was to find the optimal set of parameters defined by the model through a curve fitting procedure. In general the used simulation software allowed for curve fitting through sequentially refining an initial, arbitrary guess of parameters. That means, after each variation of any of the parameters the new curve was computed numerically and evaluated using the *least squares method* until no further improvement of the fit was possible. For large parameter sets this method requires a good initial guess to reach fast convergence. An alternative method was realized in this work concerning the rate equations modeling cooperative adsorption (Chapter 5). In that case, the adsorption rate could be represented as a one-dimensional function of the total surface coverage. This function was directly fitted to the rate-coverage representation of the experimental data through a non-linear regression procedure (*Origin 7.03*). Only afterwards numerical integration was performed to compute the curve representing the adsorption kinetics. Naturally, this way works without large numbers of repeated numerical integrations and is hence more efficient than the first method. However, in many cases the rate can not be expressed by a function of the coverage (Chapter 7), making the first method unavoidable. Regardless of the method used, the quality of the fit was evaluated with the help of the coefficient of determination.

$$R^2 = 1 - \frac{\sum_i (y_i - f_i)^2}{\sum_i (y_i - \bar{y})^2} \tag{3.2}$$

R^2: coefficient of determination; y_i: value of data point i; f_i: value of model point i; $\bar{y}$: mean of all data points

Monte-Carlo Simulation

The algorithm of the Monte-Carlo simulation was implemented using the programming language of *MATLAB 2008b*. A surface area of distinct adsorption sites was represented by a square matrix of dimension 3250. To match the dimensions of the data obtained experimentally in this work each matrix element was defined to represent a surface area of 2 nm × 2 nm. A second matrix of dimension 1000 was generated that corresponds to the instrumental response profile of the SAF microscope. With these settings simulated scan images of dimension 2250 as well as simulated adsorption kinetics were computed using

increasing cooperative lengths (r_{coop}) as input values. Random numbers to select the position of the adsorption trial of each step were generated by the standard random number generator implemented in MATLAB. With the used hardware (Intel Core 2 Duo E6420 CPU, 1.5 GB RAM) simulation times varied between 1 and 48 hours depending on the chosen cooperative radius. The simulation time was found to scale with the square of r_{coop}.

4 Validity of the Experimental Methods

Prior to evaluating and interpreting experimentally acquired data it is essential to carefully probe the potential and the limits of the experiment itself. Practically all results presented in this thesis rely on experiments based on fluorescence detection methods. In contrast to label-free detection methods, fluorescence techniques require a marker molecule attached to the analyte that emits a fluorescence signal upon laser excitation. A huge spectrum of different fluorophores that can be excited at a desired wavelength and readily attached to peptides, proteins, DNA, or other biomolecules is commercially available. However, despite its unique strength of being one of the most sensitive detection methods, the need of an additional tag to the analyte molecule implies potential risks of misinterpreting experimental data (Fig. 4.1).

Given the fact that size and mass of these dyes are comparable with those of small biomolecules, it is essential to question whether the adsorption behavior and in particular the surface affinity of the dye-labeled analyte molecules is identical to that of the native analyte molecules. Several studies report that dye-labeled proteins may exhibit a stronger adsorption affinity to the selected surfaces than unmodified proteins under identical conditions.[177-179] Thus, the influence of the attached marker molecule has to be clarified in advance to avoid fundamental errors in interpreting protein adsorption kinetics or isotherms. A second issue concerns the emission intensity of fluorescent dyes under varying local conditions. In the case of fluorescein isothiocyanate (FITC) it has been reported that the fluorescence intensity can decrease when the fluorophore approaches a negatively charged surface as a result of the re-orientation of the protein. This alteration of the local electrostatic potential is assumed to favor the protonation of the carboxyl residues of fluorescein which in turn reduces the emission intensity.[77, 87] Therefore, the dependence of the fluorescence emission efficiency, i.e., the quantum yield of the used fluorophores on varying surrounding conditions has to be probed.

Another problem inherent to fluorescence methods is the limited photostability of fluorescent dyes. Photodestruction processes, in particular the reaction of dyes with oxygen in

the excited state, can lead to their irreversible inactivation. Thus, the specific photobleaching rate of the fluorophores used in the experimental set-up should be determined prior to any quantitative investigations. Additional points for reliable protein adsorption experiments are the issue of reproducibility and, particularly in the case of assessing adsorption kinetics, the influence of transport processes.

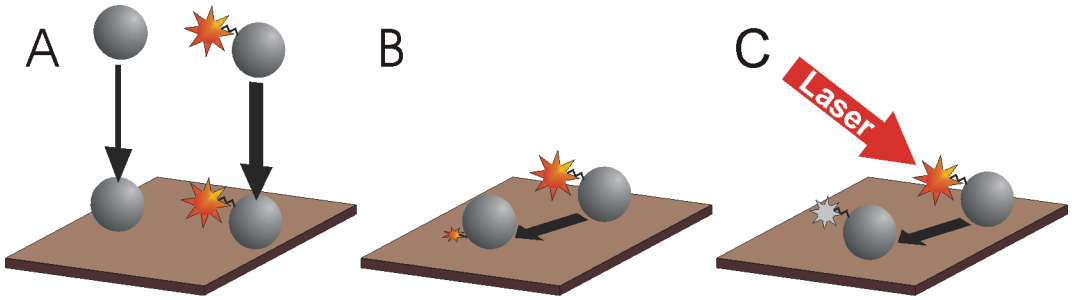

Fig. 4.1. Potential risks encountered in fluorescence detection techniques for protein adsorption studies.
A) Preferential adsorption of labeled over unlabeled proteins or vice versa.
B) Loss of fluorescence intensity due to changes of the conditions in the micro environment of the fluorophore.
C) Photodestruction of fluorophores due to a frequent laser excitation.

4.1 Probing the influence of fluorescent tags on the adsorption of proteins

The surface affinity of three commercial fluorescent dyes, Alexa® 647, Cy5, and DY-647, was tested by monitoring their adsorption behavior using the SAF biosensor (Fig. 4.2). In accordance with the conditions of most of the experiments performed in this work, the dyes were applied in citrate buffer (pH 3, 50 mM) on a hydrophilic glass surface as well as on a hydrophobic OTS-coated surface. As was expected, no adsorption took place on the hydrophilic surface because both, surface and dye molecules are negatively charged under the applied conditions and hence repel each other. On the hydrophobic surface, by contrast, dyes do adsorb to some extend: irreversible adsorption of DY-647, reversible adsorption of Cy5 (Fig. 4.2 A). The intense adsorption of DY-647 is in agreement with the relatively strong hydrophobic character of the dyes of the DY-family.[180] In a second experiment the three dyes were covalently attached to the protein BSA at dye-to-protein ratios of 0.5, that means, in average every second protein is labeled. The adsorption kinetics of these three species, Alexa® 647-BSA, Cy5-BSA, and DY-647-BSA, on the hydrophilic glass surface turned out to

be practically identical as depicted in Fig. 4.2 B. In particular the characteristic linear or even slightly upwards concave shape* is observed in all three curves, suggesting an irrelevant influence of the dye family on the adsorption behavior.

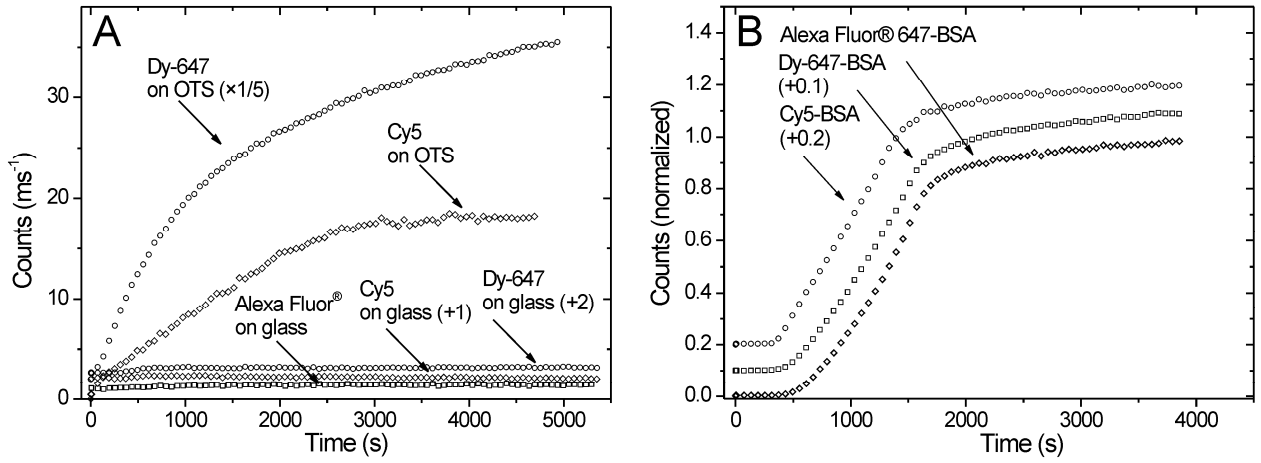

Fig. 4.2. Evaluation of potential impacts of different fluorophores on protein adsorption kinetics.
A) Adsorption of the pure fluorophores Alexa® 647, Cy5, DY-647 on the hydrophilic glass and the hydrophobic OTS-coated surface.
B) Adsorption of Alexa® 647-BSA, Cy5-BSA, and DY-647-BSA (c = 50 nM, pH = 3, 50 mM ionic strength) on the hydrophilic glass surface. For presentation reasons the curves were individually shifted upwards.

The most unambiguous confirmation of a potential influence of the fluorescent tag on the adsorption behavior is obtained from the comparison of adsorption kinetics conducted at different ratios of labeled to unlabeled proteins (p*/p – ratio). Fig. 4.3 shows pairs of adsorption kinetics of DY-647-BSA whose content of dye-conjugated proteins was set to differ by a factor of two. On examining these pairs (lower and upper adsorption curves in Fig. 4.3), it is noticed that, within the experimental error, their fluorescent intensities also differ by a factor of two. Additionally, the saturation levels are always reached after the same adsorption time independent of the content of labeled proteins. Only in the case of a preferential or a strongly inhibited adsorption of dye-conjugated proteins one would expect a factor smaller than two or different adsorption times until saturation. In the case of BSA labeled with the fluorophore DY-647 a noticeable influence of the dye can thus be excluded on both types of surfaces, the hydrophilic glass surface (Fig. 4.3 A) and the hydrophobic OTS coated surface (Fig. 4.3 B), which is a prerequisite for the study presented in Chapter 5.

* A detailed explanation of the shape of the adsorption kinetics of BSA follows in Chapter 5.

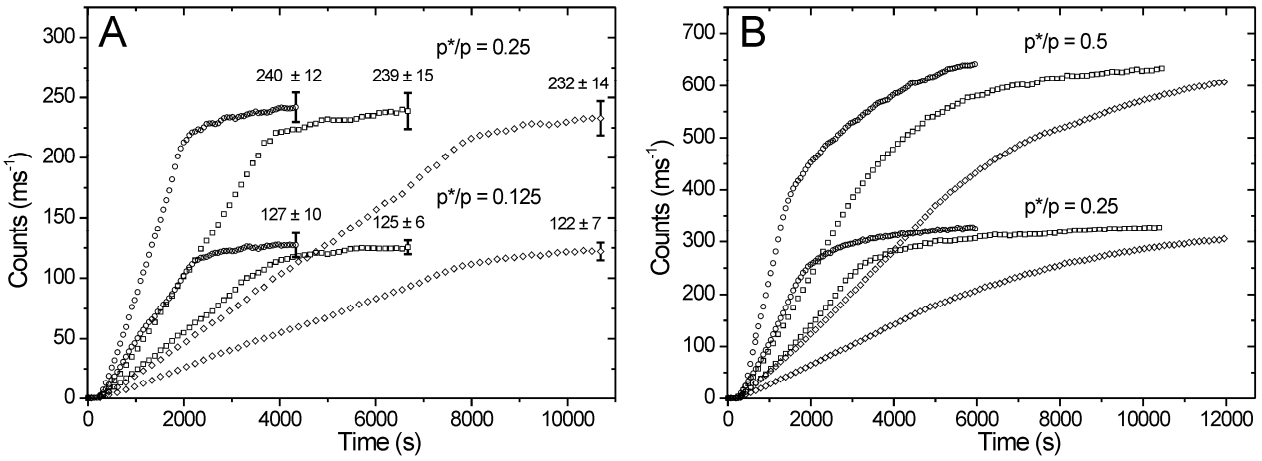

Fig. 4.3. Adsorption kinetics of DY-647-BSA at different contents of labeled proteins. The p*/p – ratios differ by a factor of two.
A) Adsorption of DY-647-BSA at bulk concentrations of 16 nM (○), 8 nM (□), and 4 nM (◊) in citrate buffer (pH 3, 5 mM) on hydrophilic glass.
B) Adsorption of DY-647-BSA at bulk concentrations of 16 nM (○), 8 nM (□), and 4 nM (◊) in citrate buffer (pH 3, 5 mM) on the hydrophobic OTS coated surface.

An analogous experiment conducted with DY-647-β-Lg at two different bulk concentrations (0.75 µM and 1.5 µM) on the hydrophilic glass surface (Fig. 4.4 A) led to comparable results as obtained with DY-647-BSA. The adsorption kinetics measured at the low p*/p – ratio exhibit count rates slightly higher than in the ideal case (~ 9%) suggesting a faintly increased adsorption affinity of labeled over unlabeled β-Lg. To ensure that this effect is unimportant for the investigation of adsorption phenomena, the following experiment, conducted in the low bulk concentration regime, was realized (Fig. 4.4 B). Two adsorption kinetics were recorded, a reference kinetic curve containing labeled β-Lg during the whole experiment (upper curve) and a second kinetic curve consisting of the adsorption of native β-Lg for the first 800 s and the adsorption of labeled DY-647-β-Lg at the same concentration thereafter. It is evident that both curves exhibit a characteristic overshoot at exactly the same point in time* which is only explainable if unlabeled proteins adsorb at a comparable rate as labeled proteins. Conclusively, the influence of the dye on the adsorption behavior of β-Lg is considered negligible at low and high bulk protein concentrations which allows for deeper investigations of the kinetics which will be the topic of Chapter 7.

* As will be discussed in Chapter 7 the overshoot takes place at a distinct critical coverage level which is equivalent to a fixed point in time at a given bulk protein concentration.

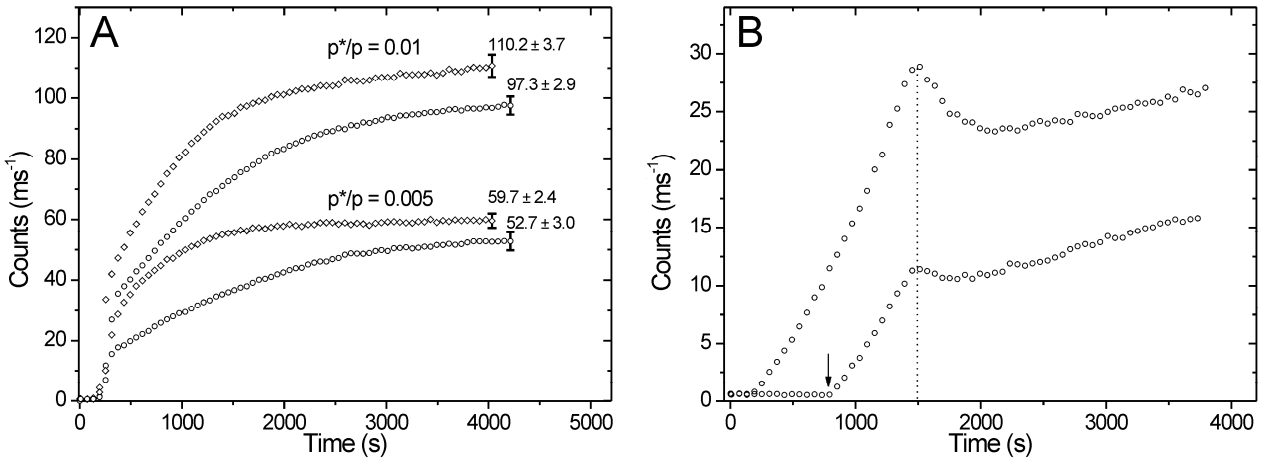

Fig. 4.4. A) Adsorption kinetics of DY-647-β-Lg at bulk concentrations of 1.5 µM (◊) and 0.75 µM (○) in citrate buffer (pH 3, 50 mM) on hydrophilic glass. The p*/p – ratios differ by a factor of two.
B) Lower curve: Adsorption of unlabeled β-Lg (50 nM) for 800s (arrow) followed by the adsorption of labeled DY-647-β-Lg at the same bulk concentration. Upper (reference) curve: Adsorption of labeled DY-647-β-Lg from the beginning.

4.2 Influences on the fluorescence emission intensity

Conformational and orientational changes upon protein adsorption are frequently observed phenomena.[77, 87, 108, 128, 148, 181] During such processes fluorophores that are covalently attached to the proteins are possibly dragged into a different environment relative to the protein's surface or to the adsorbing interface. This in turn can be accompanied by changes in the local electrostatic or dipolar potential, in particular when the interface is charged.[87] In the case of pH-dependent fluorophores like FITC such alterations result in a loss or gain of fluorescence emission intensity.[182] To check for a potential pH dependency of the main fluorophores used in this work, the fluorescence emission spectra of DY-647, Cy5, and Cy7 covalently bound to the proteins BSA and β-Lg, respectively, were recorded under pH conditions varying from pH 3 to pH 7.4 (Fig. 4.5). It is noticed that a pH dependency can be excluded for DY-647 whereas the Cy5 and the Cy7 fluorophores exhibit stronger fluorescence emission fluctuations under varying pH. A similar observation is made when the emission spectra of the three dyes bound to BSA are recorded at increasing ionic strength conditions ranging from 5 mM to 500 mM: the DY-647 fluorophore apparently shows a stronger stability towards changing the buffer conditions (Fig. 4.6). As a consequence, kinetic analyses are preferably conducted using the fluorophore DY-647. Adsorption kinetics at different pH and ionic strength conditions can hence be directly compared with each other.

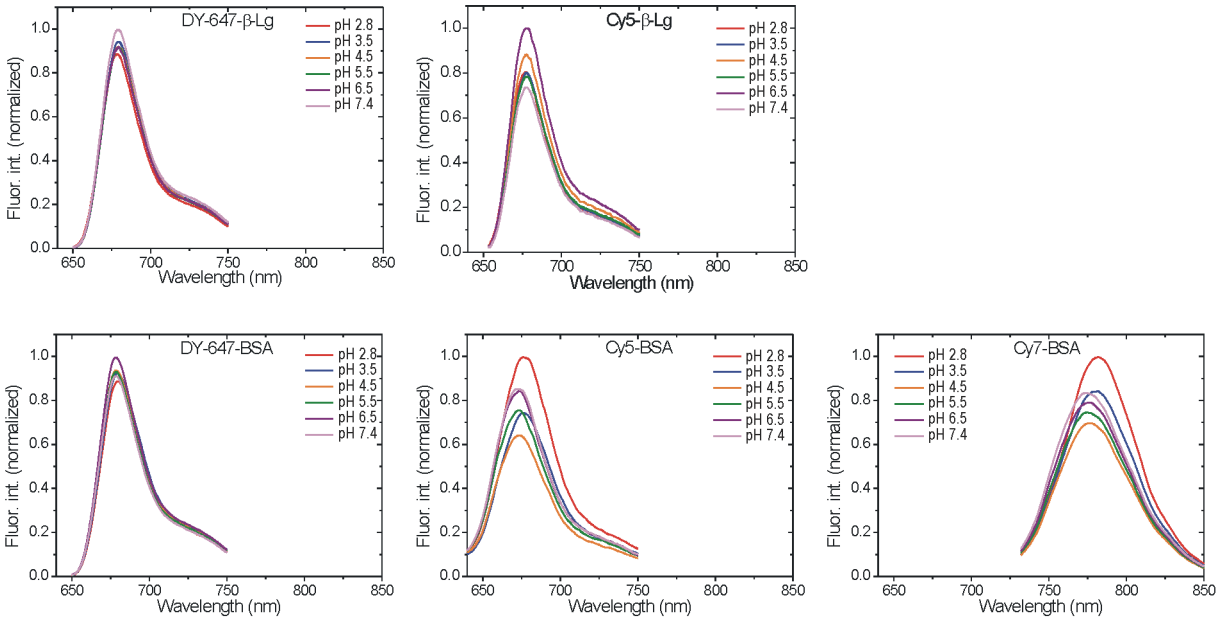

Fig. 4.5. Fluorescence emission spectra of DY-647-β-Lg, Cy5-β-Lg, DY-647-BSA, Cy5-BSA, Cy7-BSA at varying pH conditions.

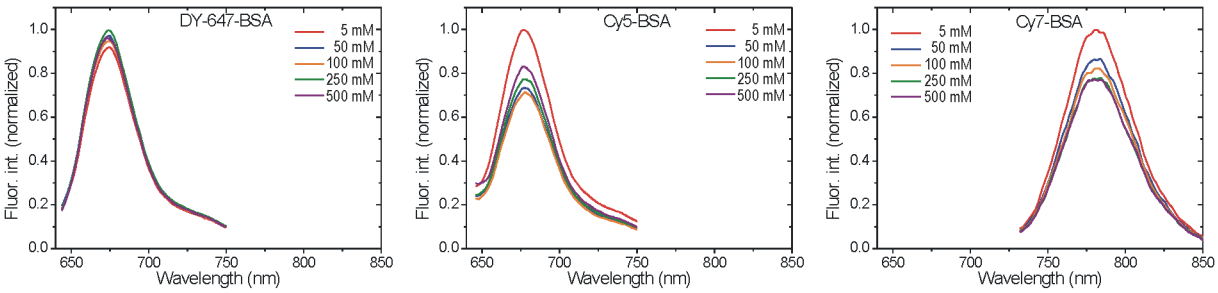

Fig. 4.6. Fluorescence emission spectra of DY-647-BSA, Cy5-BSA, Cy7-BSA at increasing ionic strength.

4.3 Photostability of fluorescent dyes

Fluorescent dyes undergo irreversible photodestruction processes upon excitation with a probability that is specific to each individual fluorophore.[183] If the photobleaching rate of a given system is comparable to the rate at which protein adsorption events take place, a quantitative interpretation of these adsorption processes is complicated. All adsorption kinetics quantitatively interpreted in this work were recorded on the SAF-biosensor. The laser beam in this set-up was expanded such that a circular area of 60 µm diameter on the surface is illuminated. Further, the total laser intensity was reduced to approximately 5 µW through a gray filter (OD 2.5) ensuring a minute laser power density. By using a shutter across the laser

beam the sample was typically excited every 60 s for a sampling time of 500 ms. The photobleaching rate of this set-up in the case of DY-647 labeled proteins was quantified with the following experiment (Fig. 4.7). DY-647-BSA was adsorbed on a hydrophilic glass surface in citrate buffer (pH 3, 50 mM). Under these conditions the adsorption of BSA is irreversible, hence the fluorescence count rate remains constant upon rinsing the surface with protein-free buffer (see Fig. 4.7 after 2000 s). Whereas the photobleaching effect is too weak to be recognized at a shutter interval of 30 s, a clear decrease of the fluorescence count rate is observed at a shutter interval of 1 s. A fit of the experimental data obtained at this short shutter interval to a mono-exponential decay revealed a photobleaching rate constant of 64×10^{-6} per excitation interval. This means, 1% of the fluorescence count rate is bleached after approximately 150 excitation intervals which is equivalent to 1% bleaching after 9000 s with the typical shutter interval of 60 s. Conclusively, the photobleaching effect can be neglected in the case of the adsorption kinetics recorded with the SAF biosensor.

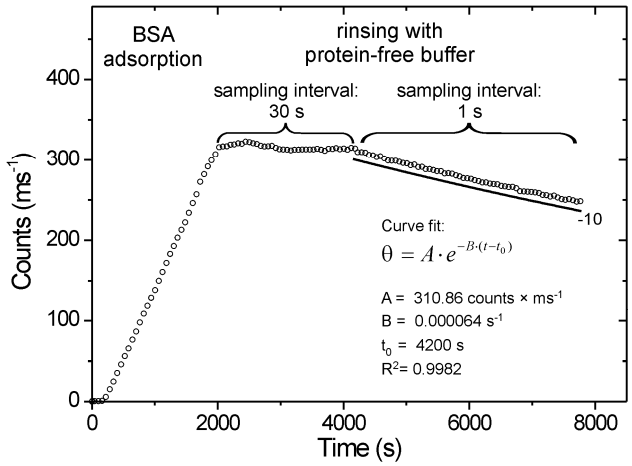

Fig. 4.7. Quantifying the photobleaching rate of the SAF-biosensor for DY-647-labeled proteins.

The optical set-up of the SAF-microscope is different from that of the SAF biosensor. Here, the laser beam is focused on the plane of the water/glass interface to a diameter of ~1 µm allowing for a diffraction limited lateral resolution. A scanning table moves the sample over a certain area with a sampling time of 1 ms per scanned pixel. The laser intensity can be varied between 0.2 µW and 600 µW through gray filters to match the requirements of the specific experiment. Typically, low laser intensities are required for high fluorophore concentrations and high laser intensities for low fluorophore concentrations. In any case, the

typically applied laser power density normalized to the sampling time is higher than the laser power density applied in the SAF-biosensor. For this reason the SAF-microscope was not used for recording quantitative adsorption kinetics.

4.4 Reproducibility of adsorption kinetics

A good reproducibility of experimental data is an essential prerequisite for the investigation of protein adsorption kinetics. Apart from carefully planned sample preparation procedures, the pre-treatment of the interface is the most critical issue affecting reproducibility. Hydrophilic glass substrates were obtained by immersing standard microscope glass coverslips (Menzel) in 0.2% aqueous deconex solution at pH 11 for at least two weeks. During this time soluble components of the upper region of the glass substrate dissolve slowly into the solution. It was noticed that after an equilibration time of two weeks or longer reproducible experimental results were obtained. A similar pre-conditioning time period of one month has been found to be necessary for achieving a stationary state of a glass substrate in a previous study.[184] The reproducibility of DY-647-BSA (Fig. 4.8 A) and DY-647-β-Lg (Fig. 4.8 B) on such a glass substrate treated with the described procedure is demonstrated. For both proteins, two adsorption experiments with varying p*/p – ratios were repeated three times resulting in similar adsorption kinetics that overlap within an acceptable variation of approximately 10%.

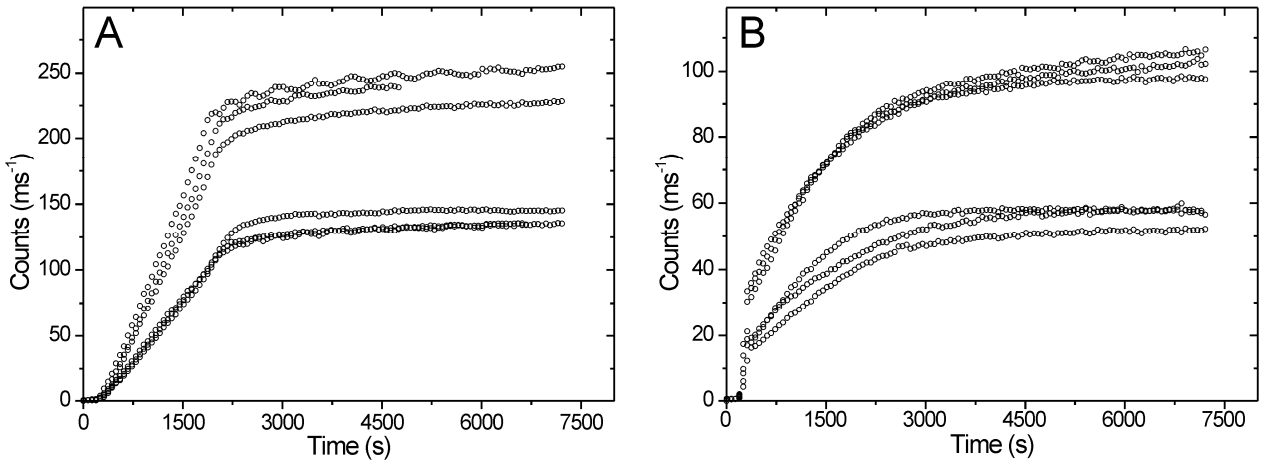

Fig. 4.8. Demonstration of the reproducibility of protein adsorption kinetics.
A) DY-647-BSA (16 nM, in citrate buffer pH 3) at p*/p = 0.5 (upper curves) and p*/p = 0.25 (lower curves).
B) DY-647-β-Lg (0.75 µM, in citrate buffer pH 3) at p*/p = 0.01 (upper curves) and p*/p = 0.005 (lower curves).

4.5 Protein transport to the sorbent surface

Sorbent surfaces act as a sink for adsorbing molecules which leads to a concentration depletion at the immediate vicinity of the surface. This in turn induces a flux of adsorbent towards the surface driven by the concentration gradient. In a flowing cell set-up the concentration of the bulk fluid that is sufficiently apart from the walls is kept constant due to a permanent supply of fresh analyte. In close proximity to the surface, by contrast, there is a thin, quasi stagnant layer of fluid through which molecules can only move via diffusion. The flux across this so called *diffusion boundary layer* or *Prandtl layer* can be calculated from Fick's first law:

$$J = k_{transport} \cdot (c_b - c_s) \tag{4.1}$$

$$k_{transport} = \frac{D}{\delta} \tag{4.2}$$

D: Diffusion coefficient; c_b: concentration in the bulk; c_s: concentration at the surface; δ: thickness of the diffusion boundary layer

Provided that the transport rate constant is significantly higher than the adsorption rate constant ($k_{transport} \gg k_{ads}$), the transport process has no important impact on the adsorption kinetics and can thus be neglected.[61, 77, 107] However, if the transport rate constant is much slower than the adsorption rate constant ($k_{transport} \ll k_{ads}$), the process is called transport limited,[185] that means the observable uptake of adsorbent is as fast as the maximum flux of proteins to the surface. Whereas the adsorption rate constant k_{ads} can be estimated from the experimental adsorption kinetics, the transport rate constant $k_{transport}$ requires an adequate model for the calculation of the boundary layer thickness δ which is dependent on the fluid velocity and viscosity, the diffusion coefficient of the adsorbent, and, most critical, on the flow cell geometry. Due to the difficulty to find an exact description that matched the geometry of the flow cell used in this work (Fig. 4.9 A), the boundary layer thickness is estimated with the help of two models that were developed for similar problems. Firstly, the model suggested by Levich describes the boundary layer thickness of a surface in the form of a plate set in a laminar flow of liquid.[186] This model was successfully applied by Ball et al. to estimate δ at the center of a flow cell with vertical in- and outlets (Fig. 4.9 B).[70]

$$\delta = 3 \cdot \left(\frac{D}{\nu} \right)^{\frac{1}{3}} \cdot \left(\frac{\nu \cdot x}{u} \right)^{\frac{1}{2}} \tag{4.3}$$

v: kinematic viscosity of fluid; *x*: distance from fluid entrance; *u*: fluid velocity

Second, Adamczyk et al. proposed an equation for the estimation of δ in a radial impinging-jet cell at a position directly in the center of the inlet flow (Fig. 4.9, C).[187]

$$\delta = 1.282 \cdot \left(\frac{D}{\alpha \cdot u} \right)^{\frac{1}{3}} \cdot R^{\frac{2}{3}} \tag{4.4}$$

$$\alpha = 1.78 + 0.186 \cdot Re + 0.034 \cdot Re^2 \tag{4.5}$$

$$Re = \frac{R \cdot u}{\nu} \tag{4.6}$$

(*Re*: Reynolds number; *R*: radius of inlet tube)

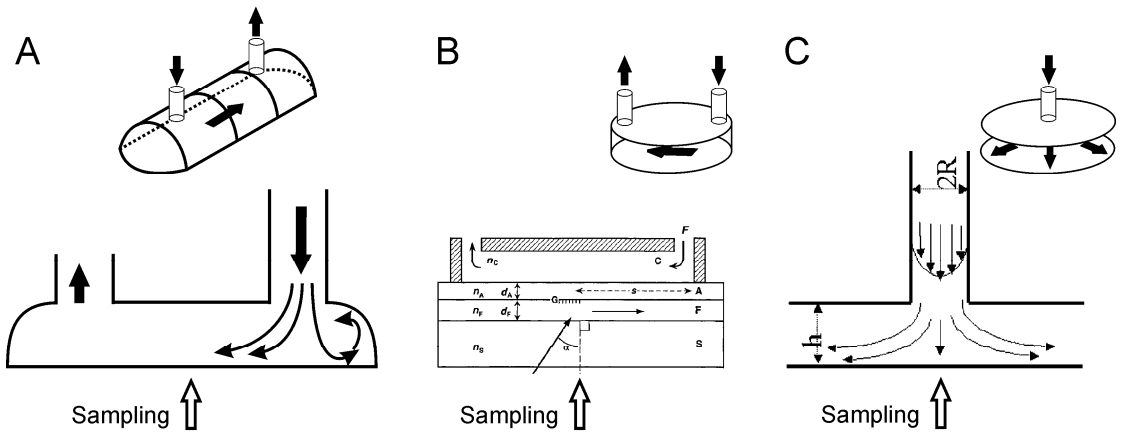

Fig. 4.9. Various flow cell geometries.
A) Geometry of the flow cell used in this work.
B) Geometry of the flow cell used by Ball et al.[70] (Fig. adapted from this reference).
C) Geometry of the flow cell described in Adamczyk et al.[187] (Fig. adapted from this reference).

From intuition it is assumed that these two models describe some sort of limiting cases, that means the reality may be found in between. The boundary layer thickness calculated according to Levich's model is probably closest to that encountered in the flow cell used in this work. As summarized in Table 4.1 the results of these two approaches differ by a factor of almost ten. Such strong differences are also found in the literature where estimated values of δ vary between 20 μm[188] and 230 μm.[70] Using the diffusion coefficients of BSA ($D = 8.5 \times 10^{-7}$ cm^2/s),[189] and β-Lg ($D = 2.7 \times 10^{-6}$ cm^2/s),[190] the transport rate constant of the proteins to the surface can be calculated according to equation (4.2) (results in Table 4.1).

Table 4.1. Values of the boundary layer thickness δ and the transport rate constant $k_{transport}$ determined with Levich's (model 1)[186] and Adamczyk's model (model 2)[187] and experimentally obtained values of the adsorption rate constant k_{ads}.

	δ (estimated) (μm)		$k_{transport}$ (estimated) (cm/s)		k_{ads} (experiment) (cm/s)	
	Model 1	Model 2	Model 1	Model 2	low ionic str.	high ionic str.
BSA	398	50	2.1×10^{-5}	16.9×10^{-5}	1.4×10^{-5} (pH 3; 5 mM ionic strength)	1.1×10^{-5} (pH 3; 50 mM ionic strength)
β-Lg	585	74	4.6×10^{-5}	36.4×10^{-5}		3.1×10^{-5} (pH 3; 50 mM ionic strength)

Comparing the maximum transport rate constant with the adsorption rate constants of BSA and β-Lg found in the kinetic analyses it turns out that the transport rate is in the same order of magnitude as the protein adsorption rates.* To this end the adsorption is certainly influenced by the transport process. However, this does not mean that the adsorption is also transport limited, one rather faces an 'intermediate range'. Experimentally this can be observed when adsorption kinetics are recorded with different flow rates as shown exemplarily for the adsorption of BSA at 5 mM and 50 mM ionic strength conditions (Fig. 4.10). Reducing the pump rate stepwise from 400 μL/s to 100 μL/s, a slight deceleration of the adsorption rate is observed which is in agreement with an increasing boundary layer thickness at decreasing fluid velocities (see equation (4.3) and (4.4)). However, even at slow fluid velocities the adsorption rate still increases during the adsorption as a result of cooperative effects which proves that the adsorption can not be fully transport limited.

* The values for the adsorption rate constants are taken from Chapter 5 and 7.

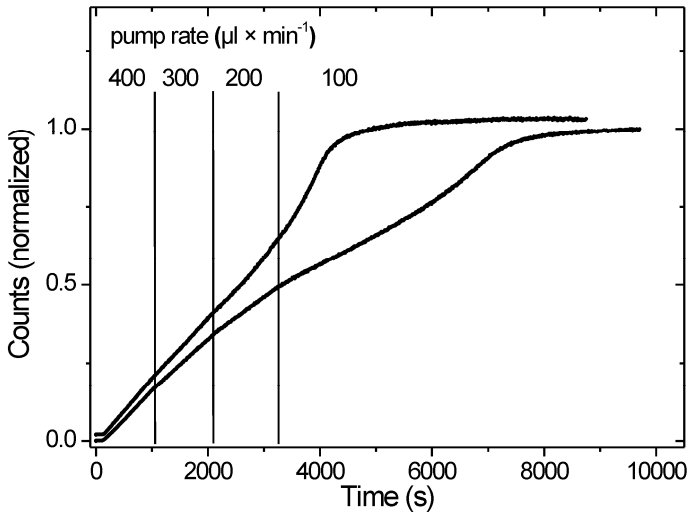

Fig. 4.10. Adsorption of DY-647-BSA on the hydrophilic glass surface at decreasing fluid velocities (c = 50 nM, pH = 3, ionic strength = 5 mM (upper curve) / 50 mM (lower curve)).

Given that the transport process appears to be not fast enough to be negligible, it is worth to evaluate the exact influence on the observable adsorption kinetics with the help of model calculations on the adsorption kinetics of BSA on a hydrophilic glass surface. Therefore, an additional rate equation accounting for the concentration depletion of the protein adjacent to the surface was added to the mathematical model of BSA adsorption.*

$$\frac{\mathrm{d}c_s}{\mathrm{d}t} = \frac{1}{h}\left(k_{transport} \cdot \left(c_b - c_s\right) - \frac{\mathrm{d}\theta}{\mathrm{d}t} \right) \tag{4.7}$$

In this equation the first term $k_{transport} \cdot \left(c_b - c_s\right)$ accounts for the transport towards the surface and the second term $-\mathrm{d}\theta / \mathrm{d}t$ corresponds to the depletion of protein due to adsorption on the surface. To match the dimensions on both sites of equation (4.7) the constant *h* has to be introduced which defines the height of the volume element that is depleted by the adsorption process. The value of *h* has no influence on the surface concentration in the equilibrium state. However, the equilibration time, i.e., the time until c_s is practically constant, is the longer the greater the value of *h*. The volume element in which the surface can attract diffusing proteins is assumed to be no more than a few tens of nanometers due to the fast screening of the electrostatic potential. However, even if *h* is set to 100 nm the equilibration time is very fast (< 1 s) compared to the experimental time scale. A comparison of the surface concentration

* The model is discussed in Chapter 5.

functions $c_s(t)$ resulting from integrating equation (4.7) with that given by the approximate equation (2.7) proposed by Corsel et al.[106] who set $dc_s/dt = 0$ throughout the whole adsorption process revealed practically identical results. Only at very low levels of the transport rate constants the better precision of equation (4.7) becomes relevant.

The extended model thus includes transport to and adsorption at the interface (equation (4.7) plus equations (5.1) - (5.5)) and is compared with the same model that neglects the transport process (equations (5.1) - (5.5)). It turns out that the two models are almost identical with respect to the shape of their kinetic curves and only differ by a certain factor dependent on the ratio between transport and adsorption rate constant (Fig. 4.11). This is understood considering that an equilibrium concentration of proteins establishes at the interface which must be smaller than the concentration in the bulk fluid. As long as the transport of proteins to the surface is not critically slower than the adsorption rate, the protein concentration at the surface is quasi constant such that the model neglecting transport processes equals the model that includes transport only at a lower concentration. This is shown in Fig. 4.11 A where the bulk concentration of the model that neglects transport processes (dashed, red line) was lowered such that it fits the model that includes the transport rate (black line). These model calculations point out that the transport process has a rather small impact on the adsorption kinetics apart from a reduced concentration at the immediate vicinity of the surface. Even if the transport rate is only half as fast as the adsorption rate, the correlation between these two models that do and do not include transport processes ($R^2 = 0.9994$) is better than the typical correlation between model and experimental data ($R^2 \sim 0.9985$).* Thus the accuracy of the experimental set-up is too weak to differentiate between them.

Fig. 4.11 B allows a more general view on the influence of transport processes on different kinetic curves. The three kinetics belonging to the same set of parameters (k_1^{on}, k_2^{on}) but different transport rate constants exhibit qualitatively equivalent shapes and almost exclusively differ by a certain factor. Thus, conclusions drawn from the shape of kinetic adsorption curves and from relations between them are not affected by transport processes.

* R^2-values characterizing the correlation between model and experimental adsorption kinetics are listed in Table 5.1 - Table 5.4.

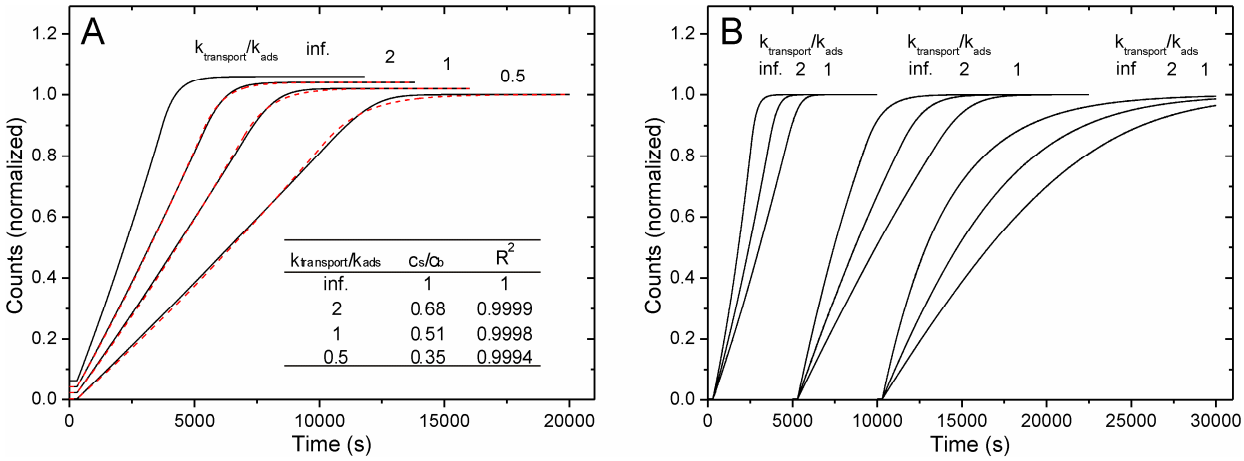

Fig. 4.11. Model calculations on BSA.
A) Comparison of the models including (black, solid lines) and neglecting (red, dashed lines) transport processes. The bulk concentration of the model that does not include transport processes was varied to 'fit' the model that does include transport at varying rates.
B) General view on the influence that the transport rate has on the shape of adsorption kinetics. Three sets of different curve shapes, upwards concave ($k_2^{on} = 2 \cdot k_1^{on}$, left), almost linear ($k_2^{on} = 0.5 \cdot k_1^{on}$, middle), and exponential ($k_2^{on} = 0$, right) are plotted at decreasing transport rates. The first curve from the left of each set presents the limit of infinitely fast transport, i.e., the case in which transport processes have no influence.

4.6 Conclusion

The results and conclusions that will be presented in the following chapters of this dissertation would suffer from a lack of legitimacy without a proper validation of the used experimental methods. It has been demonstrated that the fluorescent dye DY-647 is ideally suited as marker molecule for protein adsorption kinetics. This fluorophore hardly adsorbs to hydrophilic surfaces which are predominantly used herein, shows a very good stability towards varying pH and ionic strength conditions, and exhibits a negligible photobleaching rate in the given set-up. Further, a series of experiments based on varying label ratios of the protein solutions has confirmed that the marker molecules do not interfere significantly with the proteins' surface affinity. A critical examination of the protein transport process to the sorbent surface has revealed that the transport influences the protein adsorption rate mainly through reducing the effective bulk concentration above the surface. However, model calculations have shown that the characteristic shapes of the kinetic curves remain unaffected justifying the conclusion drawn from the kinetics. Together with an excellent reproducibility the experimental data presented in this dissertation are considered to be of high accuracy and, most importantly, to reflect the true behavior of the native, i.e., unlabeled proteins.

5 Self-Organization and Cooperativity during the Adsorption of Proteins*

Cooperativity is a frequently observed effect which is believed to generally play a major role in protein adsorption events.[63, 64, 69, 70] Despite a vast number of studies in this field a unique opinion describing protein adsorption mechanism including cooperativity is still lacking as most concepts concentrate only on specific experimental observations like the formation of two-dimensional surface aggregates,[64, 65, 67] sigmoidal adsorption isotherms,[4] or characteristic adsorption kinetics.[71, 72] Concerning the adsorption kinetics it is now widely accepted that a clear sign for the presence of a cooperative adsorption process is the enhancement of protein adsorption due to other pre-adsorbed proteins. This necessarily leads to partially constant or even increasing adsorption rates.[63, 69, 70] In the following chapter such adsorption kinetics are encountered during the adsorption of the two model proteins BSA and Fib. A consistent mechanistic model is developed which can explain not only the kinetic behavior but also a characteristic observable surface organization.

5.1 Protein adsorption kinetics of BSA at pH 3 on a hydrophilic surface

To acquire an experimental basis for the study of cooperative effects the adsorption behavior of BSA on a bare, hydrophilic glass surface in citrate buffer at pH 3 was comprehensively investigated. BSA is the most abundant plasma protein, exhibits a heart-like shape, and has a molecular weight of approximately 67 kDa. BSA has become the most important blocking and stabilization agent in assay technologies which renders it to a perfect model protein for the present study. Under the chosen condition it is net positively charged whereas the target glass surface is negatively charged.[191] The adsorption kinetics of BSA were measured by

* The results of this chapter were published in: M. Rabe, D. Verdes, J. Zimmermann and S. Seeger, *J. Phys. Chem. B,* 2008, **112**, 13971-13980.

recording the fluorescence intensity increase at the surface over a time period of up to 6 hours using the SAF surface sensor. As shown exemplarily in Fig. 5.1 A (circles) the adsorption kinetics do not follow an exponential-like adsorption behavior. Consequently, classical adsorption models like the simple Langmuir adsorption theory fail to describe the experimental data. Solid blue and solid green lines in Fig. 5.1 represent mono- and bi-exponential adsorption curves which correspond to a Langmuir adsorption pathway[192, 193] and to an overlap of two distinct Langmuir adsorption pathways, respectively.[108, 194] To this end it is clear that a more complex model is needed to describe the experimental data. Inspiration is obtained by the theoretical work from Minton.[67] As can be inferred from the red dashed line in Fig. 5.1 A this model approaches the experimental data much better than models based on the Langmuir theory. However, if the adsorption rate is plotted as rate-coverage-plot (the adsorption rate as a function of the normalized surface coverage, Fig. 5.1 B), the fit turns out to be unsatisfying. For this reason a new model needs to be developed that accurately fits the experimental data.

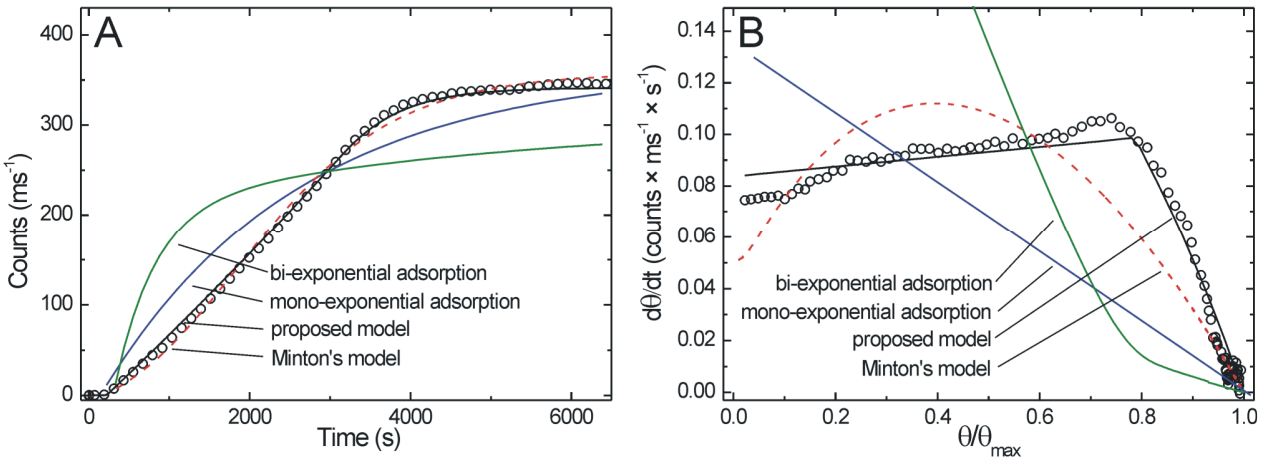

Fig. 5.1. Circles represent the adsorption behavior of fluorescently labeled BSA (16 nM) in citrate buffer (pH 3, 50 mM). The data are only poorly fitted by a mono-exponential function, i.e., the Langmuir model (blue line) or by a bi-exponential function, i.e., the overlap of two distinct Langmuir models (green line). The kinetic model proposed by Minton[67] (dashed red line) fits the data much better but not as satisfyingly as the model which is developed in this work (solid black line). To better highlight the difference between the models all time-integrated kinetics (shown in A) are re-plotted as rate-coverage plots (shown in B).

To provide sufficient experimental data that support such a model, adsorption kinetics of BSA were recorded at different bulk concentrations and in different ionic strength conditions. Fig. 5.2 shows the adsorption behavior in citrate buffer (pH 3) at 5 mM (A) and 50 mM (B) ionic strength. Both plots contain the kinetic data recorded at bulk protein concentrations of

4 nM, 8 nM, and 16 nM, respectively. As expected, the initial adsorption rates are proportional to the protein concentrations used. Also, the saturation levels at a given ionic strength are the same for all three protein concentrations. This is a clear indication that a monolayer coverage is formed in the saturation stage which is in agreement with other experimental studies on BSA.[42, 50, 195] Rinsing of adsorbed proteins with protein-free buffer yielded no measurable desorption at any point indicating that the adsorption process is essentially irreversible under the given conditions. The most important observation is that the adsorption kinetics clearly differ from an exponential-like growth that is characteristic for conventional concepts like the Langmuir-type adsorption model. Here, the adsorption rate is apparently not proportional to the available surface area but stays almost constant until about 80% of the maximum coverage is reached. In other words, it seems like adsorbing proteins do not sense the shrinkage of free adsorption sites until the surface is almost filled. More precisely, the rate-coverage plots even reveal that the adsorption rate increases within the first stage of adsorption (Fig. 5.3 A and B). The key feature of the adsorption kinetics of BSA at the given conditions, that can be deducted from this representation, is a linearly increasing adsorption rate up to a high surface coverage, followed by a sharp decline. The increasing adsorption rates imply that adsorbed proteins do not hinder but even promote further protein adsorption. From these observations it is clear that cooperative effects must contribute to the adsorption process.[63, 69, 70]

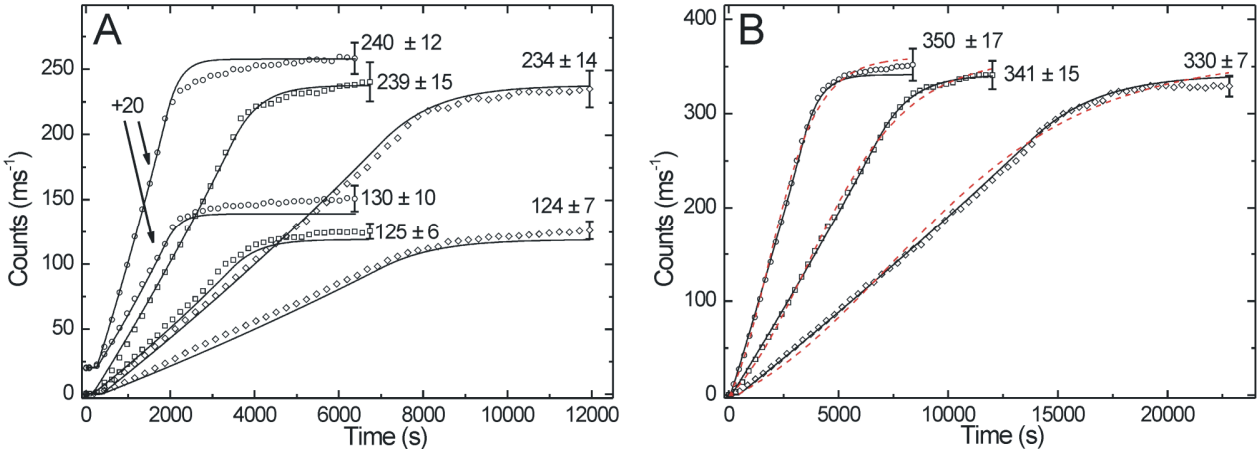

Fig. 5.2. A) Adsorption kinetics of BSA at bulk concentrations of 16 nM (○), 8 nM (□), and 4 nM (◊) in citrate buffer at pH 3 at low ionic strength (5 mM). The three lower curves refer to identical measurements in which only half as much proteins were labeled as in the upper curves (p*/p – ratio = 12.5%). The solid lines refer to the best fit of the model proposed in this work.
B) Adsorption kinetics of BSA at bulk concentrations of 16 nM (○), 8 nM (□), and 4 nM (◊) in citrate buffer at pH 3 at high ionic strength (50 mM). The solid lines refer to the best fit of the model proposed in this work; the red dashed lines refer to the best fit of a model based on the work of Minton.[67]

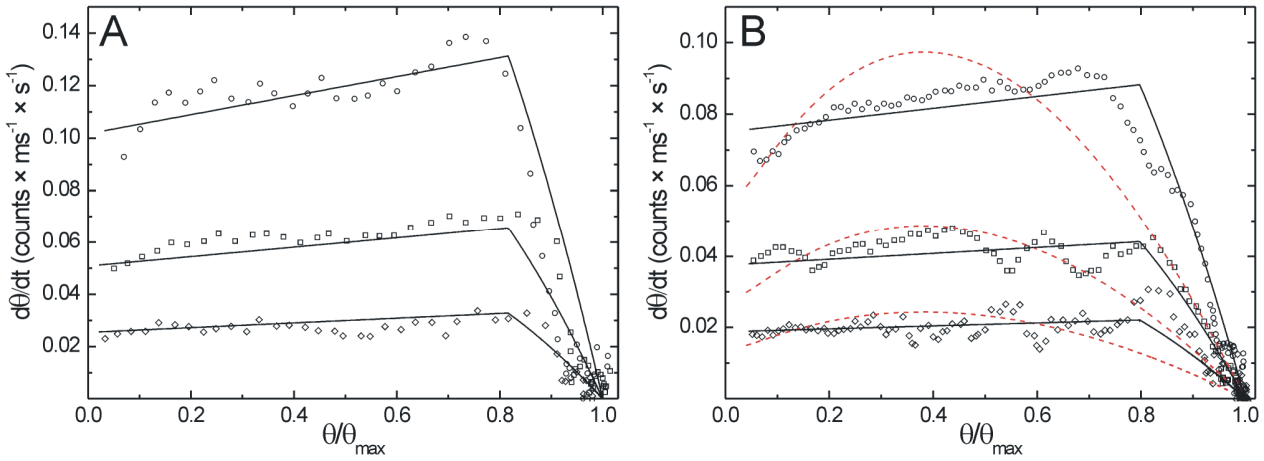

Fig. 5.3. A) Rate-coverage plots of the adsorption kinetics of BSA at bulk concentrations of 16 nM (○), 8 nM (□), and 4 nM (◊) in citrate buffer at pH 3 at low ionic strength (5 mM). The solid lines refer to the best fit of the model proposed in this work.
B) Rate-coverage plots of the adsorption kinetics of BSA at bulk concentrations of 16 nM (○), 8 nM (□), and 4 nM (◊) in citrate buffer at pH 3 at high ionic strength (50 mM). The solid lines refer to the best fit of the model proposed in this work; the red dashed lines refer to the best fit of a model based on the work of Minton.[67]

Comparing the adsorption kinetics of BSA at low ionic strength (Fig. 5.2 A and Fig. 5.3 A) and at high ionic strength (Fig. 5.2 B and Fig. 5.3 B) it is noticed that there are two quantitative differences although they look qualitatively very similar. First, the saturation level is about 30% lower at 5 mM ionic strength than at 50 mM ionic strength and second of all, the initial adsorption rates are much higher at low ionic strength. According to equation (2.2) the reduction of the buffer ionic strength from 50 mM to 5 mM increases the Debye length from 1.4 nm to 4.3 nm, i.e., the protein's electrostatic potential is less efficiently shielded.[29] As a consequence, electrostatic repulsion between the charged molecules is more pronounced at low ionic strength. This forces the proteins to adsorb onto the surface at greater distances to each other, leading to a lower surface density at saturation. The difference in the adsorption rates, on the other hand, is explained by the attractive electrostatic interactions between the negatively charged surface and net positively charged proteins. A stronger shielding of surface and protein charges at high ionic strength naturally reduces the adsorption rate.[31]

5.2 Modeling

The observed non-exponential like adsorption kinetics are explained by a preferential adsorption of proteins on a surface which already contains a certain amount of adsorbed proteins. In this respect, the influence that adsorbed proteins have on the adsorption behavior of the approaching proteins is referred to as cooperative effects. If these effects just compensate for the decelerating effect of surface occupancy, the resulting adsorption kinetics appear to be linear. In the case of even stronger cooperative effects, a slightly upwards concave shape of the adsorption kinetics is observed (see Fig. 5.2). Clearly, a consistent mathematical description of the observations presented in Fig. 5.1 - Fig. 5.3 must include the issue of cooperativity. As mentioned before, the kinetic model proposed by Minton is one approach because it describes the protein layer build-up through a cooperative growth of two-dimensional surface clusters.[67, 196] In this framework, proteins are either allowed to adsorb as individual species on the surface which can then diffuse and aggregate to a pre-existing cluster or to directly deposit at the edge of a two-dimensional surface cluster via a *piggyback*-pathway. The model was successfully applied to simulate the adsorption kinetics and the isotherm of the protein Ezrin to model membranes.[64] Herein, a version of this model was tested, that neglects surface diffusion and size exclusion effects because those have a small influence on positive cooperativity as encountered in the present study. Least-squares fits of the Minton model to the measured adsorption kinetics are presented as red dashed lines in Fig. 5.2 B and Fig. 5.3 B. Despite an overall qualitative agreement, the model does not adequately describe the experimental data measured in this study. In particular, it does not reflect the linearly increasing rate in the beginning and the abrupt decrease at a certain coverage level. This disagreement is predominantly obvious, when the rate-coverage plots of the experimental and calculated data are compared (Fig. 5.3 B). As a first conclusion from this discrepancy the concept of growing two-dimensional surface clusters for the studied systems is precluded because in contrast to the cluster concept the observable adsorption rate is a linear function of the surface coverage. Additionally, the maximum coverage of BSA at pH 3 is too low to be consistent with a surface covered with two-dimensional clusters. From quantitative measurements it is known that the saturation coverage of BSA at pH 3 is by a factor of five lower than the maximum saturation limit that is obtained at pH = pI because charged proteins generally tend to adsorb apart from each other.[42] Consequently, it is suggested that under these conditions adsorbed proteins form a layer of rather loosely

distributed molecules instead of surface clusters in which proteins would be densely ordered. Nevertheless, the distance between adsorbed proteins must be close enough such that adsorbing proteins sense the attractive influence of the nearest neighbors. In this concept the cooperative attractive forces do not accumulate when a region becomes crowded as it is the case for surface clusters whose attraction towards adsorbing proteins scales up with their size. Consequently, it is proposed that bulk proteins coming close to surface bound proteins are 'guided' to free binding sites in their vicinity but not as close as in a surface cluster. The protein density in a certain region hence determines the probability with which this cooperative adsorption pathway takes place. Bulk proteins that reach the surface in a larger distance from other adsorbed proteins are considered to adsorb without further influence through the classical Langmuir-type adsorption pathway. Thus, the overlapping of both, the Langmuir type pathway (pathway 1) and the cooperative adsorption pathway (pathway 2), leads to the experimentally observed adsorption kinetics. Fig. 5.4 illustrates schematically this adsorption mechanism.

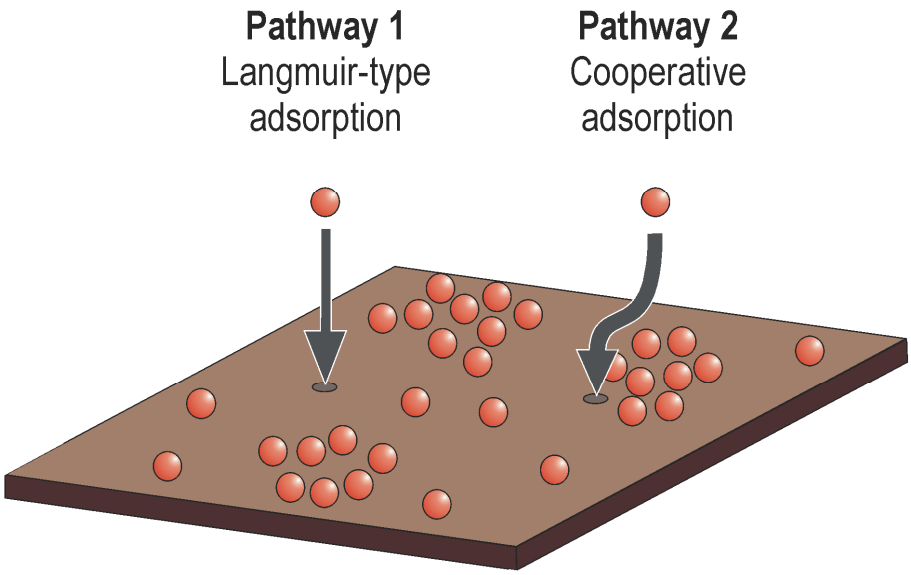

Fig. 5.4. Schematic representation of the proposed model. Proteins can either adsorb at any available binding site in an unoccupied region (pathway 1: Langmuir-type adsorption) or in close proximity to pre-adsorbed proteins (pathway 2: cooperative adsorption).

In the following the mechanism is presented by a mathematical description through rate equations. The description of pathway 1 is given by:

$$\frac{\mathrm{d}\theta_1}{\mathrm{d}t} = k_1^{on} \cdot c \cdot \Phi_1 - k_1^{off} \cdot \theta_1 \tag{5.1}$$

$$\Phi_1 = 1 - \frac{\theta}{\theta_{max}} \tag{5.2}$$

The description of the additional cooperative adsorption pathway (indicated by the subscript 2) is as follows:

$$\frac{\mathrm{d}\theta_2}{\mathrm{d}t} = k_2^{on} \cdot c \cdot \Phi_2 \cdot \frac{\theta}{\theta_{max}} - k_2^{off} \cdot \theta_2 \tag{5.3}$$

$$\Phi_2 = \begin{cases} 1 & , \quad \dfrac{\theta}{\theta_{max}} \le \alpha \\ \dfrac{1}{1-\alpha} \cdot \left(1 - \dfrac{\theta}{\theta_{max}} \right) & , \quad \dfrac{\theta}{\theta_{max}} > \alpha \end{cases} \tag{5.4}$$

In these equations θ_1, θ_2 denote the fraction of surface proteins adsorbed via the Langmuir-type or the cooperative adsorption pathway, θ denotes the total surface coverage, and θ_{max} is the experimentally observed maximum coverage. k_1^{on}, k_2^{on} and k_1^{off}, k_2^{off} are the adsorption and desorption rate constants for the corresponding pathways, c is the bulk protein concentration, and Φ_1, Φ_2 refer to the available surface function. As will be discussed in more detail below, the parameter α defines the coverage limit at which the cooperative adsorption pathway changes from the regime in which the overall coverage has no influence on the adsorption rate into the regime where the increasing coverage slows down the adsorption rate. In equation (5.4) the factor $(1-\alpha)^{-1}$ has to be included in the second part of the surface function to avoid a mathematical point of discontinuity at $\theta = \alpha \cdot \theta_{max}$. Summing up the time-integrated adsorption rates of the two pathways gives the total surface coverage.

$$\theta = \theta_1 + \theta_2 \tag{5.5}$$

To account for the cooperative effects in the second pathway the cooperative adsorption rate is set proportional to the normalized surface coverage (θ/θ_{max}). Mechanistically this ensures that the probability of a bulk protein to adsorb close to another pre-adsorbed protein increases with the increasing surface coverage. However, the cooperative adsorption rate constant k_2^{on} is independent of the number of neighboring proteins. As discussed before the intermolecular distances between adsorbed proteins are larger than in a surface cluster and hence the accumulation of attractive cooperative forces is weak when proteins assemble in a certain region.

An important effect accompanying cooperative adsorption is that approaching bulk proteins do not adsorb at random positions but are directed to favorable adsorption areas in the vicinity of pre-adsorbed proteins. This is explained by a kind of electrostatic self-organization mediated by lateral interactions from neighboring surface bound proteins.[70-72] As a consequence, the adsorption rate of cooperatively adsorbing proteins does not decrease with increasing occupancy at low to moderate surface densities which causes the observed linear adsorption kinetics (see Fig. 5.2). In order to model the sudden decrease of the adsorption rate at a fixed adsorption stage (see Fig. 5.3) a coverage limit ($\alpha \cdot \theta_{max}$) is defined up to which the available surface function Φ_2 is set constant ($\Phi_2 = 1$). Only above this limit the surface function is set proportional to the number of free binding sites.

Thus, the complete model defined by equations (5.1) - (5.5) comprises the adsorption of proteins by the Langmuir-type adsorption pathway on any available binding site and an additional cooperative adsorption pathway which is only encountered in the vicinity of pre-adsorbed proteins. In this respect k_1^{on} is a measure for the general probability of proteins to adsorb on the surface whereas k_2^{on} corresponds to the additional cooperative adsorption probability that is encountered in the vicinity of other surface bound proteins. Because of the overlap of Langmuir-type adsorption and cooperative adsorption the sum of k_1^{on} and k_2^{on} can be considered a measure for the total probability of proteins to adsorb in the vicinity of other surface bound proteins. In mathematical terms, the two rate constants k_1^{on} and k_2^{on} are most easily understood by regarding an empty position in an unoccupied region and an empty position in the vicinity of pre-adsorbed proteins. The probability by which a protein adsorbs to the position within the empty region is given by:

$$p^* = k_1^{on} \cdot c \tag{5.6}$$

Analogously, the probability by which a protein adsorbs to the position in the vicinity of pre-adsorbed proteins is given by:

$$p^{**} = \left(k_1^{on} + k_2^{on}\right) \cdot c \tag{5.7}$$

From equations (5.6) and (5.7) it follows directly that the relation of the rate constants $(k_1^{on} + k_2^{on}) / k_1^{on}$ describes by which factor the probability of a protein to adsorb in the vicinity of pre-adsorbed proteins is increased over the probability to adsorb at any random position.

The parameter α in equation (5.4) determines the surface coverage level above which the adsorption rate abruptly starts to decline towards zero. In the first stage of the adsorption the decreasing rate of the Langmuir-type adsorption pathway is overlapped by the increasing rate of the cooperative adsorption pathway. As discussed before, cooperatively adsorbing proteins are guided to preferential adsorption areas close to pre-adsorbed proteins and are hence not affected by the shrinkage of unoccupied surface. Naturally, this mechanism breaks down when the surface becomes strongly crowded such that not every bulk protein diffusing close to other adsorbed proteins is guided to a free adsorption area. In this respect, α points to the coverage limit ($\alpha \cdot \theta_{max}$) at which the cooperative adsorption rate starts to decrease. Phenomenologically, a large value of α can be explained by attractive forces ranging over a rather long distance caused by surface bound proteins. Then, the probability that a bulk protein is guided to a free adsorption area in the vicinity of adsorbed proteins is still high at increased coverage levels. Small values of α, on the other hand, indicate attractive forces that range only over short distances. From the experimental data it is evident that the adsorption rate undergoes a sharp transition between the first stage in which the available surface is irrelevant ($\theta \leq \alpha \cdot \theta_{max}$) and the second stage in which the available surface is relevant ($\theta > \alpha \cdot \theta_{max}$) (see Fig. 5.3). Hence, from an experimental point of view it is justified to approximate this behavior using a step-like transition between these two stages in the proposed model as realized by the definition of Φ_2 equation (5.2). Naturally, the step function can only represent a simplified description of the real transition between the two stages. However, a mathematically exact treatment of the protein adsorption behavior under consideration of the micro-environment of each adsorbing molecule would extend the number of rate equations to infinity.[67]

To quantitatively evaluate the parameters describing the Langmuir-type adsorption pathway (k_1^{on}) and the cooperative adsorption pathway (k_2^{on} , α) the proposed model was fitted to the experimentally acquired kinetics of BSA. Since all adsorption kinetics of BSA measured at pH 3 were found to be irreversible the off-rate constants k_1^{off} and k_2^{off} were set to zero leading to the following expression for the total rate of the irreversible adsorption:

$$\frac{\mathrm{d}\theta^{irr}}{\mathrm{d}t} = \begin{cases} m \cdot \dfrac{\theta}{\theta_{max}} + n \ , & \dfrac{\theta}{\theta_{max}} \le \alpha \\ -\dfrac{1}{1-\alpha} \cdot (m+n) \cdot \left(\dfrac{\theta}{\theta_{max}} \right)^2 + \left(\dfrac{1}{1-\alpha} \cdot m + \dfrac{\alpha}{1-\alpha} \cdot n \right) \cdot \dfrac{\theta}{\theta_{max}} + n \ , & \dfrac{\theta}{\theta_{max}} > \alpha \end{cases} \tag{5.8}$$

$$m = \left(k_2^{on} - k_1^{on} \right) \cdot c \tag{5.9}$$

$$n = k_1^{on} \cdot c \tag{5.10}$$

The function given by equations (5.8) - (5.10) is composed of a linear part characterized by the slope *m* and the intercept *n* and a quadratic function whose parameters are fixed by *m*, *n*, and *α*. To find appropriate parameters for the proposed model the maximum coverage (θ_{max}) of each data set was determined as the final saturation limit of the respective adsorption curve. The count rates of the plateaus of the kinetics measured at three different bulk protein concentrations were therefore averaged and used as maximum surface coverages. Subsequently, the derivations of the adsorption kinetics were calculated and plotted as functions of the normalized surface coverage θ / θ_{max}, i.e., as rate-coverage plots. The function defined by equation (5.8) was then fitted to all rate-coverage plots yielding estimated values for the three parameters α, k_1^{on}, and k_2^{on} (Table 5.1). For the three curves obtained in one system but at different bulk protein concentrations a global fit was performed ensuring that all parameters except the given concentration are indifferent. Finally, the estimated parameters were used to numerically integrate the set of rate equations given by equations (5.1) - (5.5) leading to the calculated adsorption kinetics presented as solid lines in Fig. 5.2 and Fig. 5.3. To evaluate the correlation between experimental data and calculated kinetics the coefficient of determination R^2 for each data set is added to Table 5.1. The obvious agreement between experiment and model (most R^2 – values given in Table 5.1 are above 0.990) highlights the validity of the overlap of Langmuir-type adsorption and

cooperative adsorption. It confirms in particular that an accumulation of cooperative forces plays no important role which is a clear indication that two-dimensional surface clusters do not exist in the studied systems. Instead the model suggests a layer of more loosely distributed proteins with a certain degree of self-organization. This means that one fraction of all adsorbed proteins has been guided to preferential adsorption areas due to cooperative effects whereas the other fraction has adsorbed on random surface positions.

Table 5.1. Estimated parameters for BSA adsorption in citric buffer at pH 3.

protein conc. (10^{-9} M)	ionic strength (10^{-3} M)	θ_{max} (counts ms^{-1})	k_1^{on} (10^6 counts ms^{-1} M^{-1} s^{-1})	k_2^{on} (10^6 counts ms^{-1} M^{-1} s^{-1})	$\frac{k_1^{on}+k_2^{on}}{k_1^{on}}$	α	R^2	Plot
16	5	238 ± 14	6.35 ± 0.26	8.63 ± 0.70	2.36	0.82 ± 0.09	0.9503	Fig. 5.2 A, Fig. 5.3 A
8	5	238 ± 14	6.35 ± 0.26	8.63 ± 0.70	2.36	0.82 ± 0.09	0.9987	Fig. 5.2 A, Fig. 5.3 A
4	5	238 ± 14	6.35 ± 0.26	8.63 ± 0.70	2.36	0.82 ± 0.09	0.9985	Fig. 5.2 A, Fig. 5.3 A
16	50	340 ± 13	4.69 ± 0.50	5.73 ± 0.69	2.22	0.80 ± 0.07	0.9985	Fig. 5.2 B, Fig. 5.3 B
8	50	340 ± 13	4.69 ± 0.50	5.73 ± 0.69	2.22	0.80 ± 0.07	0.9995	Fig. 5.2 B, Fig. 5.3 B
4	50	340 ± 13	4.69 ± 0.50	5.73 ± 0.69	2.22	0.80 ± 0.07	0.9987	Fig. 5.2 B, Fig. 5.3 B

5.3 Cooperative adsorption of BSA at pH 3 on a hydrophobic surface

An equivalent adsorption experiment as shown in Fig. 5.2 and Fig. 5.3 has been repeated on a hydrophobic model surface (Fig. 5.5 and Fig. 5.6). Such a hydrophobic surface was obtained through coating a clean glass coverslip with a C18–chain silane monolayer. Similar observations as made on the hydrophilic surface were found. At low ionic strength (Fig. 5.5 A and Fig. 5.6 A) the overall adsorption rate is higher and the saturation coverage is lower than at high ionic strength. In particular it is noticed that the cooperative adsorption rate constant k_2^{on} is increased at lower ionic strength which supports the conclusion that attractive cooperative forces are induced by the electrostatic field of the adsorbing proteins. Comparing the cooperative model (solid lines) with the experimental data (circles) in Fig. 5.5 and Fig. 5.6 reveals a satisfying correlation (most R^2 – values are higher than 0.995). It is noteworthy that hydrophobic surfaces generally exhibit stronger surface diffusion rates of adsorbed proteins.[135, 197] This effect is not implemented into the model which may explain that the curve fits are slightly worse than in the case of protein adsorption on a hydrophilic surface.

Nevertheless, the validity of the proposed model not only on hydrophilic but also on hydrophobic surfaces is concluded from this experiment. All estimated parameters found for BSA adsorption on the hydrophobic surface are summarized in Table 5.2.

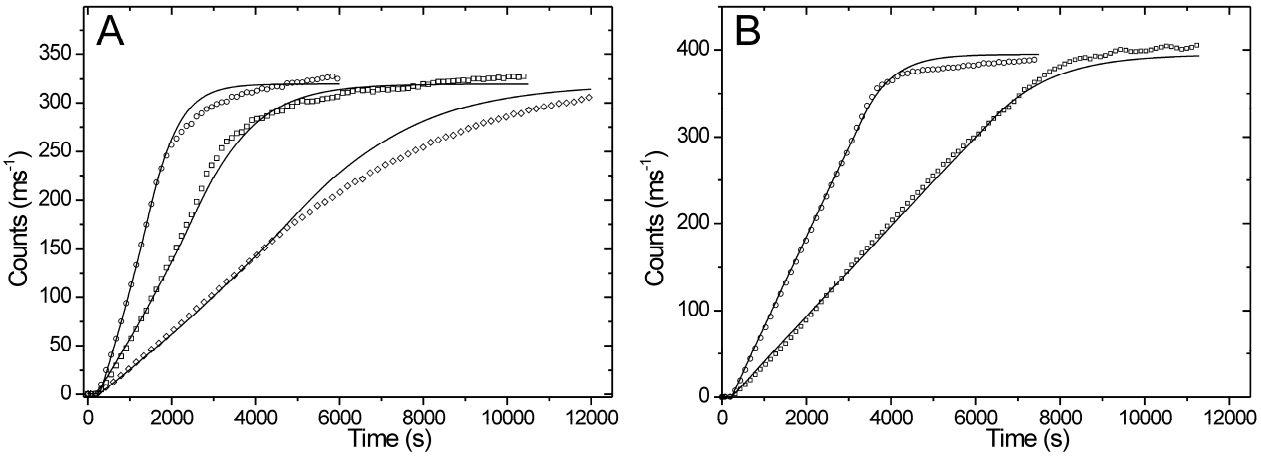

Fig. 5.5. Adsorption kinetics of BSA at bulk concentrations of 16 nM (○), 8 nM (□), and 4 nM (◊) in citrate buffer at pH 3 on a hydrophobic, OTS coated surface. The solid lines refer to the best fit of the model proposed in this work. The ionic strength was set to 5 mM (A) and 50 mM (B).

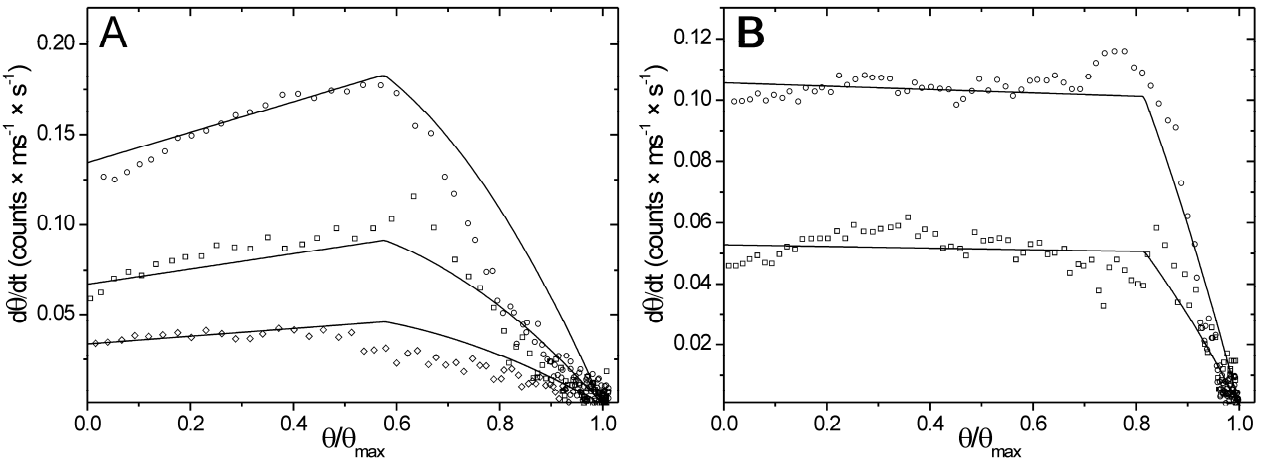

Fig. 5.6. Rate-coverage plots of the adsorption kinetics of BSA presented in Fig. 5.5. The solid lines refer to the best fit of the model proposed in this work. (A) 5 mM ionic strength; (B) 50 mM ionic strength.

Table 5.2. Estimated parameters for BSA adsorption in citric buffer at pH 3 on OTS.

protein conc. (10^{-9} M)	ionic strength (10^{-3} M)	θ_{max} (counts ms^{-1})	k_1^{on} (10^6 counts ms^{-1} M^{-1} s^{-1})	k_2^{on} (10^6 counts ms^{-1} M^{-1} s^{-1})	$\frac{k_1^{on}+k_2^{on}}{k_1^{on}}$	α	R^2	Plot
16	5	320 ± 9	8.39 ± 0.47	14.01 ± 0.24	2.67	0.58 ± 0.08	0.9955	Fig. 5.5 A, Fig. 5.6 A
8	5	320 ± 9	8.39 ± 0.47	14.01 ± 0.24	2.67	0.58 ± 0.08	0.9967	Fig. 5.5 A, Fig. 5.6 A
4	5	320 ± 9	8.39 ± 0.47	14.01 ± 0.24	2.67	0.58 ± 0.08	0.9751	Fig. 5.5 A, Fig. 5.6 A
16	50	395 ± 11	6.61 ± 0.43	6.35 ± 0.84	1.96	0.82 ± 0.05	0.9977	Fig. 5.5 B, Fig. 5.6 B
8	50	395 ± 11	6.61 ± 0.43	6.35 ± 0.84	1.96	0.82 ± 0.05	0.9977	Fig. 5.5 B, Fig. 5.6 B

5.4 In situ scan images of BSA adsorption at pH 3

To further support the microscopic interpretation of the proposed model, surface images of fluorescently labeled BSA adsorption were recorded by scanning ~4.5 µm × 4.5 µm surface areas using the SAF microscope. The adsorption process was monitored using a constant bulk protein concentration of 8 nM. Fig. 5.7 presents fluorescence intensity images that illustrate the density distribution of BSA on hydrophilic glass at increasing adsorption times. All images were subjected to a nearest-neighbor averaging prior to plotting and further analysis. Surface images at low (5 mM, left column) and high (50 mM, right column) ionic strength conditions are shown. The average coverage level ranges between 10% and 60% of the saturation limit. The images clearly show that proteins do not adsorb in a uniform layer under these conditions. Instead, an inhomogeneous distribution on the surface, comprising regions of high and low protein density, is observed. Furthermore, initial patches of high density retain a relatively high protein density throughout the adsorption process, i.e., density differences are not balanced out. The profile plots underneath the scan images, displaying the evolution of the protein density along the marked lines in Fig. 5.7, emphasize this observation. This is consistent with a preferential adsorption of proteins in the vicinity of other pre-adsorbed molecules. The probability by which proteins adsorb in close proximity to pre-adsorbed proteins is by a factor of more than two higher than the probability to adsorb in an unoccupied region (see $(k_1^{on}+k_2^{on})/k_1^{on}$ values in Table 5.1). Thus the reduced number of available binding sites in regions of high protein occupancy is overcompensated by an increased adsorption probability in the circumference of adsorbed proteins. Consequently, variations in the protein density are not balanced out. The emergence of density fluctuations is

a consequence of the cooperative adsorption mechanism as will be discussed below. However, it can not be excluded that surface inhomogeneities inherent to the glass coverslip also contribute to initial density variations.[127, 198] Naturally, an overlap of two or more distinct Langmuir adsorption pathways on surface regions of different protein affinity would result in similar intensity distributions. However, this scenario is inconsistent with the observed adsorption kinetics (see Fig. 5.1, green line) and can hence be excluded.

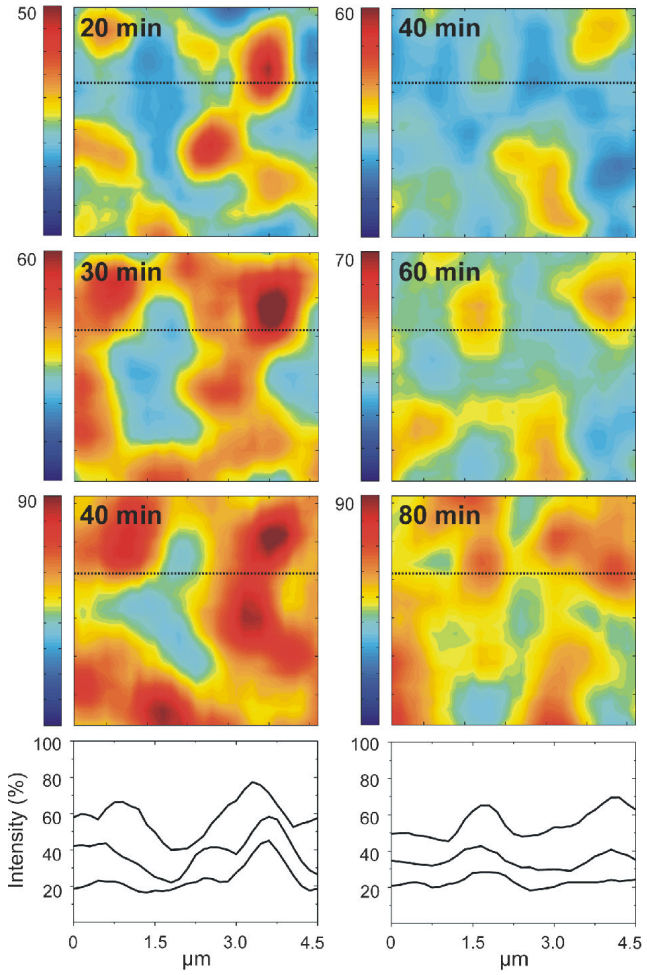

Fig. 5.7. Surface scan images recorded at different stages during the adsorption of BSA (8 nM) in citrate buffer (pH 3) at 5 mM ionic strength (left column) and 50 mM ionic strength (right column). Red color indicates patches of higher protein densities; blue color indicates regions of lower protein density. The scale of each scan image is adapted to its maximum intensity values. An intensity of 100% refers to the saturation coverage. The profile plots underneath the images show the evolution of the fluorescence intensity along the cross sections marked by the dotted lines.

5.5 Cooperative adsorption of BSA at higher pH

To evaluate if the proposed adsorption mechanism is also valid in higher pH environments, adsorption kinetics were recorded for BSA in citrate buffer (50 mM) at pH 4.85, 6.0, and 7.0, respectively (Fig. 5.8 A and B). The adsorption kinetics at different pH differ strikingly in terms of curve shape, initial adsorption rate, and saturation limit from those acquired at pH 3. Additionally, rinsing experiments revealed, that the adsorption becomes reversible at higher pH environments. To allow for the desorption of adsorbed proteins equation (5.8) is extended to:

$$\frac{\mathrm{d}\theta^{rev}}{\mathrm{d}t} = \frac{\mathrm{d}\theta^{irr}}{\mathrm{d}t} - k^{off} \cdot \theta \tag{5.11}$$

Herein the two off-rate constants k_1^{off}, k_2^{off} were set equal for simplification. Due to this approximation, the fitting procedure explained above is still valid once the off-rate constant k^{off} has been determined separately by fitting the desorption curve to a mono-exponential decay.[199]

$$\theta(t) = (\theta_0 - \theta_\infty) \cdot e^{-k_{off} \cdot (t - t_0)} + \theta_\infty \tag{5.12}$$

θ_0 and θ_∞ denote the surface coverages at the onset of rinsing and after long desorption time, t_0 is the point in time when rinsing is started. Of course, θ_{max} is always higher than the observable equilibrium level in the case of reversible adsorption and is therefore only indirectly accessible from the adsorption kinetics. An efficient way to determine all parameters in these cases is to choose initial values for the parameters α, k_1^{on}, k_2^{on} and to numerically optimize θ_{max} by time-integrating the extended model (equation (5.11)). Subsequently, α, k_1^{on}, k_2^{on} are estimated through fitting the extended model to the rate-coverage plot and used for a new optimization of θ_{max}. This cycle is repeated until self-consistency. All parameters and the coefficients of determination for the fits of BSA at pH 4.85, 6, and 7 are summarized in Table 5.3.

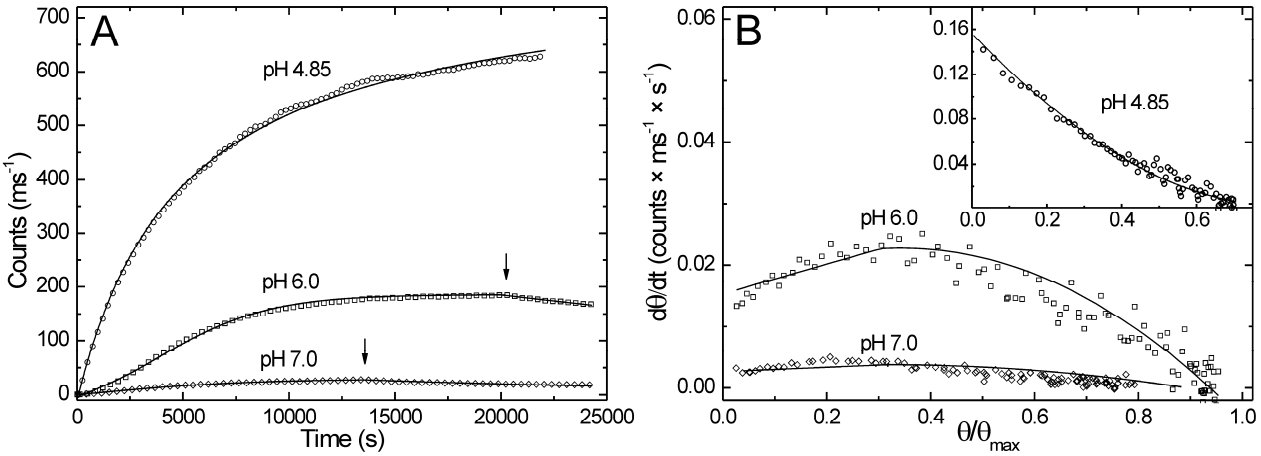

Fig. 5.8. A) Adsorption kinetics of BSA in citrate buffer (50 mM) at varying pH: pH 4.85 (64 nM, ○), pH 6 (200nM, □), and pH 7 (200 nM, ◊). Arrows indicate the points in time when rinsing with pure buffer was started. B) Rate-coverage plots of the kinetics presented in Fig. 5.8 A. Solid lines refer to the best fit obtained with the proposed model (see text).

Table 5.3. Estimated parameters for BSA adsorption in citric buffer (50 mM) at pH 4.85, 6, 7.

protein conc. (10^{-9} M)	pH	θ_{max} (counts ms^{-1})	k_1^{on} (10^6 counts ms^{-1} M^{-1} s^{-1})	k_2^{on} (10^6 counts ms^{-1} M^{-1} s^{-1})	$\frac{k_1^{on}+k_2^{on}}{k_1^{on}}$	α	k^{off} (10^{-7} s^{-1})	R^2	Plot
64	4.85	888 ± 59[a]	2.44 ± 0.69	-	-	-	7.5 ± 1.4	0.9985	Fig. 5.8
200	6.0	198 ± 18	0.076 ± 0.002	0.223 ± 0.011	3.93	0.31 ± 0.06	250 ± 50	0.9979	Fig. 5.8
200	7.0	30.5 ± 3.2	0.013 ± 0.002	0.038 ± 0.005	3.92	0.32 ± 0.08	500 ± 80	0.9756	Fig. 5.8

[a] The surface function Φ_1' is included.

The fit of the model to the adsorption kinetics of BSA at pH 6 and pH 7 displays an excellent agreement of the proposed mechanism with the observed behavior (solid lines in Fig. 5.8 A, B). From the rate-coverage plots (Fig. 5.8 B, □, ◊) it is evident that a contribution of the cooperative adsorption pathway still plays an important role in the initial stage. In comparison to the adsorption behavior at pH < pI much slower rates and lower saturation levels are noticed under pH 6 and pH 7 (see Table 5.3). This is because at rising pH values above the pI the number of negative charges within the protein and on the surface increases leading to stronger repulsions between protein molecules and between proteins and the surface. Explanations why proteins can bind to a negatively charged surface despite their own net negative charge, i.e., on the 'wrong side' of the isoelectric point, are comprehensively discussed in the literature.[200-202] Clearly, as α is rather small in these conditions (α = 0.31 at

pH 6, α = 0.32 at pH 7) the cooperative effects which are most obvious at low surface coverages can be easily disregarded especially at high bulk concentrations.

When BSA adsorbs in conditions of pH = pI (4.85) it exhibits the highest observable saturation level in its equilibrium state which is in agreement with the commonly reported behavior of this protein[42, 195] and of many other proteins.[32, 48, 203] At pH = pI the curve shape of the kinetics is exponential-like during the whole adsorption process and hence differs clearly from the kinetics at pH 3. Plotting the adsorption rate as a function of surface coverage (Fig. 5.8 B, inset) reveals no characteristic of positive cooperativity. On the contrary, the upwards concave shape of the curve is a strong indication that size exclusion effects which are comprehensively investigated in the literature have to be considered in this system.[57, 59, 204, 205] The best fit to the adsorption kinetics at pH 4.85 was obtained by eliminating the cooperative adsorption pathway ($k_2^{on} = 0$) and using the surface function $\Phi_1' = \Phi^{RSA}$ that accounts for size exclusion effects according to the random sequential adsorption (RSA) theory (see equation (2.5), parameters summarized in Table 5.3).[55]

$$\Phi_1' = \frac{\left(1-\frac{\theta}{\theta_j}\right)^3}{1-0.812\cdot\left(\frac{\theta}{\theta_j}\right)+0.2336\cdot\left(\frac{\theta}{\theta_j}\right)^2+0.0845\cdot\left(\frac{\theta}{\theta_j}\right)^3} \qquad (5.13)$$

In this equation θ_j is defined as the jamming limit which refers to a surface density of 54.7% of a close-packed monolayer. At its isoelectric point BSA has a net charge of zero such that lateral repulsions of adsorbed proteins are minimized. This explains the observed maximum surface coverage among all pH conditions evaluated. The surface function Φ_1' allows a more accurate fit of the observed kinetics at pI than using the simple Langmuir model expressed by Φ_1 (R^2 = 0.9985 when Φ_1' is used and R^2 =0.9977 when Φ_1 is used). In the absence of cooperativity proteins apparently bind to random surface sites and this is better accounted for by the RSA theory than by the simple Langmuir theory. However, the difference between these two theories is rather subtle and is only strong enough pronounced in the case of pure non-cooperative adsorption at pH = pI. In the case of an overlap of cooperative and Langmuir-type adsorption pathway (as found for all other pH conditions) the experimental data do not allow the direct observation of size exclusion effects. For this reason the simple

surface function Φ_1 was preferably implemented into the Langmuir-type adsorption pathway instead of the more complicated surface function Φ_1' which refers to the RSA model.

The evolution of the protein density distribution was also compared at pH 4.85 and pH 6 by recording scan images of a chosen area at different adsorption stages. Only very slight intensity variations were visible during the adsorption of BSA at pH 4.85 (Fig. 5.9, left column). Accordingly, the profile plots along the marked lines show that density fluctuations are rapidly balanced out during the adsorption resulting in a uniform protein distribution. In agreement with the exponential-like adsorption kinetics (Fig. 5.8 A) this is explained by the absence of cooperative effects. In contrast, the images recorded during the adsorption of BSA at pH 6 (Fig. 5.9, right column) reveal a clear distinction between regions of high protein density and regions of low density. The profile plots also confirm the preferential adsorption of bulk proteins in the proximity of other adsorbed proteins.

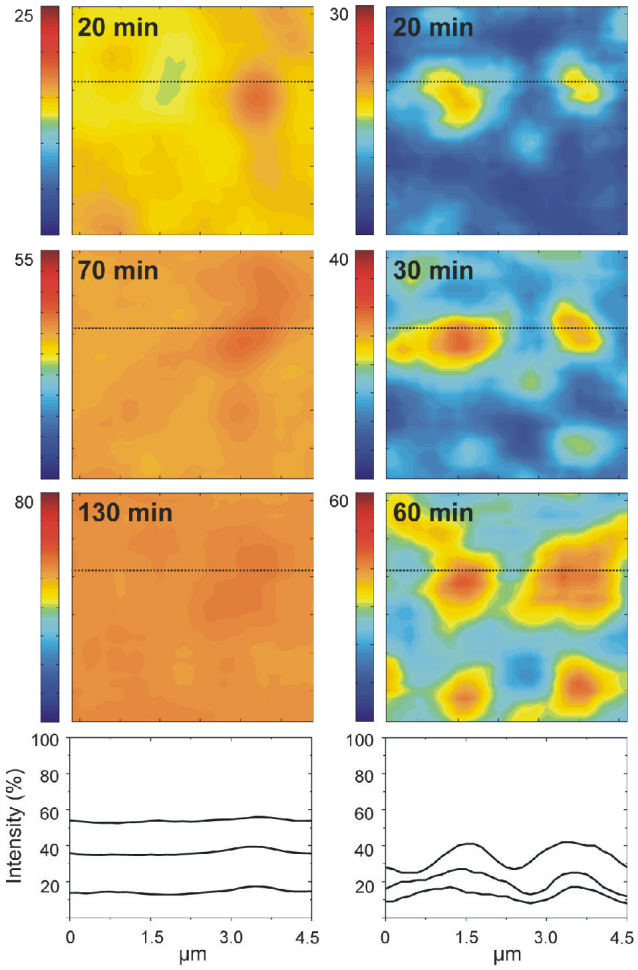

Fig. 5.9. Surface scan images recorded at different stages during the adsorption of BSA in citrate buffer at pH 4.85 (64 nM, left column) and at pH 6 (200 nM, right column). The profile plots underneath the images show the evolution of the fluorescence intensity along the cross sections marked by the dotted lines.

5.6 Cooperative adsorption of Fibrinogen

In the following analogies between the adsorption behavior of BSA and Fibrinogen (Fib) are presented, to demonstrate that the discussed mechanism is not restricted to one single protein species. Like BSA, Fib is a highly abundant plasma protein but with a significantly different structure (rod-like), a five times higher molecular weight (340 kDa), and a slightly higher isoelectric point (pI = 5.5). Nevertheless, the adsorption kinetics of Fib at pH 3, 4, 5 were found to be comparable to the kinetics of BSA (Fig. 5.10). In fact, the curve shapes of these two proteins are almost identical at pH 3 and only differ from each other at higher pH values. Conclusively, a contribution of cooperativity during the adsorption of Fib is evident. The excellent fit of the proposed model defined by equations (5.1) - (5.5) to the recorded adsorption kinetics (Fig. 5.10 A) and to the rate-coverage plot (Fig. 5.10 B) suggests that the same mechanistic description as used for BSA adsorption can be applied to the adsorption of Fib. The parameters for these fits are summarized in Table 5.4. These results suggest a rather general validity of the discussed adsorption model.

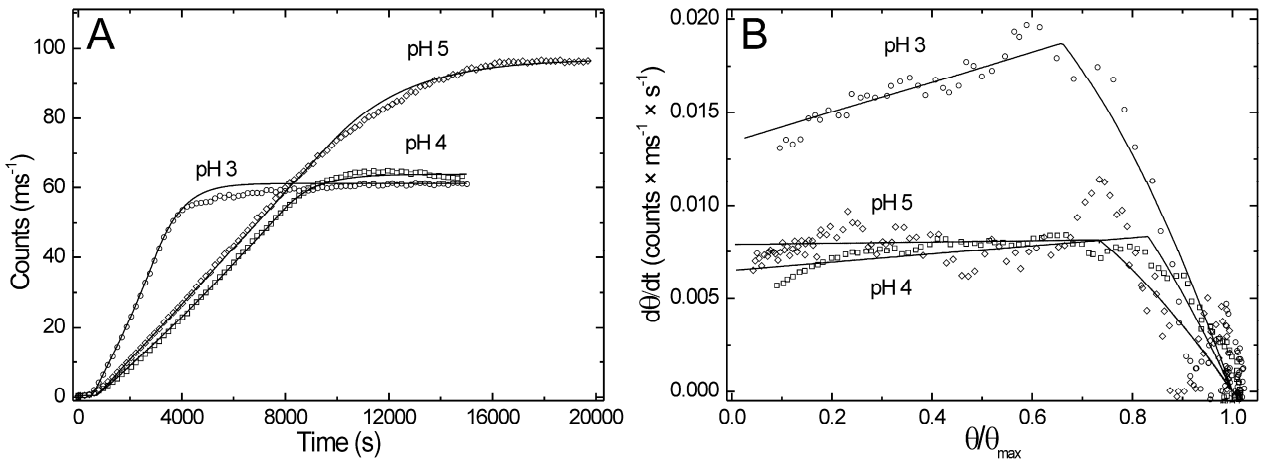

Fig. 5.10. A) Adsorption kinetics of Fib in citrate buffer (50 mM) at varying pH: pH 3 (8 nM, ○), pH 4 (8nM, □), and pH 5 (8 nM, ◊).
B) Rate-coverage plots of the kinetics presented in Fig. 5.10. Solid lines refer to the best fit obtained with the proposed model.

Table 5.4. Estimated parameters for Fib adsorption in citric buffer (50 mM) at pH 3, 4, 5.

protein conc. (10^{-9} M)	pH	θ_{max} (counts ms^{-1})	k_1^{on} (10^6 counts ms^{-1} M^{-1} s^{-1})	k_2^{on} (10^6 counts ms^{-1} M^{-1} s^{-1})	$\frac{k_1^{on}+k_2^{on}}{k_1^{on}}$	α	k^{off} (10^{-7} s^{-1})	R^2	Plot
8	3.0	61 ± 1	1.68 ± 0.10	2.68 ± 0.24	2.60	0.66 ± 0.06	0	0.9980	Fig. 5.10
8	4.0	64 ± 5	0.81 ± 0.07	1.09 ± 0.09	2.34	0.83 ± 0.02	0	0.9991	Fig. 5.10
8	5.0	97 ± 6	0.99 ± 0.02	1.03 ± 0.10	2.04	0.73 ± 0.02	0	0.9991	Fig. 5.10

5.7 Conclusion

In the present study the phenomenon of cooperative protein adsorption on solid interfaces has been experimentally investigated by the combination of kinetic analysis and in-situ surface imaging. Scan images during the course of adsorption enabled the observation of a heterogeneous protein density distribution as expressed by regions of high and low occupancy. It is shown that the adsorption of bulk proteins into regions of high protein density is related to positive cooperative adsorption whereas adsorption to any available binding site further away from pre-adsorbed proteins correlates to Langmuir-type adsorption. In the absence of positive cooperativity, proteins adsorb on random surface sites leading to a more homogeneous protein distribution which has been found for the adsorption of BSA at its isoelectric point (see Fig. 5.9, left column). On the other hand, cooperative adsorption is connected to a kind of self organization, driving incoming proteins to adsorb to binding sites close to other proteins which in turn leads to a more heterogeneous protein distribution (see Fig. 5.7 A and B, Fig. 5.9, right column). As a consequence, the growing surface occupancy does not impede the adsorption rate of adsorbing molecules which causes linear or even upwards concave shaped adsorption kinetics.[70, 71] A further conclusion is that the cooperative effects observed in this study are not related to the formation of surface aggregates or even two-dimensional clusters in which proteins bind to the surface and to each other. The experimentally acquired adsorption kinetics prove that a model based on growing surface clusters yields unsatisfying fitting results (see Fig. 5.3 B). It is shown experimentally that an abrupt change in the cooperative adsorption behavior takes place at a certain coverage limit above which the growing surface density starts to decelerate the adsorption rate. Mathematically, this is expressed by a step-like transition from cooperative to non-cooperative protein adsorption which is a certainly crude but very efficient approximation.

The model hence provides a very simple mechanistic explanation for initially linearly increasing and subsequently decreasing adsorption rates based on the overlap of Langmuir-type and cooperative adsorption pathways. Given the considerable number of equivalent experimental observations on a variety of different proteins in the literature,[61, 63, 69, 72, 74] the proposed model apparently describes a rather general adsorption behavior. Dependent on the importance of the respective Langmuir-type and the cooperative adsorption pathway (as expressed by k_1^{on} and k_2^{on}), the model perfectly fits to upwards concave ($k_1^{on} < k_2^{on}$), linear ($k_1^{on} = k_2^{on}$), or exponential-like ($k_1^{on} > k_2^{on}$) adsorption kinetics. Hence, it allows for extracting quantitative information about the positive cooperative effects from the curve shapes of protein adsorption kinetics. The wide applicability of the model is also highlighted by its ability to describe the adsorption kinetics of BSA and Fib in different pH environments. Additionally, it can be extended to account for additional phenomena such as structural re-orientation, lateral repulsion, or overshootings which will be shown in chapter 7. However, the proposed macroscopic model has some limitations such as the need for a piecewise rate equation and the abstract parameter α which can be only qualitatively explained. Further, the source of the observable density inhomogeneities of the protein layer is still not revealed. These issues will be treated with a microscopic approach in the following chapter.

6 Understanding Cooperative Adsorption at the Microscopic Scale: A Monte-Carlo Study*

The principal strategy of the study described in Chapter 5 consists of comparing experimental results with a macroscopic mathematical description that represents the proposed mechanism of cooperative adsorption. With the help of this approach the characteristic adsorption kinetics observed when proteins bind to the surface in the presence of cooperative effects can be accurately described and phenomenologically understood. Further, the model provides an explanation why variations in the protein density of adsorbed proteins are not balanced out during the course of adsorption. However, for a complete understanding of the microscopic events related to cooperative protein adsorption two more questions need to be answered. Firstly, the cooperative effect is described by a 'guidance' or 'tracking' of proteins approaching a surface site that is already occupied with another protein towards the nearest empty surface site. So far it is impossible to conclude from the experimental results up to which distance proteins can be tracked laterally by this mechanism. As discussed before, there is a critical coverage level above which the average distance that proteins have to pass to reach the nearest available binding site is too large such that the guidance mechanism breaks down (see Fig. 6.1 for an illustration of such a case). In the following this tracking distance is referred to as cooperative radius r_{coop} in units of the protein's diameter. According to the proposed mathematical description the length of r_{coop} is associated with the rather abstract parameter α which is directly amenable from the kink in the rate-coverage plots (see Fig. 5.3). The correlation between this macroscopic parameter and the real tracking distance r_{coop} can only be obtained through a microscopic approach.

* The results of this chapter have been submitted for publication

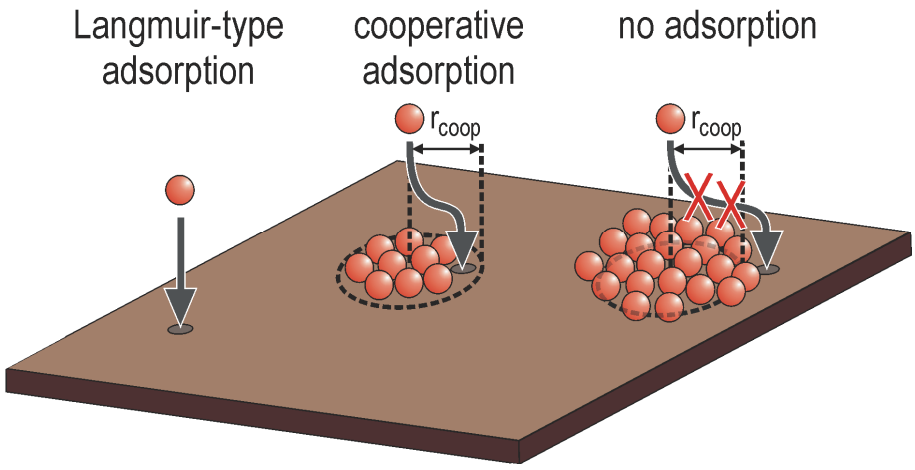

Fig. 6.1. Illustration of the tracking or guiding mechanism connected to cooperative adsorption. Middle: if the nearest available binding site is within the cooperative radius the protein adsorbs to it. Right: if the nearest available binding site is outside of the cooperative radius the protein is rejected.

The second issue concerns the experimentally observable inhomogeneities obtained from the scan images (see Fig. 5.7 and Fig. 5.9). So far it can be explained why density differences remain at the same positions during the cooperative adsorption process but the source of such inhomogeneities which are significantly more prominent in the case of cooperative adsorption as compared to non-cooperative adsorption remains obscure. Is the emergence of the intensity variation observed in the scan images a direct consequence of the cooperative adsorption? To answer this question it is necessary to unravel the molecular arrangements in which proteins organize upon surface adsorption under cooperative and non-cooperative conditions and to analyze the corresponding scan images.

Both issues are addressed comprehensively in the following with the help of a Monte-Carlo type simulation according to the proposed adsorption mechanism. The simulation was performed on a grid of 3250 × 3250 surface sites on which simulated proteins were sequentially adsorbed on random positions under periodic boundary conditions. The grid size was chosen to model a sufficiently large surface area corresponding to 6500 nm × 6500 nm that accommodates around 10 million surface sites of 2 nm × 2 nm. The adsorbing proteins are of circular-like shape with a diameter equivalent to the length of 7 surface sites, i.e., 14 nm in accordance with the longest axis of the protein BSA.[42, 165] The following algorithm was applied during the simulation:

1. a virtual protein is generated on the grid centered at a random position; if it does not overlap with any other pre-adsorbed protein the step is accepted with a probability proportional to the Langmuir-type adsorption rate constant ($p_1 \propto k_1^{on}$) and the next virtual protein is generated; the number of adsorption trials is incremented by 1

2. otherwise, if the protein does overlap with any pre-adsorbed protein the nearest empty surface site on which the protein can adsorb without any overlap is evaluated; the adsorption on the new position is accepted with the probability ($p_2 \propto k_2^{on}$) provided the distance between the initial site and the new site is smaller or equal to the cooperative radius r_{coop}, otherwise the protein is rejected; the next virtual protein is generated and the number of adsorption trials is incremented by 1

As schematically illustrated in Fig. 6.2 the simulation gives access to the adsorption kinetics and to scan images which both can be directly compared to experimental data. The kinetics and the corresponding rate-coverage plots are simply obtained by counting all proteins on the surface in intervals of 250 adsorption trials. To obtain scan images during the simulation, a discrete convolution of the protein covered surface with the point spread function is performed in intervals of 10'000 adsorption trials:

$$s(x,y) = l(x,y) * f(x,y) = \sum_{\tau_y} \sum_{\tau_x} l(x-\tau_y, y-\tau_y) \cdot f(\tau_x, \tau_y) \qquad (6.1)$$

where $s(x,y)$ is the function representing the intensity of the scan image, $l(x,y)$ refers to the point spread function, and $f(x,y)$ is the object function, i.e., the protein covered surface. The point spread function is modeled by a Gaussian function covering 1000×1000 surface sites, i.e., 2 µm × 2 µm, with a width of 2σ = 500 nm which is in line with the instrumental response profile of the SAF microscope.[147]

$$l(x,y) = N \cdot e^{-\frac{x^2+y^2}{2\sigma}} \qquad (6.2)$$

where N is the normalization factor which is chosen such that the scan image of a saturated surface scales to an average intensity of 100%. During the convolution process the movement

of the point spread function $l(x, y)$ is restricted such that it never exceeds the area of the object function. As a result, the simulated scan image exhibits a size of 2250 × 2250 surface sites corresponding to 4.5 µm × 4.5 µm.

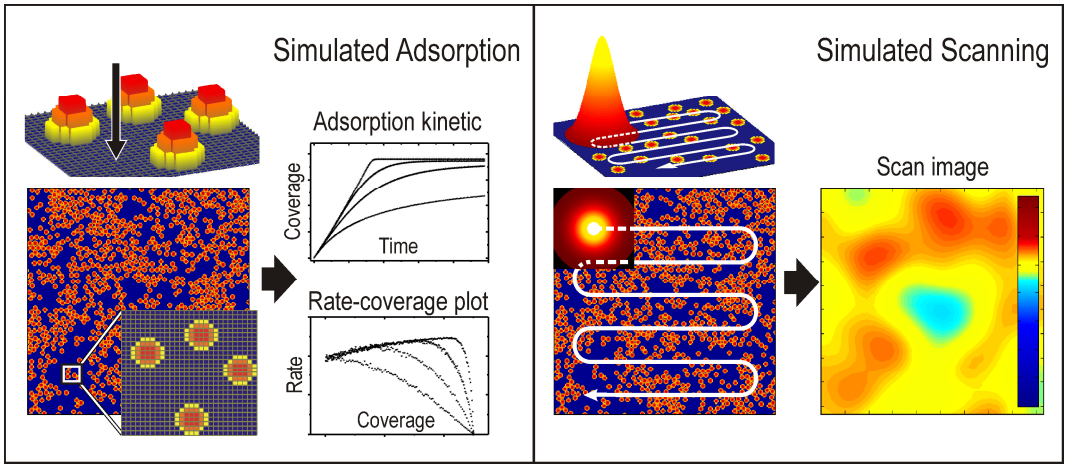

Fig. 6.2. Overview of the Monte-Carlo Simulation. Adsorption kinetics (left) and scan images (right) can be simulated and compared to experimental data.

6.1 The length of the cooperative radius

To quantify the correlation between the length of the cooperative radius r_{coop} and the parameter α, the influence of varying r_{coop} on the resulting adsorption kinetics was explored. Therefore, 18 simulations were run with values of r_{coop} ranging between 0 and 7.5 in units of the protein's diameter. The adsorption probability ratio between cooperatively and non-cooperatively adsorbing proteins was set to $p_2 / p_1 = 1.3$ which is in the magnitude of the observed ratio between k_2^{on} / k_1^{on} observed for BSA adsorption on glass at pH 3. As stated before, longer cooperative radii necessarily lead to higher values of α. Thus, a curve fit of the rate equations representing the macroscopic description of the proposed model (equations (5.8) - (5.10)) to the simulated kinetic data representing the microscopic description yields a specific value of α for every simulated r_{coop}. The fitting procedure was analogous to the fit of the model to the experimental data except that all parameters except α were fixed by the conditions of the simulation. The parameter n refers to the intercept of the rate-coverage plot

and was determined to be: n = 199. According to equation (5.9) and (5.10) the value of m is given by: $m = n \cdot \left(k_2^{on} / k_1^{on} - 1\right) \approx 60$. Examples of the simulation results are shown in Fig. 6.3 plotted as rate-coverage plots (left column) and adsorption kinetics (right column). The fit of the model is added in all plots as thin solid line and shows nicely the smooth transition between increasing and decreasing adsorption rates. The sharp kink in the rate-coverage plots is eliminated because the simulation works without the abstract parameter α and without the stepwise function defined by equation (5.4). Only the maximum tracking or guiding distance, i.e., r_{coop} and the two rate constants k_1^{on} and k_2^{on} (herein the ratio k_2^{on} / k_1^{on}) determines the shape of the adsorption kinetics. Naturally, the macroscopic approach represented by the rate equations (5.1) - (5.5) is computationally much less demanding and therefore still provides an efficient alternative to describe the observed adsorption kinetics. In fact, the time integrated adsorption kinetics resulting from the two methods, macroscopic and microscopic, can even hardly be distinguished from one another (see Fig. 6.3, left). Plotting the parameter α resulting from the curve fits as a function of r_{coop} yields the aspired connection between an experimentally amenable information and its microscopic interpretation (Fig. 6.4). One consequence of this plot is that a value of α = 0.8 which is around the experimental value found for BSA adsorption on glass at pH 3 corresponds to a cooperative radius of about $r_{coop} = 2.5$. That means, proteins which approach the surface at an occupied position can be tracked up to a distance of 2.5 times of their own diameter towards an available surface site (see Fig. 6.3 insets). To highlight the agreement between simulated adsorption kinetics and experimental data, the recorded kinetics corresponding to BSA adsorption in citrate buffer (50 mM) at pH 3 were overlaid with the plots in Fig. 6.3 B referring to r_{coop} = 2.5. Typical experimental values for the parameter α in the case of cooperative adsorption are between 0.31 and 0.84. Referring to Fig. 6.4 the underlying cooperative radii thus range from 0.75 up to 3.0. As no larger cooperative radii were observed during this study the scenario depicted in Fig. 6.3 C (inset) is a pure theoretical one which has most probably no realistic meaning.

To better highlight the effect of the cooperative adsorption pathway on the shape of the adsorption kinetics, a reference simulation using r_{coop} = 0 was run (Fig. 6.3 D). In this case the adsorption rate steadily declines with the increasing coverage as the available surface area decreases. The characteristic convex shape of the rate-coverage plot (Fig. 6.3 D, left) is a result of size-exclusion effects that are necessarily involved in the simulated adsorption process since each protein occupies more than only one surface site (namely 37). Using the formalism developed in the framework of the random sequential adsorption (RSA) theory

(equation (2.5)) the simulated adsorption kinetics under non-cooperative conditions can be accurately described (solid lines in Fig. 6.3, D).[55]

$$\frac{d\theta}{dt} = k_1^{on} \cdot c \cdot \Phi^{RSA} \tag{6.3}$$

Experimentally, a pure non-cooperative scenario was found in the case of BSA adsorption on glass at pH = pI. The corresponding data (already shown in Fig. 5.8) are added to the simulation results of $r_{coop} = 0$ in Fig. 6.3 D.

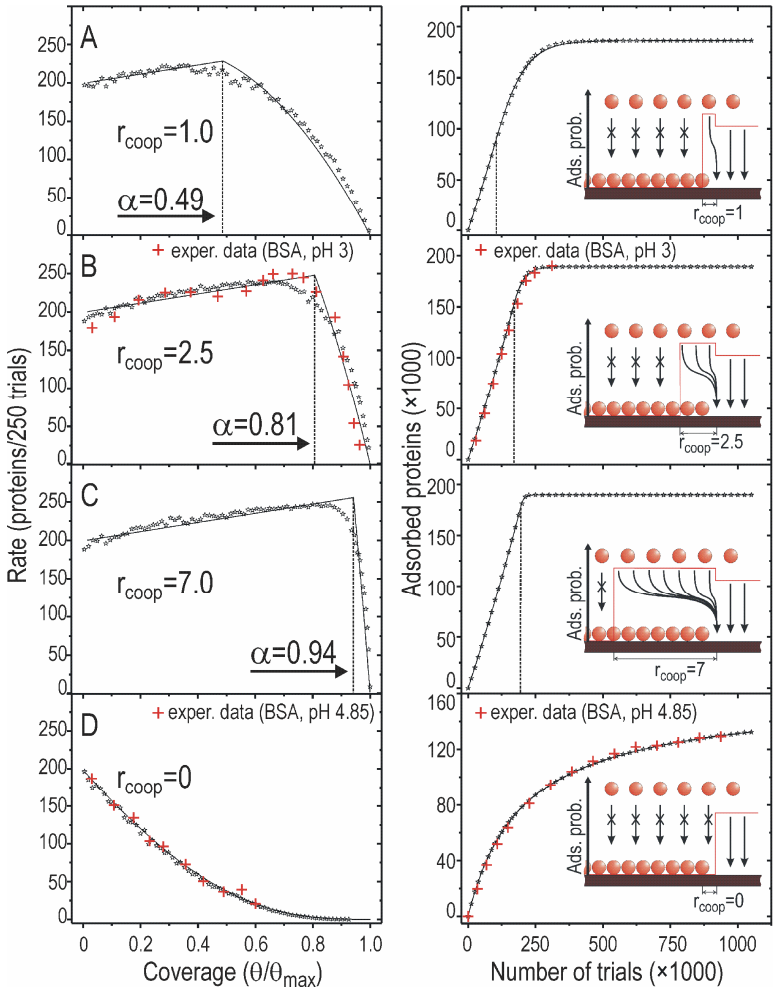

Fig. 6.3. Simulated adsorption kinetics (right) and corresponding rate-coverage plots (left) for varying r_{coop}: 1.0 (A), 2.5 (B), 7.0, (C), and 0 (D). The simulated data points were fitted by the proposed model (solid lines). Experimental data (+) are added to charts (B) and (C). Insets: schematic illustrations of the 'guiding' mechanism. Proteins approaching the surface on an occupied region adsorb with increased probability provided they are within the cooperative radius.

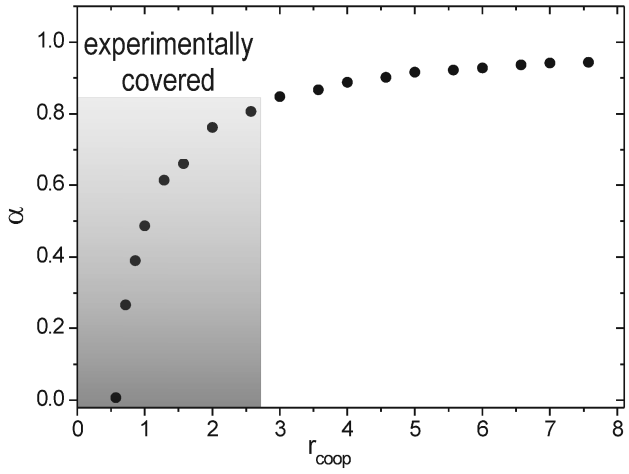

Fig. 6.4. Correlation between the macroscopic parameter α and the microscopic value of r_{coop}.

6.2 Self-organization of adsorbed proteins

To explore the source of the experimentally observed inhomogeneities in the scan images and their relation to the self-organization of proteins, simulated scanning was performed at different coverage levels. The parameters for this simulation were fixed to $r_{coop} = 2.5$ and $p_2 / p_1 = 1.3$ referring to the experimental results of BSA adsorption on glass at pH 3. Fig. 6.5 presents the simulation results showing the arrangement of surface adsorbed proteins at different coverage levels (middle column: complete view; left column: magnified view). The convoluted images, i.e., the simulated scan images are shown in the right column of Fig. 6.5. In the center of these images one can notice a local intensity minimum, thus a region of low protein density. This local minimum is present in practically all scan images ranging from a total coverage of ~25% in the beginning up to ~80% after 180'000 simulation steps. The profile plots (inset in Fig. 6.5) reveal that the intensity difference between the low density region in the center and the high density region in the circumference scales to ~8% of the saturation coverage. To work out the major characteristics of cooperative protein adsorption the results shown in Fig. 6.5 are compared with a reference simulation of a pure non-cooperative adsorption ($r_{coop} = 0$) whose results are presented in Fig. 6.6. As can be seen clearly in the simulated scan images, protein density variations in the non-cooperative case are less pronounced as they scale only to a maximum of ~4% of the saturation coverage (see profile plots in the inset of Fig. 6.6). Moreover, the distribution of regions of higher and lower protein density at one point is clearly uncorrelated with their distribution at a later point. The

contour lines in the middle column of Fig. 6.6 indicate randomly changing positions of regions of higher and lower protein density whereas in the case of cooperative adsorption (middle column in Fig. 6.5) the contour lines indicate practically constant positions of such low and high density regions.

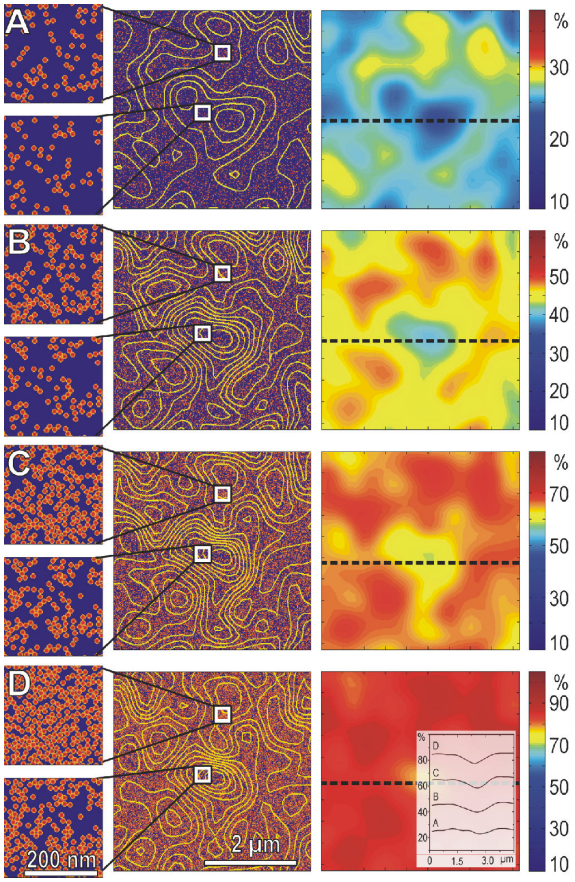

Fig. 6.5. Simulated scanning for cooperative adsorption. The protein distribution on the surface (middle and left column) and the corresponding scan images (right column) are presented. Inset: Profile plots along the dashed lines. Sampling was performed after 60 × 10^3 (A), 100 × 10^3 (B), 140 × 10^3 (C), and 180 (D) × 10^3 adsorption trials.

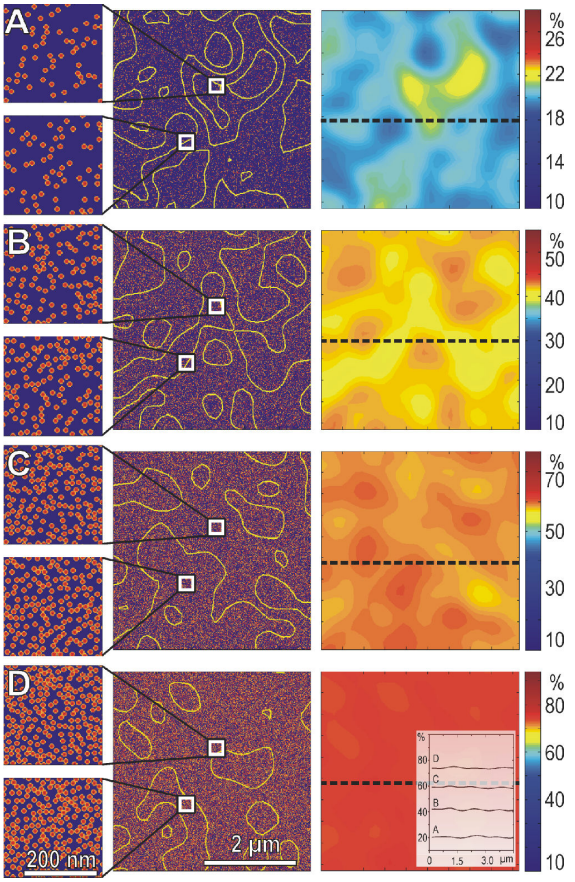

Fig. 6.6. Simulated scanning for non-cooperative adsorption. Scan images (right) and contour lines (middle) show altering distributions of high and low density regions. The protein distribution is more homogeneous at all times (left). Sampling was performed after 60 × 10^3 (A), 180 × 10^3 (B), 400 × 10^3 (C), and 1000 × 10^3 (D) adsorption trials.

This observation is the expected result of a simple Langmuir-type adsorption behavior: if there are differences in the protein density on the surface resulting from random processes they are balanced out during the course of further adsorption. Thus, the simulation reveals that the cooperative adsorption process is directly linked to inhomogeneities in the surface distribution of adsorbed proteins. During their continuous adsorption proteins arrange

spontaneously in a way such that regions of higher and regions of lower occupancy are observed in the scan images. Examples for such protein arrangements are shown as magnified views on the left of Fig. 6.5. By contrast, intensity inhomogeneities are also found during non-cooperative adsorption but to a significantly lower extent than in the case of cooperative adsorption. Accordingly, the protein arrangements (Fig. 6.6, left) are of nearly uniform appearance.

To highlight that the surface inhomogeneities are significantly more pronounced in the case of cooperative adsorption as compared to non-cooperative adsorption, a statistical evaluation of the intensity variations was performed. Therefore, 100 independent simulations for each case were run starting from an empty surface. In Fig. 6.7 A the mean differences between maximum and minimum intensities of the simulated scan images are plotted as a function of surface coverage. It turns out that intensity fluctuations of up to 4% of the saturation coverage appear in the beginning in both cases, cooperative and non-cooperative adsorption. However, during the non-cooperative adsorption variations are quickly balanced out whereas during the cooperative adsorption the initial density fluctuations provoke the formation of even stronger intensity differences after continued adsorption. As a consequence, the divergence between the surface inhomogeneities becomes most obvious at coverage levels above 50%. An analogous analysis was performed on experimental results using 30 subsections of a large scan image that was repeatedly scanned until protein adsorption reached the saturation level. The plots of the maximum intensity differences presented in Fig. 6.7 B suggest qualitative agreement between observed and simulated protein surface distributions. However, the most important conclusion from this analysis is that the stronger inhomogeneities resulting from cooperative adsorption (red data points in Fig. 6.7) as compared to non-cooperative adsorption is significant in both cases, simulation and experiment. The experimentally obtained scan images (Fig. 5.7 and Fig. 5.9) are thus consistent with the proposed mechanism of cooperative adsorption. Because of the guiding behavior proteins organize preferably in patches of high protein density which naturally also leaves some regions of low protein density behind. Such a surface organization is recognized as an inhomogeneous intensity image when the surface is scanned with the SAF microscope.

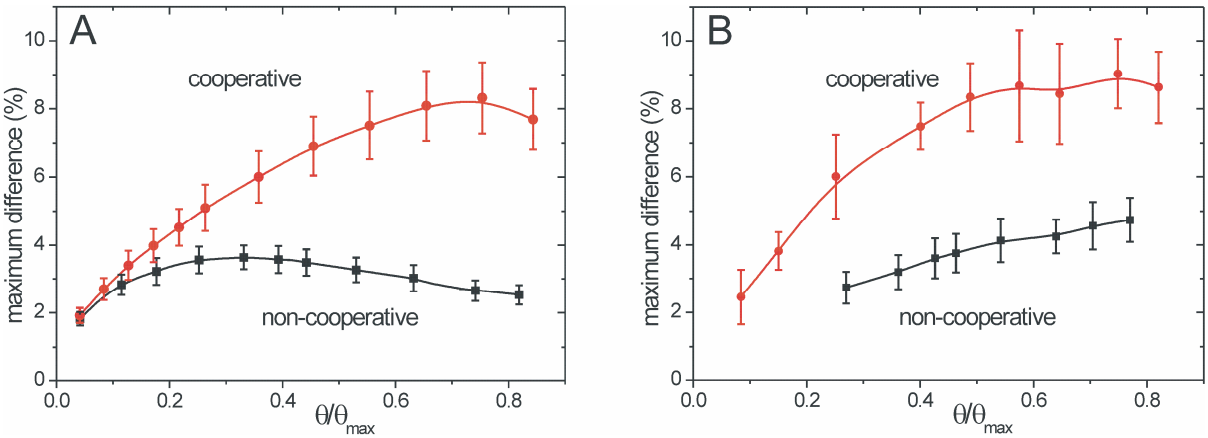

Fig. 6.7. Statistical evaluation of density variations in the scan images at different adsorption stages. The average difference between intensity maximum and minimum on all scan images was plotted as a function of surface coverage for both cases, cooperative (red line) and non-cooperative (black line) adsorption. Error bars indicate the standard error calculated from 100 (A) and 30 (B) values at each point, respectively. (A) Simulation; (B) Experiment.

6.3 Conclusion

In the present study the microscopic events behind the cooperative adsorption of proteins to solid surfaces is explored with the help of a Monte-Carlo type simulation. The implemented algorithm represents the proposed mechanism of cooperative adsorption introduced in the preceding chapter whose key feature is that a protein approaching the surface in an occupied region is not necessarily rejected like in the classical Langmuir-type adsorption model. Instead, the protein is tracked to the nearest available binding site guided by the complex local electrostatic field arising from the pre-adsorbed charged proteins and the surface. From the simulation data information with regard to the adsorption kinetics and to the surface organization of adsorbed proteins was extracted. The simulation settings and conditions were chosen such that a direct comparison with experimental results of Chapter 5 was possible. First, simulated adsorption kinetics were found to be in excellent agreement with experimental data and with the calculated kinetics using the proposed rate equations (5.1) - (5.5) (see Fig. 6.3). Compared to this macroscopic approach, however, the simulation represents certainly a more realistic situation as it works without the abstract parameter α. Thus, the piecewise description of the adsorption rate becomes needless and the kink in the rate coverage plots can be avoided. In fact, the simulation reveals that there is indeed a sharp transition between the increasing and decreasing parts of the adsorption rate but this appears clearly not in a step like fashion. However, the accuracy of experimental data is insufficient

for an unambiguous assignment of the transition behavior. The macroscopic approach presented in Chapter 5 can therefore still be considered as a straight-forward and sufficiently accurate method to evaluate experimental adsorption kinetics. Since the present study provides a correlation between the parameter α and the tracking distance r_{coop}, a microscopic interpretation of experimental data is now possible.

Apart from the adsorption kinetics the surface organization behavior of proteins is also explored from a microscopic point of view. It was found that the random adsorption of proteins on a surface causes minute density fluctuations which, under cooperative conditions, evolve into persistent density differences after continued adsorption. The simulation reveals that cooperative adsorption causes the formation of patches of several proteins next to loosely covered surface regions. Macroscopically this necessarily results in the observed scan images showing characteristic density inhomogeneities (see Fig. 6.5). To demonstrate that the discussed effects are tightly connected to cooperativity, reference simulations and experiments under non-cooperative conditions were shown for comparison (Fig. 6.5 - Fig. 6.7). Because of the wide agreement between various macroscopic observations with the results of the simulation presented herein this study highlights the validity of relating cooperative adsorption to the proposed tracking or guiding mechanism.

7 Adsorption Phenomena of β-Lactoglobulin*

The main objective of this chapter is to investigate the adsorption behavior of the chosen model protein β-Lactoglobulin (18.4 kDa) in great detail. This protein exhibits a combination of several adsorption phenomena including not only cooperative effects as studied in the previous chapters but also an overshooting effect and several transitions or relaxations from one state into another. To ensure reliant conclusions about the adsorption mechanism and in particular to obtain a useful adsorption model, a comprehensive set of experimental data is crucial. The focus is put on the protein's adsorption and desorption kinetics which can be described by rate equations that imply a certain adsorption mechanism. All kinetics were recorded using the SAF biosensor on which a flow cell maintaining a quasi constant bulk protein concentration near the surface was mounted. Ideally, a unified adsorption model should accurately describe the protein's adsorption behavior over a broad range of applied bulk concentrations. Therefore, adsorption kinetics at bulk protein concentrations starting from as low as 5 nM up to 1.5 µM were recorded. Other influencing parameters such as temperature, ionic strength, buffer pH, and the chosen surface were kept constant to ensure a reasonable framework of this study. More precisely, the adsorption kinetics were measured at room temperature on negatively charged hydrophilic glass coverslips using citrate buffer at pH 3 and an ionic strength of 50 mM. Apart from a basic scientific point of view the adsorption behavior of β-Lactoglobulin is also of interest in the dairy industry where it is involved in fouling processes.[10, 11, 74]

* The results of this chapter were published in: M. Rabe, D. Verdes, M. Rankl, G. R. J. Artus and S. Seeger, *ChemPhysChem,* 2007, **8**, 862-872.

7.1 Real-time adsorption kinetics

As was discussed in Chapter 4 it was made sure that measuring the fluorescently labeled protein β-Lactoglobulin with the SAF technique reflects the true adsorption behavior of the native protein. Also the risk of signal loss at higher surface coverages resulting from self-quenching effects was minimized by diluting fluorophore (DY-647) labeled proteins (DY-647-β-Lg) with unlabeled, native proteins at p^*/p-ratios of 1:100. In this way the average distance between two fluorophores bound to surface adsorbed proteins was much larger than the distance at which homo energy transfer or self-quenching is possible.

In the following the adsorption behavior of β-Lg is explored in a large range of bulk protein concentrations to finally develop a general mathematical description of the adsorption mechanism. Beginning in the high concentration range ($c_{bulk} = 0.125 \times 10^{-6}$ M - 1.5×10^{-6} M) the first investigated issue was the reversibility of the non-specific binding in the presence of protein-free buffer. In a first step, protein adsorption and subsequent desorption during rinsing with buffer was monitored using a bulk concentration of 0.75×10^{-6} M (p^*/p = 1.0%). As clearly depicted by the experimental data shown in Fig. 7.1 A the adsorption of the protein under the chosen conditions is only partially reversible. The major part of the molecules apparently binds almost irreversibly to the surface such that after a reasonable rinsing time the fluorescence intensity reaches a quasi plateau far above the baseline. This is a common phenomenon encountered for non-specifically adsorbing proteins which has led to the conclusion that the mechanism can not be explained with one single state of the surface bound protein.[23, 25, 110] A comparison of the desorption curves further reveals that the amount of proteins that are removed from the surface upon rinsing slowly decreases in time (see inset of Fig. 7.1 A) which is typically explained by a relaxation of a reversibly adsorbed state to an irreversible state. In agreement with other studies the transition of reversibly adsorbed β-Lg to an irreversible state is a rather slow process as it takes at least one hour to observe an unambiguous effect.[108, 206] It should be mentioned that in reality there are most likely more than two states of the adsorbed protein differing in their conformation or orientation and consequently in their desorption rate.[110] Herein the ensemble of all relaxed states is regarded as one single quasi irreversible species for the sake of simplicity. Rinsing experiments after long adsorption times reveal that the relaxed state is not completely irreversible as a minute off-rate of this state can be observed. Even after an extended adsorption time of more than 10 hours the same desorption rate as after three hours is

observed (data not shown). The solid lines also plotted in Fig. 7.1 A refer to the calculated kinetics obtained from the model which is developed below.

To learn more about the adsorption and desorption behavior of β-Lg it is important to study the interaction of non-specifically adsorbed proteins with other proteins that are approaching the surface. When the solution of labeled molecules is replaced by an equally concentrated solution of unlabeled molecules the adsorption on the surface continues in the same way but only the molecules already adsorbed are fluorescently labeled and hence detectable. This is important because the desorption rate of β-Lg turns out to be influenced by the proteins that are about to adsorb. In Fig. 7.1 B the adsorption and desorption kinetics of a 0.75×10^{-6} M β-Lg solution are depicted. Two distinct points in time (700 s and 3000 s) were chosen to compare the desorption processes in the presence of pure buffer and unlabeled proteins. Rinsing with protein-free buffer apparently leads to a slower off-rate compared to rinsing with a 0.75×10^{-6} M solution of unlabeled proteins. Thus, incoming molecules enhance the desorption of adsorbed proteins. As early as in the 1970s Vroman et al.[81, 83] found analogous experimental results and concluded that surface bound proteins can be removed by other adsorbing proteins. Later this effect has been confirmed by other studies for the adsorption behavior of a set of different proteins[31] as well as for a single protein species.[76]

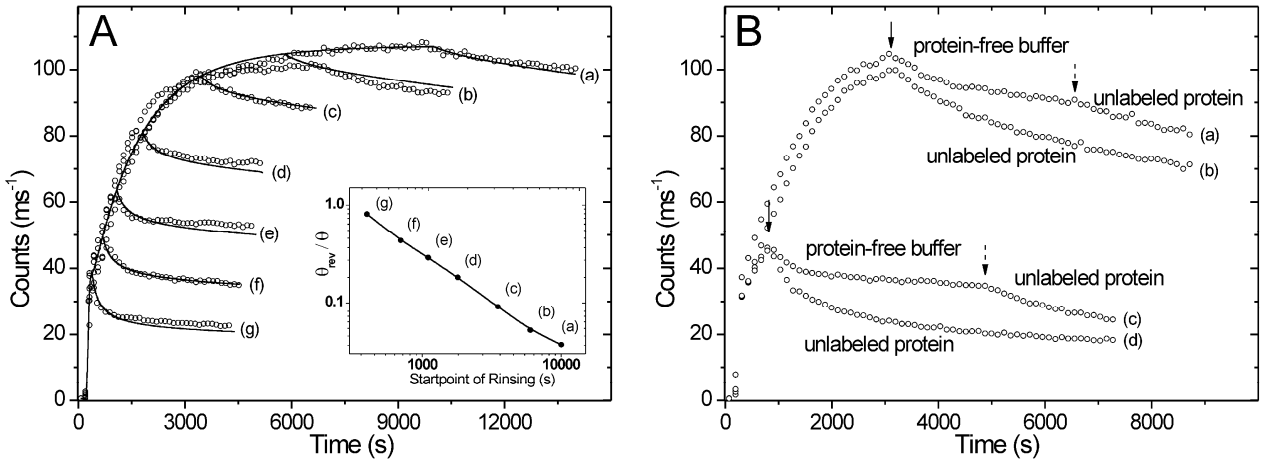

Fig. 7.1. A) Desorption kinetics of β-Lg after different adsorption times. Rinsing with protein-free buffer was performed in 7 separate experiments after adsorption of the protein (0.75×10^{-6} M) for 10000s (a), 6000s (b), 3500s (c), 1800s (d), 1100s (e), 700s (f), and 400s (g) (circles, only every second data point is plotted). The solid lines represent the calculated kinetics. Inset: calculated fraction of the amount of the reversibly adsorbed species (logarithmic scale) as a function of the point in time when rinsing was started (logarithmic scale).
B) Desorption kinetics of β-Lg in the presence of unlabeled protein solution. In 4 separate experiments adsorbed proteins (0.75×10^{-6} M) were rinsed with protein-free buffer and a solution of equally concentrated unlabeled protein after 3000s (a, b) and 700s (c, d), respectively (solid arrows). In the case of rinsing with pure buffer (curves a, c) unlabeled proteins were also added after 5000s, and 6500s, respectively (dashed arrows).

To better characterize concentration dependent phenomena the adsorption kinetics of β-Lg were recorded at stepwise decreasing bulk protein concentrations starting from 1.5×10^{-6} M down to 0.5×10^{-8} M (Fig. 7.2). As can be noticed for higher bulk concentrations above 0.125×10^{-6} M (Fig. 7.2 A, curves a-c) the adsorption curves tend to reach approximately equal saturation values corresponding to their equilibrium coverages. Conclusively, there must be an upper limit for the equilibrium coverage (~110 counts × ms^{-1}). This limit can be attributed to a monolayer coverage of maximum density. From calculations and from ellipsometry measurements it is known that a close-packed monolayer of β-Lg on a flat surface has a density of 2.7 mg × m^{-2}.[11, 206] Naturally, the equilibrium coverage level of each adsorption curve depends on the applied bulk concentration since the final relaxed state of the adsorbed protein has a non-negligible desorption rate. This is in accordance with typical adsorption isotherms that converge to a maximum which is defined by the saturation level. The build-up of a second or higher order layer on the surface can be excluded as it would exhibit at least two plateaus at different count rates instead of a defined upper saturation limit.[11] In agreement with this conclusion ellipsometry based works reported monolayer coverages for β-Lg on hydrophilic surfaces in comparable conditions.[11, 206]

An important observation of this study is that β-Lg exhibits an overshoot in the early adsorption process. At high bulk concentrations (Fig. 7.2 A, curves a-c) this feature appears as a ‘kink’ in the adsorption kinetics whereas a clear peak shape is encountered at low bulk concentrations (Fig. 7.2 B). It is noticed that the overshoot occurs at roughly equal surface coverage levels of approximately 30±5 counts × ms^{-1}. Consequently, the adsorption time before the overshoot is the longer the lower the bulk protein concentration is. According to the observed kinetics presented in Fig. 7.2 the adsorption process can be divided into three stages. In the beginning the free surface is rapidly populated with adsorbing proteins in a non-exponential-like manner. A closer look into the curvatures of the adsorption kinetics in the low concentration range (Fig. 7.2 B) reveals that the initial rate increases with a growing surface coverage. Once the coverage reaches a critical density a ‘peak’ or a ‘kink’ in the adsorption kinetics is observed resulting in a temporal decrease of the total coverage. The peak widths of the overshoots are broad at low bulk concentrations and narrow for higher concentrations. Afterwards, the surface density passes through a local minimum and continues to grow in an exponential-like manner until the equilibrium coverage is reached.

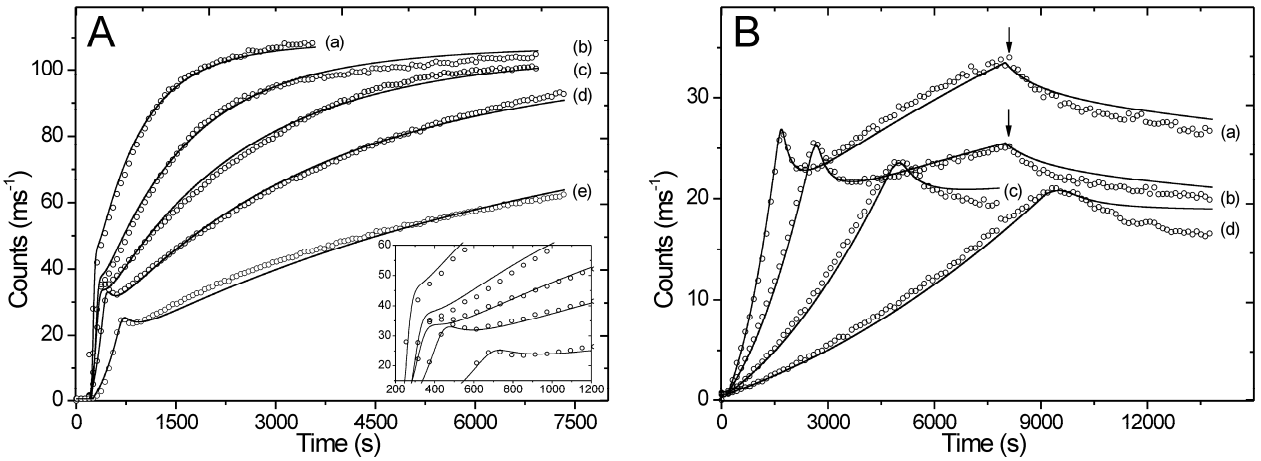

Fig. 7.2. A) Adsorption kinetics of β-Lg for bulk concentrations of 1.5×10^{-6} M (a), 0.75×10^{-6} M (b), 0.5×10^{-6} M (c), 0.25×10^{-6} M (d), and 0.125×10^{-6} M (e) (circles). The solid lines represent the calculated kinetics. Inset: Enlarged scale for the first 1200s.
B) Adsorption kinetics of β-Lg for bulk concentrations of 4.0×10^{-8} M (a), 2.0×10^{-8} M (b), 1.0×10^{-8} M (c), and 0.5×10^{-8} M (d) (circles, only every second data point is plotted). In the case of the two higher concentrations (curves a, b) rinsing with protein-free buffer was performed after 8000s (arrows). The solid lines represent the calculated kinetics.

The interpretation of these phenomena turns out to be rather complex because simple models usually predict exponential-like kinetics throughout the whole adsorption process.[74, 108, 128, 181] Similar increasing rates in the initial adsorption kinetics were observed by Vasina et al. for the adsorption of the two proteins Lysozyme and α-Chymotrypsin on mica using radiolabeling techniques.[72, 157] As discussed in Chapter 5 such upwards concave adsorption kinetics are a clear sign of cooperative effects which will have to be considered for the adsorption mechanism of β-Lg. Overshoots during non-specific protein adsorption kinetics have also been reported by several research groups.[41, 77, 84] As was discussed in the theoretical part of this dissertation there is still no unique explanation for this phenomenon. When the adsorption of protein mixtures is studied the effect is referred to as the Vroman effect.[81-84] In this case, fast adsorbing molecules initially cover the surface before they are replaced by slowly adsorbing molecules of a higher surface affinity. This explanation is not valid for the present work although the applied protein solution was composed of the two variants β-Lg A and B. This assumption was confirmed by repeating some of the discussed experiments with one isolated variant that showed the same overshooting behavior as the mixture of both variants (data not shown). This is not surprising because the two genetic variants of β-Lg are very similar as they differ by only two amino acids (Asp-64, Val-118 in A, and Gly-64, Ala-118 in B) causing a mass difference of only 70 Da.[160] It should also be noted that in the given

conditions (pH 3.0, low ionic strength) the monomeric rather than the dimeric form of β-Lg is predominant.[169, 207]

Nonetheless, overshoots were also observed during the adsorption of single protein species. Wertz et al.[41] found that Lysozyme on hydrophobic surfaces initially adsorbs in a dense layer which later relaxes to a loose but energetically favored layer. They postulated a rollover mechanism driving the orientation of the adsorbed protein from end-on to side-on. In opposite to the observations in the present study the authors showed that under their conditions the overshoot in the adsorption kinetics of Lysozyme only occurs at high bulk concentrations and vanishes in the low concentration range. Daly et al.[77] also reported overshoots during the adsorption of Lysozyme labeled with FITC dye on hydrophilic mica. In contrast to the afore mentioned work, they attributed the overshoot to an intensity loss of the fluorescent label when the protein changes its orientation on the surface which finally moves the dye in a different local pH environment. This explanation essentially requires a pH-dependent fluorescent label and specific binding sites for the dye within a certain region in the protein. None of these conditions were encountered in this work (see Fig. 4.5 and Fig. 4.6). Furthermore, an increase of the adsorption kinetics after the overshoot as encountered in the experiments presented herein could not be explained in this way.

To elucidate the mechanism of the overshoot in this work, further rinsing experiments were performed during the initial adsorption stage. Naturally, this is only reasonable in the low concentration range where the initial growth is slow enough. Fig. 7.3 presents the desorption behavior of β-Lg after different periods of adsorption ($c_{bulk} = 5.0 \times 10^{-8}$ M) in the presence of protein-free buffer. It is remarkable that proteins attach completely irreversibly on the surface in the early stage of the adsorption before the overshoot takes place. Even after extended rinsing with pure buffer no decrease of the fluorescence intensity is observed (Fig. 7.3, curves c, d). However, if rinsing with buffer is started close to the peak maximum (Fig. 7.3, curve b) or later (Fig. 7.2 B, curves a, b) a typical desorption curve is obtained. Thus, at this stage β-Lg appears to be partially reversibly bound. From these observations it is concluded that at a certain surface density there must be a transition of the initially irreversibly adsorbed species to a reversible species. In the following this threshold coverage level is referred to as the critical surface coverage θ_{crit}.

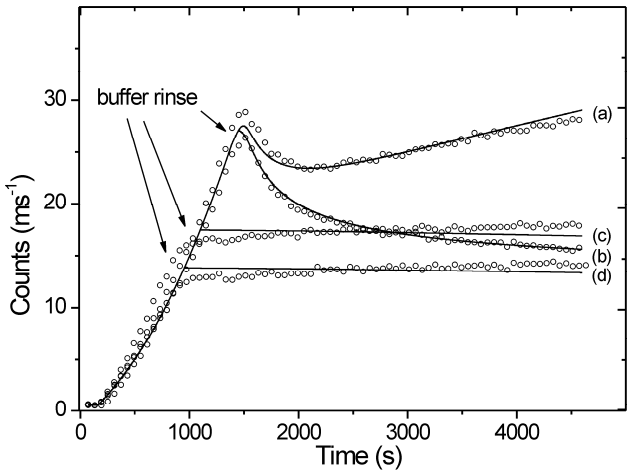

Fig. 7.3. Desorption behavior of β-Lg. Curve a represents the reference adsorption kinetics measured without desorption at 5×10^{-8} M (circles). Rinsing with protein-free buffer was performed in three separate experiments after 1450s (b), 1100s (c) 900s (d), (solid arrows). The solid lines represent the calculated kinetics.

An efficient approach to probe the fate of the initially adsorbed proteins is to replace the labeled proteins by an equally concentrated solution of unlabeled proteins in the beginning of the adsorption (Fig. 7.4 A). The surface coverage continues to grow at the same rate as before but only the behavior of the labeled molecules which were adsorbed on the surface prior to rinsing is visible. That means the system represented by curve c in Fig. 7.4 A is exactly in the same state as presented by the reference curve (a) but the unlabeled proteins adsorbing on the surface are invisible. During the first minutes after starting the adsorption of unlabeled proteins the fluorescence intensity practically remains on a constant level confirming that the initially adsorbed molecules bind irreversibly to the surface. However, due to the adsorption of unlabeled β-Lg the system also reaches the state in which the critical coverage is exceeded. At this point the transition process is triggered affecting all surface bound proteins including the initially adsorbed labeled proteins. As a consequence, a partial desorption of the initial species is observed proving that proteins adsorbed in the beginning must be affected by the transition from the irreversible to the reversible state. To provide experimental certainty on this issue a slightly modified experiment was performed that confirms the proposed transition behavior (Fig. 7.4 A, curve b). Here, the labeled protein solution is firstly replaced by protein-free buffer leading to no visible change of the coverage level for almost one hour. Thereafter, unlabeled protein solution replaces the protein-free buffer which leads to the transition of the irreversibly adsorbed proteins into the reversible state and causes the observable desorption. Note that this happens not right at the point when the unlabeled protein solution is added but a few minutes later namely at the point where the added proteins have increased the total

coverage up to the critical coverage level. The complementary experiment in which firstly unlabeled and secondly labeled proteins were adsorbed onto the surface is shown in Fig. 7.4 B (curves b, c). As expected, the overshooting behavior is only observed if labeled proteins are added before the critical coverage is reached (curve b), otherwise the exponential-like behavior occurring after the overshoot is observed (curve c). As discussed before this experiment also proves the equal behavior of fluorophore-labeled and native proteins (see also Fig. 4.4). Thus, the overshooting is definitely not a phenomenon which is restricted to labeled proteins. It is worth to mention that abruptly increasing protein desorption rates as a result of crowding on the surface has been observed during the adsorption of the protein Fibronectin (440 kDa) before.[129] However, it has not been formulated that his phenomenon occurs at a certain critical surface density.

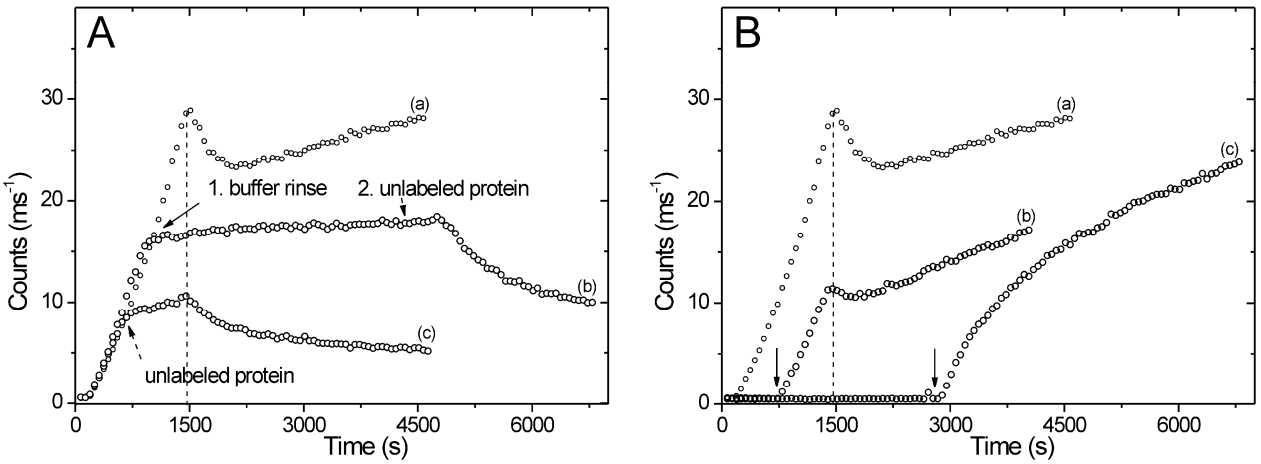

Fig. 7.4. A) Adsorption of labeled and unlabeled β-Lg. Curve a is the reference curve, curve b was obtained after first rinsing with protein-free buffer (solid arrow) and second applying unlabeled proteins (dashed arrow). Curve c was obtained by replacing labeled with unlabeled proteins (dashed arrow).
B) Adsorption of unlabeled and labeled proteins. Unlabeled proteins were adsorbed for 750 s (curve b) and 3000 s (curve c) and subsequently replaced by labeled proteins (arrows).

The transition of the surface affinity from tight and irreversible to loose and reversible is also the key process explaining the overshooting behavior during the adsorption. Since the observable desorption behavior changes abruptly, the transition between the two states must be much faster than the desorption process. For this reason the surface suddenly is populated with a large fraction of reversibly bound proteins which then desorb within a short period of time. Provided that the bulk protein concentration is not too high the desorption (off-)rate exceeds the adsorption (on-)rate at this stage leading to a temporal decrease of the total

coverage. In the following the on-rate remains constant due to a constant bulk concentration whereas the off-rate decreases with the depletion of reversibly bound proteins on the surface. Therefore, the overall coverage passes a minimum before it continues to grow again with a significantly slower rate that is now the sum of adsorption and desorption rate (see Fig. 7.4 B, curve c). As shown before there is also a slow relaxation of the reversible state to a strongly bound final state such that the fraction of reversibly bound proteins further decreases. The adsorption kinetics after the overshoot are exponential-like and show no evidence for cooperative effects. In the final stage the surface is mainly populated with the relaxed state of the protein.

7.2 Modeling

Based on the experimental observations discussed in the preceding paragraph a mathematical model is developed that describes the adsorption and desorption behavior of β-Lg in the given conditions. To work out the most important characteristics of the adsorption process the model is required to be as simple as possible with a minimum of different adsorbed states and surface processes. During the rinsing experiments presented in Fig. 7.1 A and Fig. 7.3 it was recognized that there are three different desorption behaviors in different stages of the adsorption process. Accordingly, it is proposed that the surface bound proteins can adopt three different states. At low surface coverage β-Lg mainly adsorbs in an essentially irreversible initial state (init) which does not desorb in the presence of protein-free buffer (see Fig. 7.3, curves c, d). Beyond the critical coverage, proteins transform into a reversible state (rev) with a relatively high desorption rate constant (see Fig. 7.3, curve b). In the long term, the reversible species is found to relax into an almost irreversible state with a quite low desorption rate constant (see Fig. 7.1 A) which is simply referred to as the irreversible state (irr). In agreement to the experimental observation the whole adsorption process can be characterized by dividing it into three stages which are illustrated schematically in Fig. 7.5.

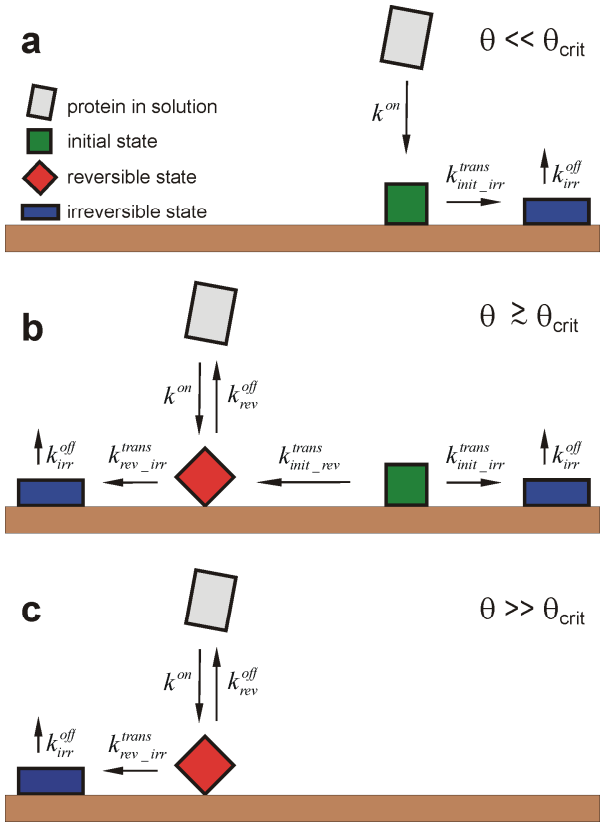

Fig. 7.5. Schematic representation of the kinetic model at different stages of the adsorption process: (a) in the beginning ($\theta << \theta_{crit}$), (b) around the critical coverage ($\theta \sim \theta_{crit}$), (c) after long term adsorption ($\theta >> \theta_{crit}$). Note that only processes occurring directly on or very close to the surface are depicted.

In the first stage which comprises the period between start and overshoot the adsorption proceeds at low surface densities. This may last a few minutes at high bulk concentrations and up to several hours at low concentrations. Since the surface density in the beginning is rather low, any kind of lateral interaction between bound proteins is regarded as negligible and the adsorption of proteins in the initial state is the predominant process. The initial species is then allowed to slowly convert into the final irreversible state via structural re-orientations described by the transition rate constant $k_{init\_irr}^{trans}$. In the second stage of the adsorption the surface density has increased to an extent that lateral interactions between adsorbed proteins are no longer insignificant. From experimental data it can be concluded that the initial state abruptly becomes energetically disfavored whereas the reversible state turns into the preferred one. This causes a transition of the surface bound proteins from the initial to the reversible state. The data fits reveal a relatively high transition rate constant ($k_{init\_rev}^{trans}$) for this process implying a low free energy barrier between the two states. For this reason comprehensive

intramolecular reorganizations within the protein are not expected. Typically, such structural changes during the transition are found to proceed slowly.[108, 206] In agreement with other published results it is conceivable that the initial and the reversible state simply represent two different possible orientations of the protein which differ in their surface affinity.[41, 72, 77] As soon as the initial state is energetically disfavored the proteins are expected to no longer approach the surface in the initial but directly in the reversible state. This probably happens because the negatively charged surface and the adsorbed proteins create a complex potential energy landscape which forces the incoming molecules to adopt a specific state once they are in close proximity to the surface.[72] Surely, the force field has no influence on the proteins diffusing farther away in the bulk volume where the electrostatic field is screened by charged and polar molecules present in the vicinity of the interface. As is discussed in the context of potential alternative models in the following section it is found that proteins practically exclusively adsorb either in the initial or in the reversible state depending on the surface density. This means, proteins coming close to the surface adopt the initial state at low coverages and the reversible state at coverages beyond the critical surface density. An analogous behavior was also concluded from computational studies which suggest that prior to adsorption proteins are forced to adopt a certain preferred orientation through the long-range interactions between adsorbing and pre-adsorbed proteins.[33, 34] After completion of the transition from the initial to the reversible state the model implies that practically no protein in the initial state is left on the surface. In the following third stage the predominant process is the adsorption of proteins in the reversible state and their slow relaxation into the final irreversible state described by $k_{rev\_irr}^{trans}$. An additional direct adsorption of the irreversible species as proposed in some other models[23, 25] was not considered because the quality of the fit of the experimental data did not improve significantly when this pathway was included into the model. The following rate equation system is used to express the observed behavior.

$$\frac{\mathrm{d}\theta_{init}}{\mathrm{d}t} = k^{on} \cdot c \cdot \Phi - k_{init\_irr}^{trans} \cdot \theta_{init}\,, \qquad \theta \le \theta_{crit} \qquad (7.1)$$

$$\frac{\mathrm{d}\theta_{init}}{\mathrm{d}t} = -k_{init\_rev}^{trans} \cdot \theta_{init} - k_{init\_irr}^{trans} \cdot \theta_{init}\,, \qquad \theta > \theta_{crit} \qquad (7.2)$$

$$\frac{\mathrm{d}\theta_{rev}}{\mathrm{d}t} = 0\,, \qquad \theta \le \theta_{crit} \qquad (7.3)$$

$$\frac{\mathrm{d}\theta_{rev}}{\mathrm{d}t} = k^{on} \cdot c \cdot \Phi + k^{trans}_{init\_rev} \cdot \theta_{init} - k^{trans}_{rev\_irr} \cdot \theta_{rev} - k^{off}_{rev} \cdot \theta_{rev}, \quad \theta > \theta_{crit} \tag{7.4}$$

$$\frac{\mathrm{d}\theta_{irr}}{\mathrm{d}t} = k^{trans}_{init\_irr} \cdot \theta_{init} + k^{trans}_{rev\_irr} \cdot \theta_{rev} - k^{off}_{irr} \cdot \theta_{irr} \tag{7.5}$$

$$\theta = \theta_{init} + \theta_{rev} + \theta_{irr} \tag{7.6}$$

$$\Phi = 1 - \frac{\theta}{\theta_{\max}} \tag{7.7}$$

To account for the sudden change of the processes taking place before and after reaching the critical surface density, the rate equations for the initial and the reversible state are defined for the two cases that $\theta \leq \theta_{crit}$ and $\theta > \theta_{crit}$. In these equations c represents the concentrations of the proteins located in close proximity to the surface. θ_{init}, θ_{rev}, and θ_{irr} denote the amount of surface bound proteins in the initial, reversible, and irreversible state in units of counts × ms^{-1}, θ is the sum of all states, hence the measurable surface coverage. Φ refers to the available surface function which is approximately described by the ratio between uncovered surface and maximum available surface. Surface exclusion effects as discussed in Chapter 5 were not included as their influence on the data fits turned out to be negligible.

The abrupt change of the adsorption processes taking place before and after the critical surface density as defined by equations (7.1) - (7.4) implies that there is a sudden inversion of the free energy difference between the initial and the reversible state. This means that energetically the initial state becomes unstable and the reversible state turns into the favoured one. Although this concept is a simplistic description it gives acceptable results. The bulk proteins approaching the surface are expected to easily transform into a specific state which is most probably nothing else than a different orientation. Thus, this process has no rate-limiting effect. The transition between the initial and the reversible state that takes place on the surface, by contrast, is slower compared to the adoption of the reversible state in the solution and therefore has an important influence on the adsorption kinetics. Again, this can be explained by a protein re-orientation that is certainly connected with a higher energy barrier on the surface than in the solution. It has been shown by statistical mechanical approaches that the free energy difference of two different adsorbed states as a function of the surface coverage can only be calculated approximately due to a vast number of contributing parameters.[60, 65, 208]

The equations discussed so far allow to explain the observed phenomena encountered during the non-specific adsorption of β-Lg in the chosen conditions. However, in order to yield satisfying agreement between model and experimental data several refinements which account for frequently observed lateral interactions need to be included.[73-75] As discussed before, the most obvious effect where the interaction between adsorbed proteins plays an important role is the increasing adsorption rate in the first stage. Clearly, this feature is easiest observed at low bulk concentrations and rather poorly resolved when the kinetics are measured at high protein concentrations where the adsorption proceeds very fast. Since an increasing adsorption rate is only observable in the first stage of the adsorption the on-rate constant is set to depend linearly on the number of proteins adsorbed in the initial state. This formalism is equivalent to the concept developed in Chapter 5 (see equations (5.1) - (5.3)).

$$k^{on} = k_0^{on} + c_1 \cdot \frac{\theta_{init}}{\theta_{max}} \tag{7.8}$$

In this equation k_0^{on} denotes the on-rate constant in the absence of positive cooperative effects which is encountered in the beginning when the surface is uncovered and c_1 describes the increase of the adsorption rate with the growing coverage of proteins in the initial stage. Referring to the notation used in Chapter 5 k_0^{on} is equal to k_1^{on} (Langmuir-type adsorption pathway) and c_1 is equal to k_2^{on} (cooperative adsorption pathway). Note that this is only true during the first stage of the adsorption, i.e., before the overshoot takes place.

As shown in Fig. 7.1 B the desorption rate is influenced by the bulk protein concentration. There are two main ideas in the literature to implement this concentration dependent off-rate into mathematical models. On the one hand an exchange mechanism between adsorbing and bound proteins is proposed[109] whereas on the other hand the desorption rate constant was set to be a function of the surface coverage.[73-75] In the present work the best results were obtained using a linear dependency of the desorption rate on the total surface coverage.

$$k_{rev}^{off} = k_{rev,0}^{off} + c_2 \cdot \frac{\theta_{rev}}{\theta_{max}} \tag{7.9}$$

In analogy to equation (7.8) $k_{rev,0}^{off}$ refers to the off-rate constant in the absence of adsorbed proteins whereas c_2 accounts for increasing repulsions at growing densities.

Lateral interactions between adsorbed proteins are also envisaged during the transition from the initial to the reversible state. It is important to note that the peak widths of the overshoots presented in Fig. 7.2 increase as the applied bulk concentrations decrease. This is best explained by assuming that the transition is induced by the surrounding adsorbed proteins. Furthermore, the rinsing experiments presented in Fig. 7.3 prove that the process is irreversible. That means the reverse direction of the transition does not occur which is in agreement with similar published observations.[77] Hence, the transition continues until no more molecules in the initial state are left on the surface once the process has started. This behavior is modeled by introducing a transition rate constant that is proportional to the coverage of proteins in the reversible state.

$$k_{init\_rev}^{trans} = c_3 \cdot \frac{\theta_{rev}}{\theta_{max}} \tag{7.10}$$

At the point where the total coverage exceeds the critical coverage proteins start to adsorb in the reversible state and induce the transition of the initially adsorbed proteins. The more reversible proteins attach to the surface the faster the initially adsorbed proteins transform into the new state. In this respect θ_{crit} can be regarded as the maximum total surface coverage up to which all adsorbed proteins remain on the surface in the initial state even if rinsing with protein-free buffer is performed. If, on the other side, the critical coverage is exceeded rinsing essentially results in the desorption of proteins because of the transition from the initial into the reversible state (see Fig. 7.3).

A comparable coverage dependency is observed for the transition of the reversible state to the irreversible state.

$$k_{rev\_irr}^{trans} = c_4 \cdot \frac{\theta_{rev}}{\theta_{max}} \tag{7.11}$$

The third transition rate constant, $k_{init\_irr}^{trans}$, was assumed to be coverage independent because the corresponding process is only relevant in the first stage of the adsorption where the absolute surface density is low.

7.3 Curve fitting

The mathematical description of the adsorption mechanism found in this work is a combination of known and new concepts into one single model describing all phenomena observed during the kinetic measurements rather than concentrating only on selected features. This is an important difference to the model proposed in Chapter 5 which only focuses on the cooperative adsorption behavior. In the often encountered case that the adsorption is completely irreversible the rate equations reduce to a relatively simple algebraic expression for the adsorption rate as a function of the surface coverage (equation (5.8)) which allows a fast parameter estimation applying the least-squares fitting method. In the model proposed in this Chapter, by contrast, cooperative effects are only one feature among others, such as transitions between different states. As a consequence, the adsorption rate is a non-trivial function of three arguments (θ_{init}, θ_{rev}, θ_{irr}) which can not be described with an algebraic expression. Thus, the fitting procedure is more complicated and involves the numerical integration of all rate equations after each parameter variation. Fig. 7.6 A shows calculated adsorption kinetics for 10 different bulk protein concentrations (1×10^{-8} M – 1.5×10^{-6} M) using one set of parameters. It shows nicely how the overshoot visible at low concentrations continuously transforms into a sort of kink when the concentration is increased. Fig. 7.6 B presents the rate coverage plots of some chosen adsorption kinetics of Fig. 7.6 A to illustrate that the rate can not be expressed as a function of the total coverage as was done in Chapter 5.

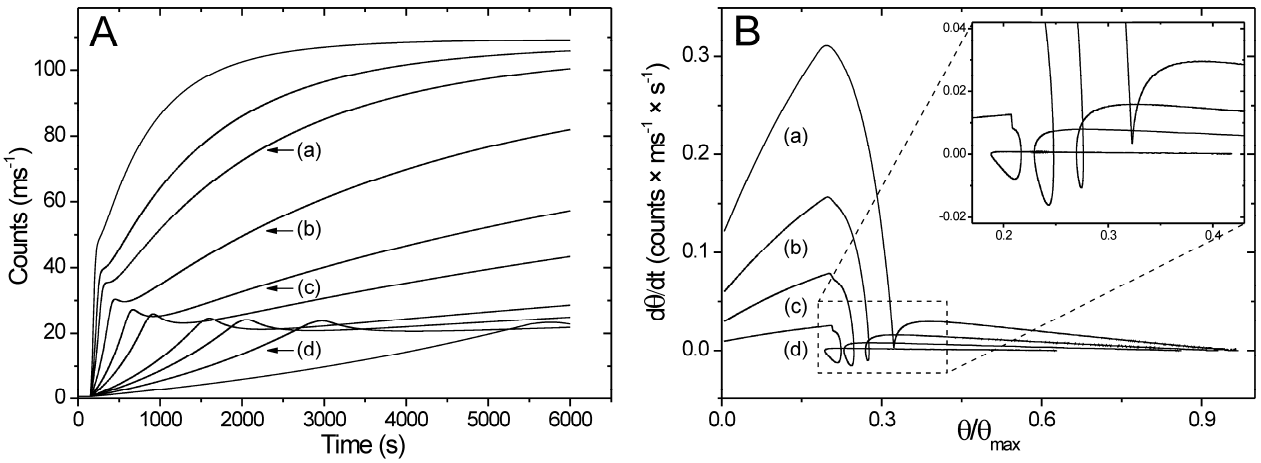

Fig. 7.6. A) Calculated adsorption kinetics for bulk protein concentrations varying between 1×10^{-8} M and 1.5×10^{-6} M. The model is in perfect agreement with the experimental observations that the overshoot is clearly visible at low bulk concentrations and vanishes at higher concentrations.
B) Rate-coverage plot for 4 selected kinetics. The rate can not be expressed as a function of the total coverage.

To obtain protein adsorption kinetics from the proposed model a numerical integration of the system of rate equations defined by equations (7.1) - (7.7) was necessary. Suitable values for the implemented parameters valid for all bulk concentrations had to be found. Therefore, five representative data sets were chosen for which the parameters were optimized individually applying the least-squares fitting method. In the low concentration range the adsorption kinetics measured at 2.0×10^{-8} M and 4.0×10^{-8} M were used to optimize all parameters except the saturation level θ_{max}. This level is not sufficiently approached within the measured time. In the high concentration range three adsorption curves measured at 0.75×10^{-6} M were used. In this case some processes that are important at low concentrations such as the increase of the adsorption rate in the beginning are very fast and therefore poorly resolved. For this reason the values of the corresponding parameters, namely c_1, $k_{init\_rev}^{trans}$, and $k_{rev,0}^{off}$, were taken from the fit in the low concentration range and set as invariable. All five data sets were composed of adsorption and desorption kinetics as rinsing with protein-free buffer was performed after varying adsorption time periods. The bulk protein concentration was set to zero at the point when rinsing was started to obtain the desorption curves. Including desorption kinetics into the parameter estimation procedure allowed to more accurately determine desorption and transition rate constants as the adsorption rate was zero during rinsing experiments. An appropriate initial guess for the parameter estimation was obtained by an iterative approximation of the calculated kinetics to the respective data set. Therefore, the parameters were fitted individually in a cyclic iteration until a good overlap was obtained. Afterwards, all variables were optimized for each of the five data sets. Using the mean value of each parameter over the five fits which are listed in Table 7.1 the kinetics of all bulk concentrations were calculated. However, the adsorption rate constant k_0^{on} and the critical surface coverage θ_{crit} were not averaged but fitted individually to the data sets and are summarized in Table 7.2. This turned out to be necessary because these two variables were very sensitive to the surface chemistry and topology which are generally difficult to keep constant from one measurement to the next.[184]

Once all parameters were determined the adsorption kinetics of the total coverage as well as the kinetics of the initial, reversible, and irreversible state could be computed at any desired bulk protein concentration. Fig. 7.7 A depicts the contribution of the three states to the measurable total surface coverage for the adsorption of a 4×10^{-8} M β-Lg solution. In the figures shown before (Fig. 7.1 A, Fig. 7.2, and Fig. 7.3) the calculated total coverage as a

function of time (solid lines) was added to the experimental data (circles). The excellent accordance between model and experiment is obvious and also clearly reflected by the coefficients of determination of the individual data sets (see Table 7.2). Only in the lowest concentration range the prediction of the model slightly deviates from experimental data. In that case the adsorption process is very slow and additional side effects might have a stronger influence.

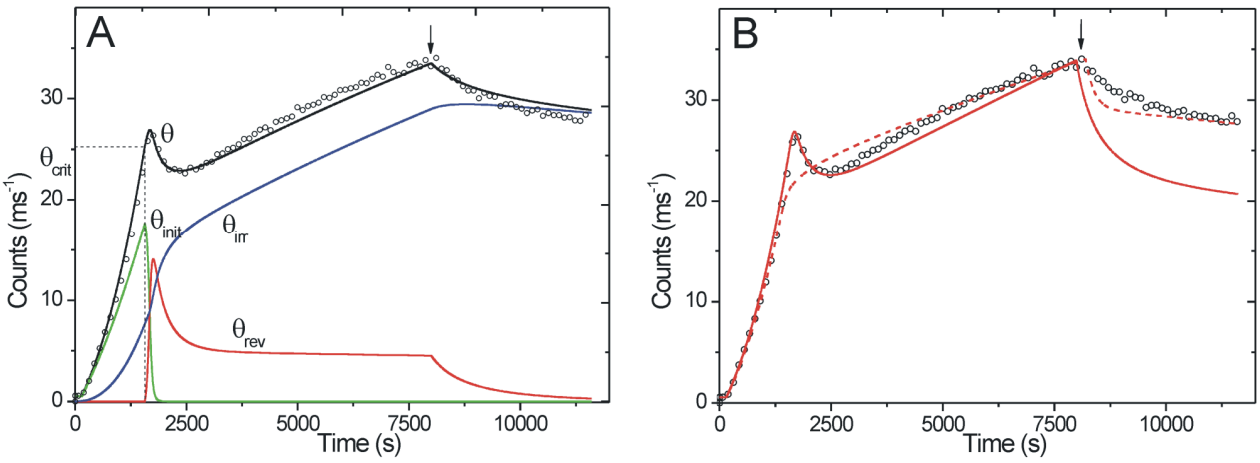

Fig. 7.7. A) Presentation of the kinetic model. The plot shows the contribution of the initial (green line), the reversible (red line), and the irreversible (blue line) state to the total coverage (black line) calculated for a bulk protein concentration of 4.0×10^{-8} M. The kinetics of the total coverage are compared to experimental data (circles).
B) Calculated adsorption and desorption kinetics of an alternative model in which the direct adsorption of proteins in the reversible state is forbidden. This alternative model may either fit correctly the overshooting behavior (red, solid line) or the behavior upon buffer rinse (red, dashed line) but not both features with the same set of parameters. Arrows mark the point in time when rinsing was started.

7.4 Alternative Models

The comparison of experimental data with the prediction of other models is also a strong argument to exclude several alternatives. This is demonstrated for one example in which the direct adsorption of proteins in the reversible state is excluded. In this case only the transition on the surface converting the initial to the reversible state is allowed (Fig. 7.7 B). As the corresponding plot outlines clearly, the model overestimates the desorption rate when rinsing is performed after a relatively long adsorption time although the shape of the overshoot matches perfectly (red, dashed line in Fig. 7.7 B). If, on the other hand, the parameters were changed such as to better predict the desorption behavior the curve would exhibit no

overshoot (red, solid line in Fig. 7.7 B). A similar argument justifies the path in the model that allows proteins adsorbed in the initial state to directly convert into the irreversible state without passing the reversible state. This transition must be included because the minima after the overshoots in the low concentration range would be too deep if there were only reversibly attached proteins at the time when the overshoot takes place. Naturally, the insertion of additional paths or even states, like different irreversible states, would further improve the quality of the fits. However, it was decided not to implement further processes whose benefit on the quality of the fit was too small to justify the addition of a further parameter. However, a simpler model containing for instance only two instead of three different states of adsorbed proteins could not satisfactorily explain the experimental data.

Table 7.1. Estimated parameters I. Using five representative data sets all fitted parameters except k_0^{on} and θ_{crit} were averaged and used for the calculations of the binding kinetics.

c_{bulk} (10^{-8} M)	Rinsing[a] (s)	θ_{max} (counts×ms^{-1})	k_{irr}^{off} (10^{-6} s^{-1})	$k_{rev,0}^{off}$ (10^{-6} s^{-1})	$k_{init\_irr}^{trans}$ (10^{-6} s^{-1})	c_1 (counts×ms^{-1} ×M^{-1}×s^{-1})	c_2 (10^{-3} s^{-1})	c_3 (10^{-3} s^{-1})	c_4 (10^{-3} s^{-1})
2.0	8000	110.0[b]	14.6	531.1	693.5	12.65	8.222	172.1	11.18
4.0	8000	110.0[b]	14.1	530.3	612.7	12.54	8.770	164.0	10.51
0.75	750	110.0[b]	13.3	530.7[b]	653.1[b]	12.59[b]	9.247	182.7	12.87
0.75	3500	110.2	13.3	530.7[b]	653.1[b]	12.59[b]	9.392	197.8	12.67
0.75	10000	111.3	12.5	530.7[b]	653.1[b]	12.59[b]	9.381	216.7	12.94
Mean[c]		111	14	531	653	12.6	9.00	187	12.0
STDV[c]		1	1	1	57	0.1	0.51	21	1.1

[a] Point in time when protein solution was replaced by buffer.
[b] Parameters were set as constant and not included into the calculation of mean values.
[c] Rounded values.

Table 7.2. Estimated parameters II. k_0^{on} and θ_{crit} were determined for all applied bulk concentrations individually.

c_{bulk} (M)	Rinsing[a] (s)	k_0^{on} (10^5 counts×ms^{-1} ×M^{-1}×s^{-1})	θ_{crit} (counts×ms^{-1})	R^2	Plot
0.5×10^{-8}	-	2.510	20.50	0.979	Fig. 7.2 B, d
1.0×10^{-8}	-	2.579	22.97	0.990	Fig. 7.2 B, c
2.0×10^{-8}	8000	2.596	24.21	0.988	Fig. 7.2 B, b
4.0×10^{-8}	8000	2.235	25.28	0.989	Fig. 7.2 B, a
5.0×10^{-8}	-	2.112	25.70	0.992	Fig. 7.3
0.125×10^{-6}	-	2.341	20.67	0.993	Fig. 7.2 A, e
0.25×10^{-6}	-	2.549	24.98	0.997	Fig. 7.2 A, d
0.5×10^{-6}	-	2.070	21.70	0.998	Fig. 7.2 A, c
0.75×10^{-6}	-	2.205	21.34	0.996	Fig. 7.2 A, b
1.5×10^{-6}	-	2.162	21.75	0.998	Fig. 7.2 A, a
0.75×10^{-6}	400	2.205[b]	21.34[b]	0.869	Fig. 7.1 A, g
0.75×10^{-6}	700	2.205[b]	21.34[b]	0.959	Fig. 7.1 A, f
0.75×10^{-6}	1100	2.205[b]	21.34[b]	0.943	Fig. 7.1 A, e
0.75×10^{-6}	1800	2.205[b]	21.34[b]	0.961	Fig. 7.1 A, d
0.75×10^{-6}	3500	2.205[b]	21.34[b]	0.998	Fig. 7.1 A, c
0.75×10^{-6}	6000	2.205[b]	21.34[b]	0.979	Fig. 7.1 A, b
0.75×10^{-6}	10000	2.205[b]	21.34[b]	0.989	Fig. 7.1 A, a
Mean[c]		2.34	22.9		
STDV[c]		0.21	2.0		

[a] Point in time when protein solution was replaced by buffer.
[b] Parameters were set as constant and not included into the calculation of mean values.
[c] Rounded values.

7.5 Conclusion

The non-specific adsorption of β-Lg, a model protein of intermediate size, was investigated on a hydrophilic surface in acidic buffer. Measurements in a broad concentration range (0.5×10^{-8} M - 1.5×10^{-6} M) and various rinsing experiments yielded a large set of information which served to develop a full mathematical model of the adsorption behavior of this protein. To account for the observable differences in the desorption behavior the model comprises three states of adsorbed proteins. In the beginning all proteins adsorb in an irreversible initial state on the surface. Once the critical surface density is exceeded the molecules approaching the surface undergo a transformation and adsorb in the reversible state. At the same time all surface bound proteins in the initial state start to transform into the reversible state. In the long term surface bound proteins slowly relax into a final and almost irreversible state.

One key finding of the present work is that non-specifically adsorbed proteins do interact with each other which has a direct influence on the adsorption, desorption, and transition rates during the course of adsorption. As a consequence, principal properties of adsorbed proteins like the reversibility and the conformation or orientation change with the growing surface density. In this respect the concept of a critical surface density (θ_{crit}) was introduced where the surface affinity of adsorbed proteins changes abruptly. Experimental evidence for the existence of θ_{crit} was provided in the present work by rinsing experiments conducted with either protein-free buffer or unlabeled protein solutions. The proposed model nicely confirmed that the abrupt alteration of the desorption behavior necessarily causes an overshoot in the adsorption curve. Further it has been shown that there is a slow transition from the reversible to a relaxed and almost irreversible state caused by a conformational re-orientation which is a typical effect during non-specific adsorption processes. In addition to this well known phenomenon, the proposed model reveals that the transition rate from the reversible to the irreversible state is influenced by lateral interactions of adsorbed proteins. Thus not only the initial adsorption rate increases due to the influence of pre-adsorbed proteins as was discussed for the protein BSA in Chapter 5. To this end the proposed model of the present study implies that cooperative effects can be of diverse nature affecting adsorption, transition, and desorption rates.

To set a reasonable framework of the experimental work, this study was designed to focus on the most important parameter, namely the bulk protein concentration, and to keep all other parameters, such as pH, ionic strength, temperature, or surface conditions fixed. For this reason transferring the conclusion of this work to other systems must be done with care. However, it is generally accepted that regardless the surrounding pH proteins usually contain charged residues such that electrostatic interactions play an important role in practically all non-specific adsorption events.[32, 209, 210] Thus, the understanding of elementary processes and phenomena in the studied system certainly contributes to a deeper insight into the complex and controversy field of non-specific protein adsorption in general.

8 Protein Aggregates on Surfaces*

As stated already several times protein adsorption phenomena are usually a combination of the individual behavior of isolated proteins and the behavior of proteins acting in an ensemble. In Chapter 5 and 6 the ensemble effect of cooperativity was discussed in detail. One of the consequences found was the preferred organization into patches of high protein density whereas a contact between surface adsorbed proteins was ruled out for the applied conditions. In the following Chapter model systems with other specific conditions are presented in which protein aggregation mechanisms and peculiarities can be studied. As is schematically illustrated in Fig. 8.1 protein aggregation can be a process of antithetic facets. On the one hand aggregates can evolve in the solution and subsequently deposit onto the surface (Fig. 8.1 A). Such a scenario was found for BSA at very low bulk concentrations in an acidic buffer. On the other hand, protein aggregation can proceed directly on the surface (Fig. 8.1 B). In this case proteins do touch each other which is in contrast to the protein patches (Fig. 8.1 C) that were identified to be a result of cooperative adsorption. On-surface growth of protein aggregates was found for the protein α-Synuclein (α-Syn) at low bulk concentrations and under neutral pH conditions. It is, of course, natural that the processes depicted in Fig. 8.1 are accompanied by the simultaneous adsorption of protein monomers (Fig. 8.1 D). The most efficient way to suppress the influence of this process is to reduce the bulk concentration to a minimum.

* The results of this chapter were partially published in: M. Rabe, D. Verdes and S. Seeger, *Soft Matter,* 2009, **5**, 1039-1047.

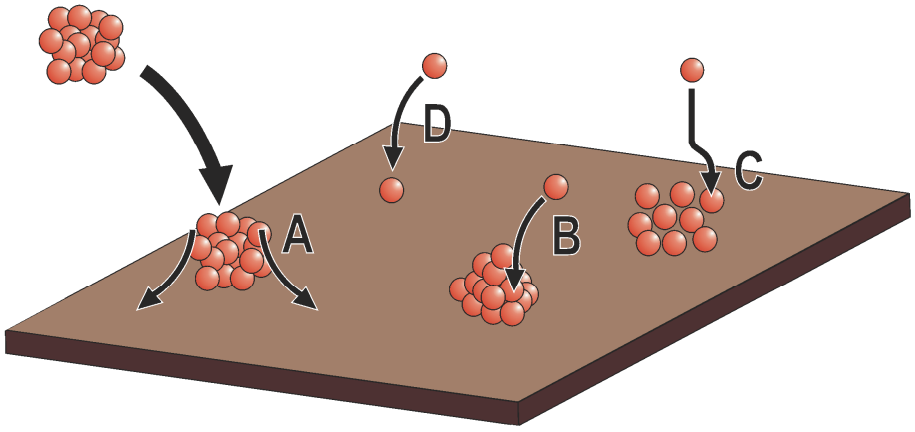

Fig. 8.1. Schematic illustration of protein aggregation events. Aggregates can evolve in the solution and deposit afterwards onto the surface (A). Alternatively, proteins can aggregate directly on the surface (B). As a comparison the formation of protein patches is not considered as a real aggregation (C). The adsorption of protein monomers is an accompanying process (D).

8.1 Detection of BSA clusters

During the previous experimental work on protein adsorption it was noticed that the plasma protein bovine serum albumin (BSA) has a tendency to form surface aggregates under acidic pH and moderate ionic strength conditions. This effect was only observable when low bulk protein concentrations (1 nM) were used. Additionally, a certain equilibration time of the protein solution of a few hours prior to the adsorption experiment turned out to be crucial. Ideal conditions to promote the formation of adequate quantities of BSA clusters were the use of citrate buffer at pH 3 and 50 mM ionic strength and a bulk concentration of 1 nM. At acidic pH the protein BSA is known to be unfolded,[211] which is a frequently reported requirement for protein aggregation processes.[94, 212] However, protein clusters were also observed at pH 5 and pH 6. Reducing the buffer ionic strength from 50 mM to 5 mM results in a significant decrease of the number of detectable clusters due to increased lateral repulsions when the protein's charge is less shielded.[31, 213, 214] Images of Cy5-labeled BSA clusters on a 60 µm × 60 µm area were recorded at different times with the SAF microscope (Fig. 8.2), and showed protein clusters on the surface as spots of high fluorescence intensity indicating the presence of several fluorophores within a small region of the scan image.

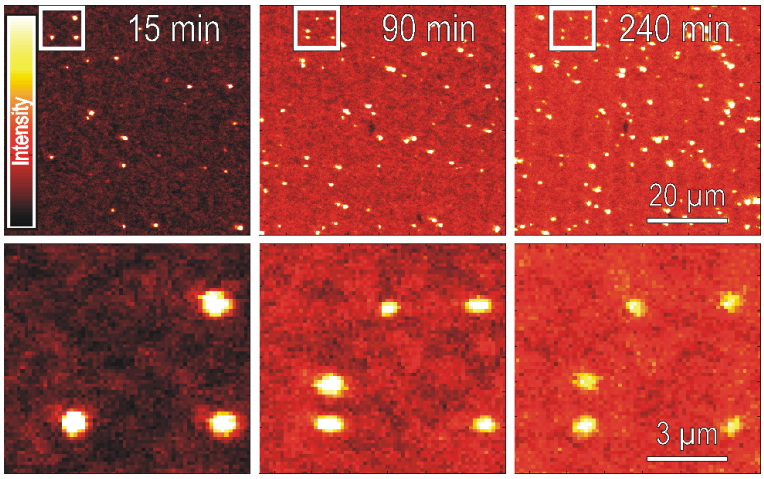

Fig. 8.2. Adsorption of Cy5-labeled BSA (1 nM) in citrate buffer, pH 3, (50 mM) onto a hydrophilic glass surface after 15, 90, and 240 min. Protein clusters are detected as bright spots. Over time, the background layer of protein monomers becomes dense. The lower row shows magnifications of the section marked by the white square in the upper row.

These clusters appeared very static upon adsorption, with no lateral movement observed on the surface. Rinsing experiments established that protein clusters did not desorb from the surface at buffer conditions of either pH 3 or pH 6. The total number of clusters increased over time while the fluorescence intensity of the individual clusters remained practically constant or even decreased slightly as a result of photobleaching after several scanning cycles (see Fig. 8.2, lower row). Hence, the continued aggregation of monomers onto surface bound clusters was not observed. Due to a constant supply of protein solution through the flow cell, the cluster deposition was accompanied by the continuous adsorption of protein monomers, resulting in an increase of the background fluorescence in time.

To determine whether the detected clusters are protein assemblies that have grown on the surface or whether they are aggregates that deposited directly from the solution onto the surface, the evolution of the cluster size, i.e., the fluorescence intensity of all proteins belonging to one cluster, was observed by repeatedly scanning the same area (15 µm × 15 µm). The monomer solution was composed of only one part (0.1 nM) Cy5-labeled protein and nine parts (0.9 nM) unlabeled protein. In this way the probability that two labeled proteins come into contact with each other inside a cluster generated from this composition was reduced and thus the risk of mutual quenching effects between adjacent Cy5 molecules was minimized.[170] The integrated intensity in the scan site area rose in a single step and remained steady over the following 30 min, indicating that the cluster was grown in the solution (Fig. 8.3). A second experiment in which only one line of the surface was scanned

(time resolution: 0.9 s) showed that clusters appeared suddenly on the surface, indicating that their formation on the surface was practically impossible under the given conditions. A magnified view of the site showed a sudden intensity jump above the background level to the maximum level from one line to the next as the clusters deposited on the surface (Fig. 8.3, inset). Due to photobleaching processes resulting from the frequent laser excitation, the intensities of the scanned clusters decayed over time. The step-like appearance of the protein clusters on the surface implied that the aggregation of proteins in this system is not a surface-induced process as previously reported.[88, 89] Rather, protein clusters form in the buffer solution under these conditions and then adsorb onto the surface. The absence of an increase in fluorescence intensity of the clusters within either 30 min (Fig. 8.3) or 240 min (Fig. 8.2) indicated that there was no growth of the clusters on the surface. Calibration of the fluorescence intensity indicated that the average cluster size was in the range of several hundreds of monomers.

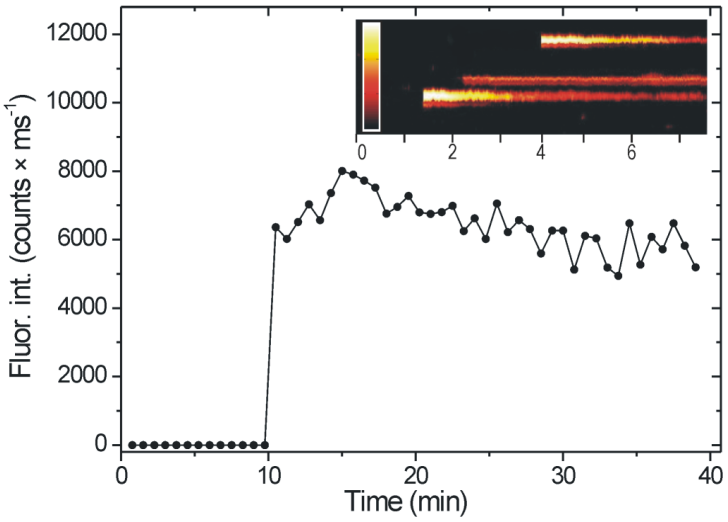

Fig. 8.3. Integrated fluorescence intensity of all pixels belonging to one protein cluster as a function of time (time resolution: 45s). The step-like intensity jump suggests a direct deposition of the cluster from the solution onto the surface; the intensity decrease afterwards results from photobleaching. Inset: Repeated scan of one single line (1 line per 0.9 s). The intensity increases suddenly when a protein cluster deposits on the surface.

8.2 FRET imaging of BSA clusters

Protein clusters can be easily detected when the surface is sparsely covered with monomer proteins (see Fig. 8.2). However, as the background layer became denser, the border between

clusters and protein monolayer was indistinct which, in turn, concealed the exact information about the cluster size. Possibly, small protein clusters may even be screened by the background layer and hence are not detectable. Additionally, direct fluorescence detection does not allow to extract any information about intermolecular distances between aggregated proteins within a cluster. A powerful technique to overcome these limitations is Förster resonance energy transfer (FRET) imaging. Herein, a mixture of equal quantities of Cy5-labeled BSA and Cy7-labeled BSA with dye/protein ratios of approximately 3:1 is prepared to ensure the aggregation of donor- and acceptor labeled monomers in one cluster. The FRET pair Cy5/Cy7 exhibits a Förster radius of 7.15 nm, assuming freely rotating dipole moments, and is excited at 635 nm. The fluorescence emission is split into donor and acceptor fluorescence signals which serve for the calculation of the FRET image (Fig. 8.4). The protein clusters clearly exhibit an energy transfer yielding a strong signal in the acceptor channel. The background monolayer, by contrast, shows practically no detectable energy transfer and is consequently only detectable in the donor channel. Even at the saturation level of the BSA monolayer, the average donor-acceptor distance between surface bound proteins is too large to observe a significant energy transfer (data not shown). Thus, the distance between the protein bound dye pairs is much larger than the Förster radius. As was discussed in Chapter 5 BSA is known to adsorb in a relatively loose package onto interfaces under the applied conditions, such that the proteins are not in contact with each other.[42, 50] Within a protein cluster, however, the molecules are tightly packed and are in contact with each other. Given that the axes dimensions of BSA are 4 nm × 14 nm (prolate spheroidal)[165] and that, on average, each BSA molecule is labeled with three donor or acceptor dye molecules, the spacing between dye pairs is certainly within the range of 1 nm to 10 nm. The high energy transfer rates within protein clusters and the absence of energy transfer between surface bound monomers is exploited to differentiate between clusters and the background layer. Signals that are only detected in the donor channel can be assigned to loosely distributed monomers, whereas all signals that are detected in both the donor and the acceptor channels can be assigned to protein clusters. From the magnified sections in Fig. 8.4 (lower row), it is evident that small protein clusters were hardly distinguishable from the background monolayer in the donor channel. In the acceptor channel, however, the clusters were more clearly visible due to a low signal of the background protein layer. Based on the energy transfer image, it can be estimated that the average distance between donor and acceptor molecules inside a protein cluster must be well within the range of the Förster radius (R_0 = 7.15 nm).

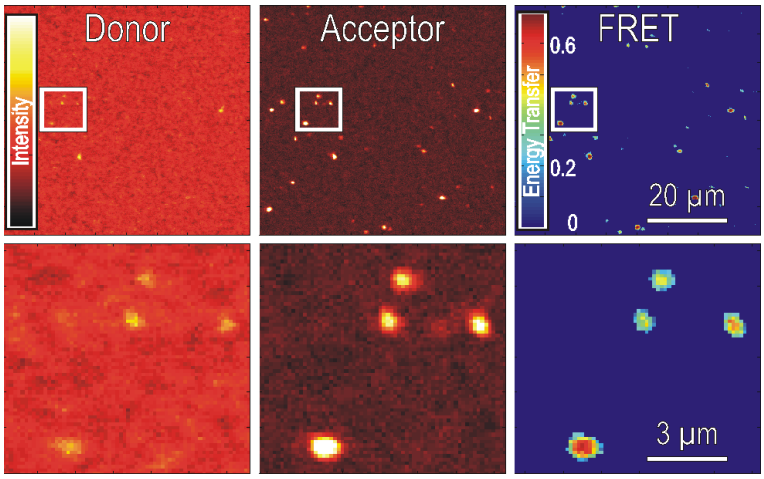

Fig. 8.4. Scan images acquired with the donor (left) and the acceptor (middle) channel after adsorption of Cy5-BSA/Cy7-BSA (0.5 nM each) for 2 h. From the data of these two channels, the FRET image (right) is calculated. The lower row shows magnifications of the section marked by the white square in the upper row.

8.3 Surface-induced spreading of BSA clusters

Since the efficiency of the energy transfer is dependent on the inverse sixth power of the spacing between donor and acceptor, the FRET technique reveals even minute changes of intermolecular distances between cluster proteins. Using FRET imaging to observe surface deposited protein clusters in time uncovers dynamics within the clusters which are not accessible by single channel fluorescence microscopy. As the surface chemistry usually influences surface processes, all cluster dynamics were examined on two distinct model surfaces, a hydrophilic glass surface and a hydrophobic OTS-coated surface. Energy transfer images of the same area (15 µm × 15 µm) were acquired at different times during the continuous flow of protein solution (Fig. 8.5). All protein clusters that deposited on the surface remained in the same position until the end of the analysis. However, as indicated by a change of their color (Fig. 8.5), the energy transfer diminished over time, and this process was considerably faster on the OTS-coated surface than on the glass surface. The new clusters on the OTS surface that appeared between 10 min and 25 min after starting the experiment exhibited a high energy transfer whereas the older clusters that had appeared within the first 10 min changed to a lower energy transfer (Fig. 8.5, lower row). The behaviors of protein clusters deposited on glass were similar, but on a much slower time scale (Fig. 8.5, upper row). The corresponding profile plots display the evolution of the energy transfer along the respective marked lines and emphasize the decreases in the transfer efficiencies.

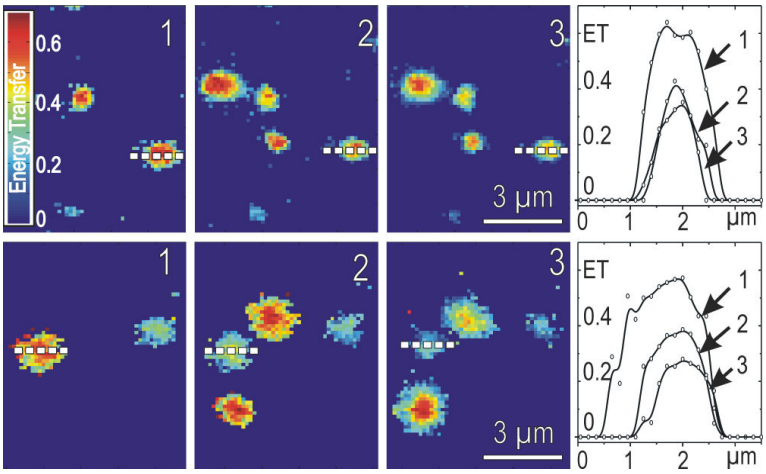

Fig. 8.5. FRET images of surface deposited protein clusters on the hydrophilic glass surface (upper row) and the hydrophobic OTS coated surface (lower row) as a function of time. Hydrophilic surface: 40 min (1), 140 min (2), 300 min (3); hydrophobic surface: 10 min (1), 25 min (2), 50 min (3). Profile plots on the right depict the energy transfer (ET) efficiency of one cluster on each surface along the corresponding dashed lines.

Assuming a fully randomized orientation of all protein bound dye molecules at any time, the FRET efficiency is predominantly dependent on the average distance between donor and acceptor. Thus, the observed decrease of the average energy transfer indicates an enlargement of the mean distance between donor and acceptor which is equivalent to an expansion of the mean inter-protein distance. In other words, protein clusters spread in time after contact with the surface. The quantitative contribution of dye photobleaching to the apparent energy transfer is discussed below.

To accurately investigate the spreading of the protein clusters, the evolution of the energy transfer of 20 selected clusters appearing on a scanned surface (60 µm × 60 µm) was analyzed. Prior to calculating the FRET efficiency the donor and acceptor intensities of all pixels belonging to one cluster were corrected for the background emission and for the crosstalk between the two channels.[215]

$$I_d(t) = \frac{S_d(t) - B_d - \alpha_{a\to d} \cdot \left(S_a(t) - B_a\right)}{1 - \alpha_{a\to d} \cdot \alpha_{d\to a}} \tag{8.1}$$

$$I_a(t) = \frac{S_a(t) - B_a - \alpha_{d\to a} \cdot \left(S_d(t) - B_d\right)}{1 - \alpha_{d\to a} \cdot \alpha_{a\to d}} \tag{8.2}$$

In these equations, $S_d(t)$, $S_a(t)$ refer to the measured signals in donor and acceptor channels, B_d, B_a is the respective background emission and α corresponds to the crosstalk correction.

Based on the emission spectra of Cy5 and Cy7, the crosstalk correction factors were determined to $\alpha_{d\to a} = 0.065$ for the donor-to-acceptor crosstalk and $\alpha_{a\to d} = 0.064$ for the acceptor-to-donor crosstalk. The corrected donor (I_d) and acceptor (I_a) signals were subsequently used to calculate the energy transfer efficiency $E_{FRET}(t)$ under consideration of the detector efficiencies at the given wavelengths and the quantum yields of the fluorophores:[215]

$$E_{FRET}(t) = \frac{I_a(t)}{I_a(t) + I_d(t) \cdot \phi_a / \phi_d \cdot \eta_a / \eta_d} \tag{8.3}$$

The ratio of the donor and acceptor detection efficiencies η_a / η_d was determined to be 1.32 in the used set-up. Both quantum yields, ϕ_d and ϕ_a, for Cy5 and Cy7 amount to 0.28.

Through repeated imaging of the same protein clusters on a 60 µm × 60 µm area over a time range of up to 20 h, a statistical analysis was performed. As the background layer of protein monomers does not show an acceptor emission, all pixels that exceed a threshold of three times the noise in the acceptor channel were attributed to a cluster. The intensities of these pixels were integrated in both channels such that the average FRET efficiency of each cluster could be calculated. The frequencies of the average FRET efficiencies of 20 selected clusters were plotted in histograms ($\Delta ET = 0.02$) and fitted by assuming a log-normal distribution of the distance between donor and acceptor (Fig. 8.6). This analysis was conducted on both, the glass and the OTS-coated model surfaces. It is obvious that at the beginning of the analysis, all freshly adsorbed protein clusters exhibited similar mean FRET efficiencies of ~65%, indicating that the initial protein density within a cluster is independent of the surface chemistry. This observation is consistent with the former conclusion that the cluster formation process occurs in the solution where the influence of the surface is negligible. The narrow energy transfer distribution implies a certain structural stability of the clusters before they deposit on the surface. In the subsequent scans, the average energy distributions clearly shift to lower values indicating the continuous spreading of the protein clusters. The time scale for this shift is considerably longer on the hydrophilic glass surface than on the hydrophobic surface. After a lengthy time (~ 20 h), the mean FRET efficiency has decreased to ~18% of the initial values for those clusters deposited on the hydrophilic surface and to ~7% for those on the hydrophobic surface. The inset images in Fig. 8.6 present the appearance of one representative protein cluster per surface after 7 h and 20 h. An intensity

increase in the donor channel (D) and an intensity decrease in the acceptor channel (A) is clearly visible. For the hydrophobic surface, the signals in the acceptor channel decrease towards values that are too weak for a reasonable differentiation of the clusters from the background. At this point further spreading of the clusters to even larger inter-protein distances exceeds the range within which the FRET technique is applicable. In the case of the hydrophilic surface, reasonable values of the energy transfer are still found after 20 h which is in agreement with a much slower rate of cluster spreading.

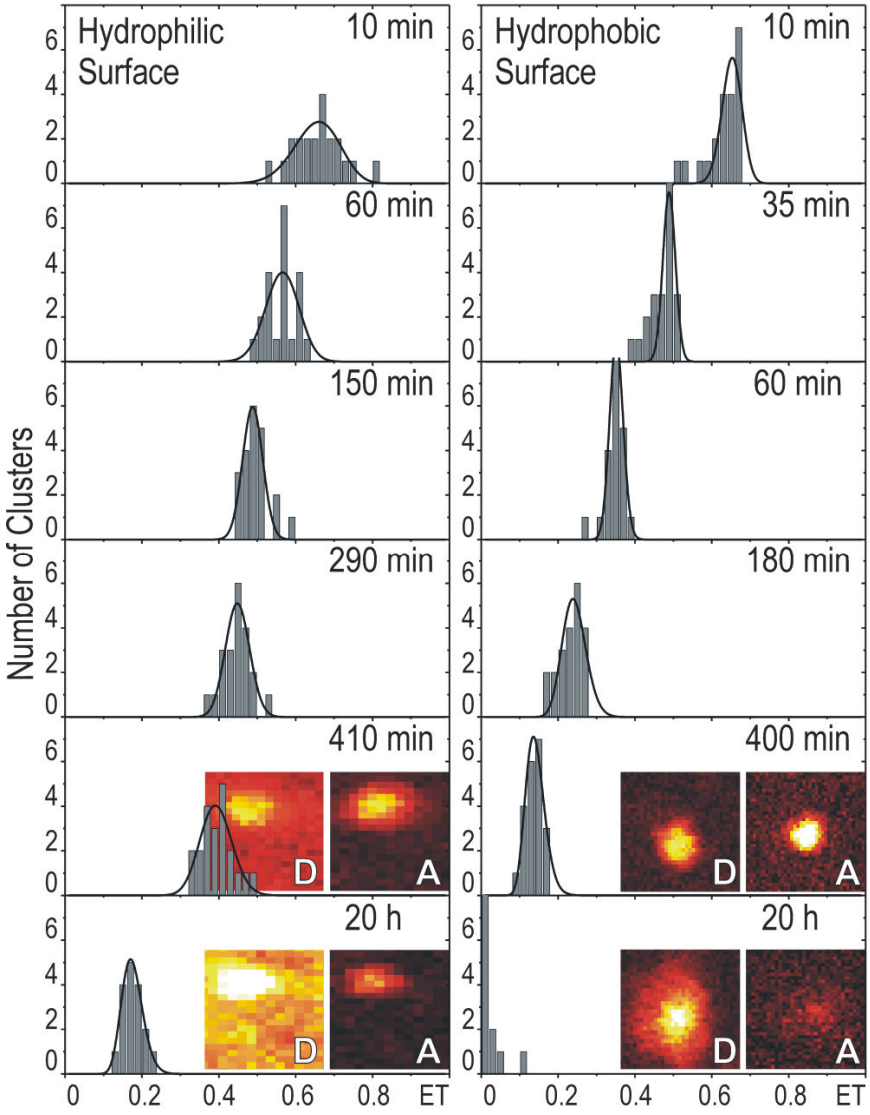

Fig. 8.6. Protein cluster analysis. The histograms present the energy transfer (ET) efficiency distribution of 20 selected clusters at different times (left column: hydrophilic bare glass; right column: hydrophobic OTS-coated glass). Insets: representative images of one surface deposited cluster on each surface after 7 and 20 h (D: donor channel; A: acceptor channel). After 20 h on the hydrophobic surface, the cluster has spread so far that it exceeds the range where the FRET technique is applicable. No scanning of the images was performed between 7 h and 20 h.

The mean FRET efficiencies measured in time can be used to calculate mean intermolecular distances between cluster proteins using the Förster theory. Therefore, it is assumed that the FRET decrease is predominantly the result of increasing distances between cluster proteins which is in line with the observed complete loss of energy transfer after a long time. As the first histograms in Fig. 8.6 show a similar energy transfer for 20 protein clusters just deposited onto the surface it is considered that the clusters formed in the solution reach a metastable equilibrium state with constant inter-protein distances before they deposit on the surface.[216] It is therefore practical to calculate the relative rather than the absolute increase of the inter-protein distance using the first value obtained immediately after cluster deposition $r(0)$ as a reference. In this way quantitative errors resulting from multiple acceptor transfer are circumvented.

$$r(t) = \left(\frac{E^0_{FRET}}{1 - E^0_{FRET}} \right)^{\frac{1}{6}} \cdot \left(\frac{1 - E_{FRET}(t)}{E_{FRET}(t)} \right)^{\frac{1}{6}} \tag{8.4}$$

In this equation $r(t)$ denotes the relative mean distance between dye molecules as a function of time, $E_{FRET}(t)$ is the mean FRET efficiency at any point in time during the spreading process and E^0_{FRET} is the mean FRET efficiency immediately after deposition which is assumed to be constant. The mean energy transfer values $E_{FRET}(t)$ including standard errors are obtained from the curve fits of the histograms presented in Fig. 8.6. Clearly, the relative inter-protein distance r(t) obtained from equation (8.4) reflects a mean value averaged over all donor and acceptor dye pairs contained in the cluster that dynamically change their relative positions. Possibly, in the early stage of spreading some sub-populations of dye pairs inside the cluster may remain at fixed distances and consequently have a negligible contribution to the observed FRET decrease. On the contrary, those proteins which are in contact with the surface play the major role to the variation of $r(t)$ and directly reflect how fast a cluster spreads in its surrounding environment. In Fig. 8.7, the mean relative distance $r(t)$ is plotted and shows the striking difference between the rates at which clusters spread on the hydrophobic (upper curve) and the hydrophilic (lower curve) surface. To quantify the influence of photobleaching on the measured FRET efficiencies, a small area (15 µm × 15 µm) was repeatedly scanned within a short time of 20 min. As the influence of spreading can be considered negligible within this short time period, the apparent distance increase during

these measurements can be fully assigned to photobleaching effects. Based on these measurements, the contribution of photobleaching was assumed to be no more than 10% during 25 scan cycles and all data were corrected by subtracting an amount of 0.4% per scan cycle. The corrected plots of $r(t)$ allowed a more quantitative interpretation of the cluster spreading process (dashed lines in Fig. 8.7). In the first 200 min, the mean donor-to-acceptor distance increased by approximately 10% on the bare glass surface and about 30% on the OTS-coated surface, indicating that the spreading of protein clusters upon contact with a hydrophobic surface proceeded three times faster than on a hydrophilic surface. Such a difference can be understood considering that proteins generally interact in a different manner with hydrophobic surfaces as compared to hydrophilic ones.[135, 136, 197] Hydrophobic surfaces may facilitate the spreading process which proceeds through maximizing the contact sites between the hydrophobic patches of the cluster proteins and the surface.

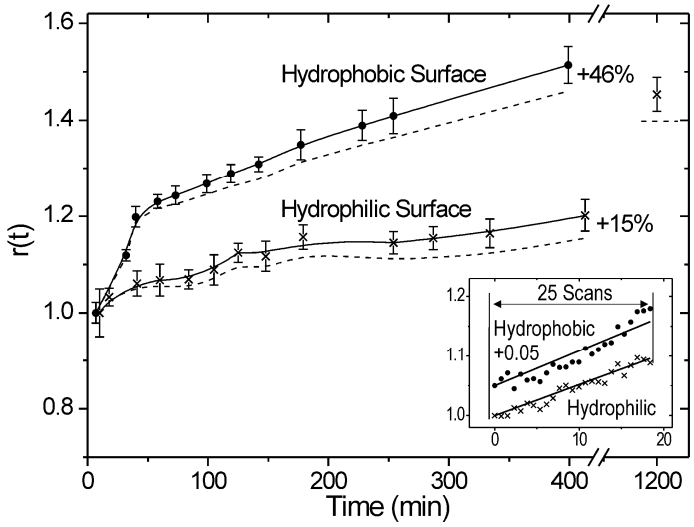

Fig. 8.7. Relative mean inter-protein distance of protein clusters on the hydrophilic and the hydrophobic surfaces as a function of time. All values are normalized to the initial inter protein distance ($r_0 = 1$). The dashed lines represent *r(t)* corrected by the effect of photobleaching. Inset: The contribution of photobleaching amounts to approximately 10% of the relative increase of *r(t)* after 25 scanning cycles regardless on which surface is measured. For the sake of clarity, the data points corresponding to the hydrophobic surface were shifted up by 5%.

8.4 Interaction of BSA clusters with a protein monolayer

A remaining question is to which extent the cluster deposition and spreading is influenced by pre-adsorbed proteins. Interestingly, it is found that protein clusters do deposit on the hydrophobic OTS-coated surface even if it is already covered with proteins. Fig. 8.8 shows one surface section at different times where a protein cluster solely consisting of Cy7-BSA molecules deposits on the surface that was pre-covered with a layer of Cy5-BSA. The Cy5-channel visualizes the Cy5-labeled protein monolayer whereas the Cy7-channel detects the deposition of one single cluster. The fluorophore Cy7 is simply used as a second dye whose direct excitation with the laser leads to a detectable emission in the Cy7-channel.

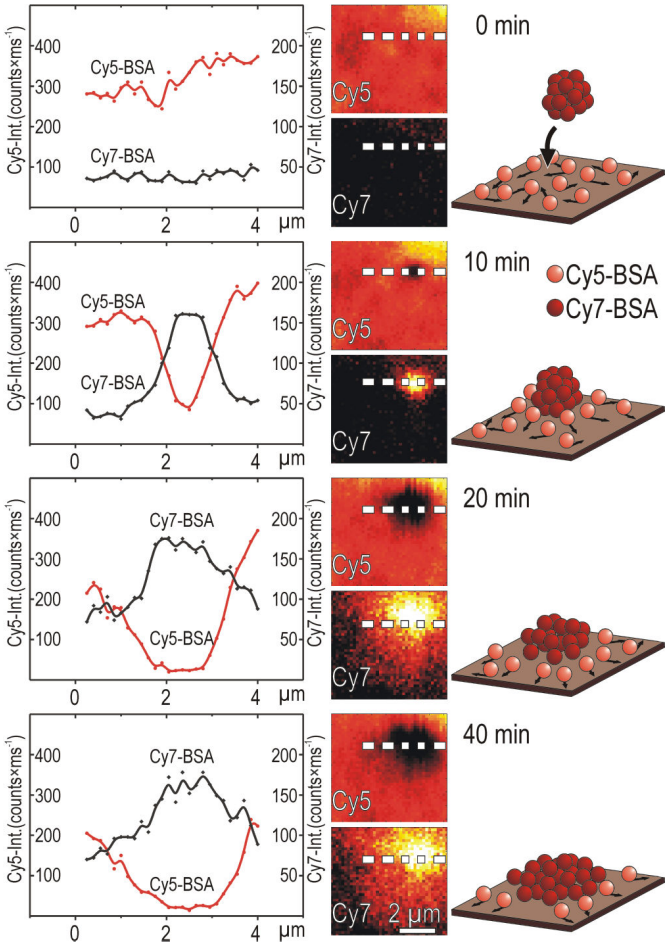

Fig. 8.8. Interaction of Cy7-labeled protein clusters with a pre-adsorbed monolayer of Cy5-labeled BSA on the hydrophobic OTS coated surface. Left: Profile plots along the marked lines showing the movement of Cy5-labeled protein monomers in the Cy5-channel and the expansion of the cluster in the Cy7-channel. Middle: Images of one representative protein cluster in the Cy5- and the Cy7-channel. Right: Schematic illustration of the cluster depositing and spreading on a protein monolayer.

On the left of Fig. 8.8 the two profile plots along the marked lines are presented at each time. It can be clearly seen that a protein cluster initially occupies a small surface area which becomes larger in time indicating its continuous spreading. Moreover, according to the scan images and the profile plots depicting the Cy5-labeled proteins, the pre-adsorbed monomers recede completely from the region that is occupied by the expanding cluster. The schematic representations on the right of Fig. 8.8 illustrate the expansion of the cluster whereas surface bound protein monomers simultaneously move apart.

To ensure that the signal decrease in the Cy5-channel at the area where the cluster expands is not a result of energy transfer to the Cy7-labeled cluster proteins, a complementary experiment was performed in which the Cy7-labeled BSA clusters were replaced by unlabeled BSA clusters (Fig. 8.9). In agreement with the observation in Fig. 8.8 the same receding of pre-adsorbed protein monomers upon deposition of unlabeled protein clusters is noticed. Hence, protein monomers indeed move apart from that area and the possibility that a protein cluster deposits and spreads on top of the pre-adsorbed layer can be excluded.

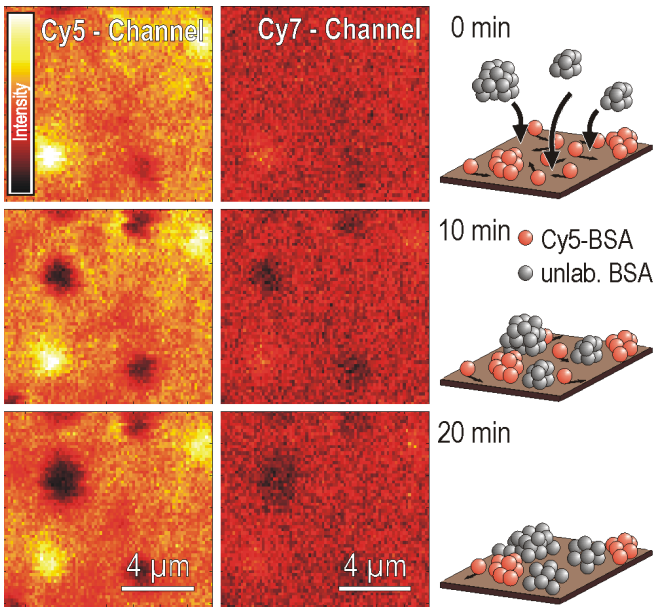

Fig. 8.9. Interaction of Cy5-labeled and unlabeled protein clusters with a pre-adsorbed monolayer of Cy5-labeled BSA on the hydrophobic OTS coated surface. First, Cy5-labeled BSA (1 nM) was applied to the OTS coated surface resulting in a Cy5-BSA background monolayer plus Cy5-BSA clusters (bright spots). Second, under the same conditions, unlabeled BSA (1 nM) was added over resulting in the deposition of unlabeled BSA clusters (dark 'holes'). The background Cy5-BSA monomers recede upon deposition of clusters and thereby create 'holes' which expand in time. Adapted to a low scale the Cy7-channel shows the same images as the Cy5-channel but at much lower intensities resulting from the bleed through of the Cy5 emission into the Cy7-channel.

For the understanding of the molecular mechanisms behind the spreading behavior it is important to note that a similar experiment conducted on a hydrophilic surface revealed the opposite behavior. No cluster was observed to deposit onto a protein covered hydrophilic surface.

8.5 Interpretation of the spreading phenomenon

The experiments discussed in this chapter have revealed that protein clusters consisting of BSA monomers can evolve in solution under certain conditions and subsequently deposit onto the surface where they spread. This process was found to be much faster on a hydrophobic surface than on a hydrophilic surface. Additionally, it was shown that cluster deposition even takes place on a protein covered surface provided that it is rendered hydrophobic. On a hydrophilic surface, by contrast, protein clusters were prevented from adsorption by such a protein layer. Combining these experimental observations leads to the conclusion that BSA molecules exhibit a rather high mobility on the hydrophobic surface which allows the cluster proteins to spread rapidly whereas pre-adsorbed protein monomers move apart laterally at the same time. This suggestion is in agreement with previous works that recognized a higher diffusion rate or mobility when proteins such as BSA and HSA were adsorbed on hydrophobic surfaces as compared to hydrophilic ones.[135, 197] From the first two scans shown in Fig. 8.8 it is obvious that the initial contact between protein cluster and surface must take place over a small area below the resolution of the SAF microscope. The cluster apparently finds a way to the surface through the gaps left between the pre-adsorbed protein monomers. Enabled by the diffusive activity of the monomers the cluster can ‘anchor’ on the surface through the augmentation of its contact patches. In general, surface bound proteins repel each other, particularly when they bear a net charge as is the case under the applied conditions, such that the diffusion direction of the monomers points away from the cluster. However, if protein monomers on the surface diffuse too slowly, this mechanism breaks down since the cluster proteins do not find unoccupied, favorable contact sites. As discussed before, the adsorption of cluster proteins on the top of pre-adsorbed monomers does not take place (see Fig. 8.9). Consequently, the cluster can not ‘anchor’ on the surface and hence its deposition and spreading is not possible. Such a scenario was observed in the case of BSA clusters on a hydrophilic surface: cluster deposition and spreading only occurred on a loosely covered

surface, whereas no cluster deposition was observable once the surface was densely covered with protein monomers. Fig. 8.10 schematically illustrates the cluster deposition and spreading mechanism on protein covered hydrophobic and hydrophilic surfaces.

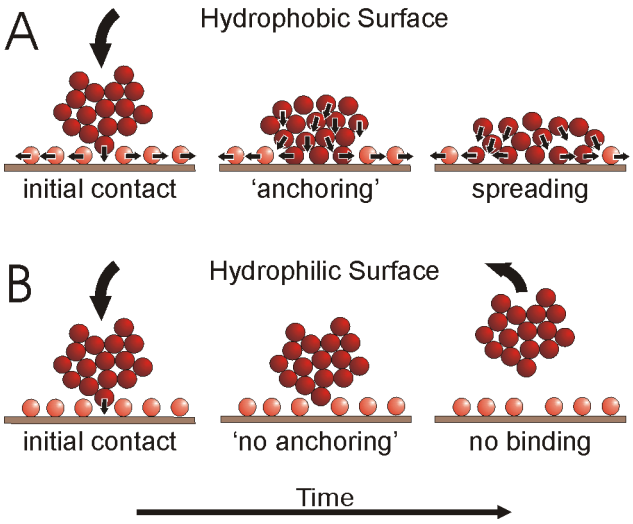

Fig. 8.10. Schematic illustration of the mechanism of the spreading process of a protein cluster in time on the hydrophobic (A) and the hydrophilic (B) surface.

Concerning the spreading process of protein clusters deposited on an empty surface free of pre-adsorbed monomers, the following mechanistic description is suggested for either surface, hydrophobic or hydrophilic. The cluster proteins that are in direct contact with the surface diffuse apart laterally and thereby open gaps for proteins in the upper part of the cluster to migrate downward to the surface. In time, more and more cluster proteins come into contact with the surface while the whole cluster expands and flattens until an equilibrium state is reached. According to the experimental results, this process continues over the range of several hours (hydrophobic surface) up to a few days (hydrophilic surface), depending on the surface chemistry. Thereby, clusters can spread to a diameter of 2 to 3 µm, which is much larger than the apparent initial diameter of the clusters (see Fig. 8.8 and Fig. 8.9). Even though FRET imaging can not resolve the final state of a deposited protein cluster, it is reasonable to assume that it approaches a flat, pancake-like structure after a sufficient equilibration time. This proposed mechanism allows that globular protein clusters deposit from the solution onto the surface and that these clusters subsequently spread until they exhibit a structure similar to a two-dimensional surface cluster.[88, 89]

Under the specific conditions chosen herein, protein clusters were found to deposit from the solution onto the surface, but the converse, formation of clusters directly on the surface, was not observed. This process can be understood by considering that proteins generally undergo orientational or conformational changes to maximize surface-protein interactions.[16] In the case of BSA, the final orientation leads to inter-protein repulsions, preventing a tight packing of adsorbed protein monomers.[42, 50] Hence, the aggregation of surface adsorbed protein monomers through surface diffusion processes is strongly suppressed.

Why do protein clusters cease to grow after their deposition on the surface? As the presented data show proteins within a deposited cluster slowly move apart from each other during the spreading process. Thus, there is a continued alteration of the arrangement of proteins within a cluster. Very likely, the contact between a cluster and the surface induces orientational changes of the cluster proteins such that attractive protein-surface interactions are maximized, in a manner analogous to the known behavior of protein monomers.[42, 50] As a result, the properties of surface bound protein clusters may differ strikingly from those of protein clusters in solution. The altered arrangement of proteins in surface bound clusters apparently suppresses the aggregation of further proteins from the bulk solution. Consequently, the attractive protein - protein interactions within a surface deposited cluster are weaker than the interactions between protein and surface, which is the driving force for the spreading process.

8.6 On-surface aggregation of α-Synuclein

So far in this chapter it was shown that protein aggregation can be a solution process which is found in the case of BSA at acidic pH conditions. However, the aggregation can also be a surface process which is observed for the protein α-Syn at neutral pH (pH 7.4). α-Syn is a 140 amino acid containing protein (MW: 14.5 kDa) found in neural tissue. Its normal biological function is still unclear although recent findings suggest a protective activity against injury of nerve terminals.[217] The wide interest in α-Syn, however, results from the perception that increased concentrations of this protein in vivo are associated with Lewy body formation in Parkinson's disease. Unraveling the aggregation mechanism of α-Syn and screening the conditions that promote or prevent this process are subjects of current research.[218, 219]

In an experiment which is similar to the one presented in Fig. 8.8 the protein α-Syn (0.1 nM in PBS, pH 7.4) labeled with the donor fluorophore DY-647 was exposed to a hydrophilic glass surface for about 40 min (Fig. 8.11). Thereafter, the solution of donor labeled proteins was replaced by a solution containing exclusively acceptor (Cy7) labeled α-Syn (1nM in PBS). In time more and more acceptor labeled proteins bind to the pre-adsorbed donor labeled proteins which leads to increasing FRET signals (upper row of Fig. 8.11). Thus, in comparison to the results obtained with the protein BSA which was proven not to aggregate on the surface the protein α-Syn behaves inversely: α-Syn aggregates grow on the surface.

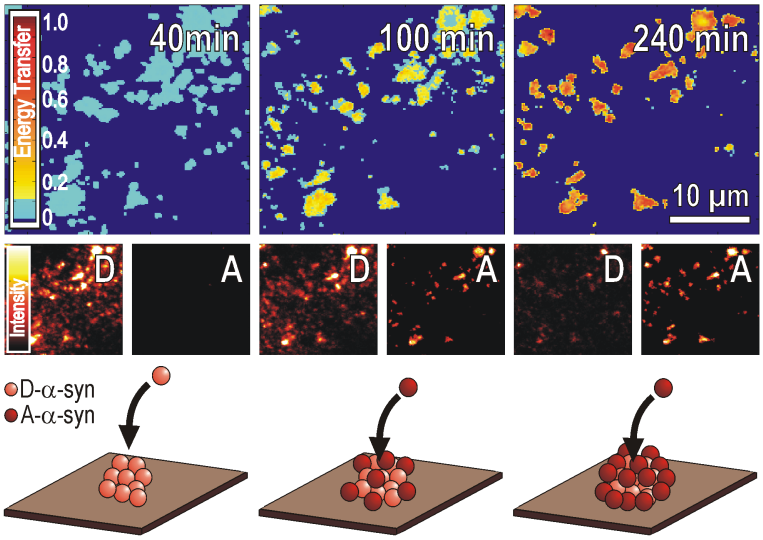

Fig. 8.11. FRET images and scheme of the aggregation process of α-Syn. For the first 40 min only donor labeled proteins were added. Subsequently, only acceptor labeled proteins were exposed on top. The change of the color in the upper row from yellow to red indicates increasing energy transfer efficiency. For the sake of clearness the light blue color in the first image corresponds to the areas were only donor fluorescence and no acceptor fluorescence is detected. The lower row presents the decrease of the donor signals and the increase of the acceptor signals.

It turns out that α-Syn aggregates are tightly tethered to the surface as none of them is removed in time. After the solution of donor labeled proteins is replaced by the solution of acceptor labeled proteins it can not be figured out if there evolve new nucleation sites. Therefore, a complementary experiment is performed in which donor and acceptor labeled proteins (0.5 nM each, in PBS, pH 7.4) are mixed together and exposed to the surface (Fig. 8.12). To mimic a more realistic system, a model membrane was established on the glass

substrate prior to the experiment. This is particularly important as the α-helix content of the natively unfolded α-Syn drastically increases upon binding to lipids.[164, 220]

The FRET images in Fig. 8.12 reveal the formation of initial protein patches within a short time period which continuously expand up to elongated structures in the long term (16 h). The time-dependent increase of the energy transfer can be explained by a growing protein density within the patches including the possibility of increasing coordination numbers when approaching proteins attach not only next to but also on the top of other surface bound proteins. The more acceptor labeled molecules are in the circumference of the donor molecule the higher is the energy transfer efficiency.

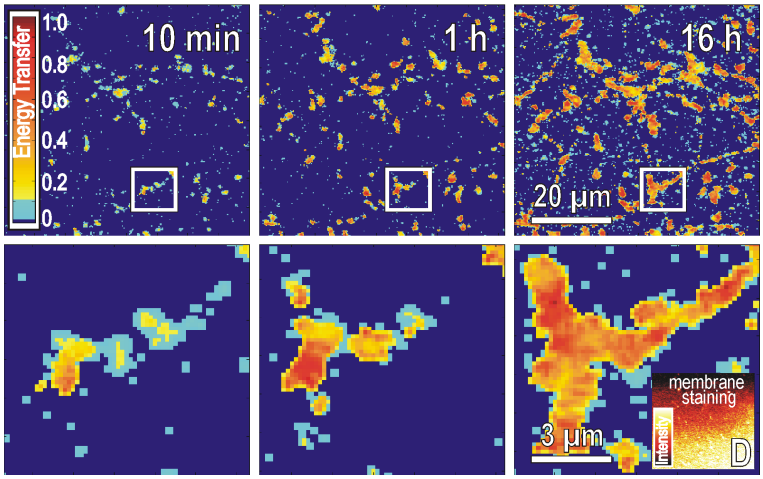

Fig. 8.12. FRET images acquired during the exposure of a mixture of donor (DY-647) and acceptor (Cy5) labeled α-Syn on a model membrane. The energy transfer efficiency increases in time as indicated by a change of the color from yellow to red. The lower row shows magnifications of the regions marked with a white square in the upper row. Inset on lower right: At the end of the experiment the model membrane was stained with a membrane intercalating dye to prove that it was not removed.

Interestingly, most aggregates seen after long time exposure had already appeared within the first 10 min. That means the aggregation of nuclei proceeds in a fast process in the beginning. After 10 min, however, hardly any new nucleus is noticed to appear and only the growth of already existing aggregates is observed. Thus the local positions on which α-Syn aggregates start to grow is determined within a few minutes in the very beginning of protein exposure to the surface. After a long time the aggregates adapt elongated amyloid fibril-like structures which is a frequently observed effect for the amyloidogenic protein α-Syn under specific conditions and after a certain lag-time.[218, 221] However, the observation that these

structures can evolve in the presence of a surface upon minute bulk concentrations (1 nM) and the fact that the anchoring sites of the aggregates are determined in the initial stage opens a new perspective on this widely investigated problem.

Finally, it is shown that the elongated structures presented in Fig. 8.12 (16h) are indeed amyloid fibrils. Therefore, the previous experiment was repeated under identical conditions and the fibrils formed after a sufficiently long time (> 16 h) were stained with Thioflavin T (ThT) which is a fluorescent dye that binds to extended cross β-sheet patterns characteristic for amyloid fibrils.[222] The binding event shifts and enhances the fluorescence emission which can be easily probed using a commercial epifluorescence microscope (*Nikon Eclipse TE2000*) (Fig. 8.13). As a result of ThT application to the curly structures encountered in Fig. 8.13 A the fluorescence emission strongly rises as seen in Fig. 8.13 B. Images C and D of Fig. 8.13 concentrate on a fiber-shaped feature whose one end is probably tethered to the surface (C). The other end of this fiber is only visible when the focus is shifted by a few µm deeper inside the bulk solution (D). This is a clear indication that surface tethered fibrils are not exclusively surface bound but can protrude into the solution. Using the SAF technique, by contrast, only those parts of the fibrils are visible which are in close proximity to the surface. In this sense the images presented in Fig. 8.11 and Fig. 8.12 can be considered to predominantly visualize the anchoring sites of the amyloid fibrils growing on them in the long term.

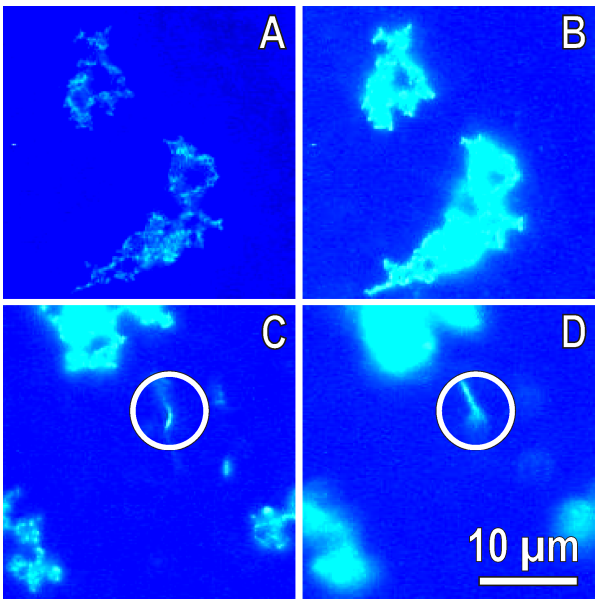

Fig. 8.13. Epifluorescence microscopy images of α-Syn fibrils formed after long time exposure of the protein (1 nM) to a model membrane. A and B show the same surface sections at the beginning and at after some time of ThT addition. Images C and D show the same surface section with the focus set to the surface and deeper inside the bulk solution.

8.7 Conclusion

The aggregation of proteins is a known and frequently observed phenomenon.[92, 94, 97, 98] However, detailed mechanistic studies of the aggregation process and of the behavior of protein aggregates on surfaces are scarce. In this chapter it has been shown that protein aggregation can be a solution or a surface process. The most important method used to study the corresponding model systems was FRET imaging. Proteins were either labeled with a donor or with an acceptor fluorophore which has led to a measurable energy transfer when proteins assembled into tight aggregates or clusters.

Protein aggregation in solution has been observed when BSA was exposed at low bulk concentrations at pH 3 to a hydrophilic or hydrophobic surface under the condition of a sufficiently long equilibration time. The initial structure of these protein clusters turned out to be solely determined by the solution conditions. Freshly deposited protein clusters exhibit comparable inter protein distances independent of the surface characteristics. Subsequently, however, the cluster proteins spread apart from the cluster core in any direction at a rate that is strongly influenced by the surface chemistry: fast spreading on a hydrophobic surface, slow spreading on a hydrophilic surface. After investigation of the interplay between protein clusters and a monolayer of pre-adsorbed proteins it was concluded that the cluster spreading mechanism is connected to the ability of protein molecules to move on the surface. A high surface mobility correlates with a high spreading rate whereas a low mobility slows down the spreading process. As a consequence, the deposition of protein clusters on the surface can be suppressed by a dense protein monolayer provided that it displays a low surface mobility of adsorbed proteins. In this case protein clusters diffusing in the bulk solution can not disrupt the layer of adsorbed proteins and hence a deposition on the surface does not take place. Such a scenario was found when BSA was adsorbed on a hydrophilic surface. On a hydrophobic surface, by contrast, a dense monolayer of BSA could not hinder the deposition and subsequent spreading of protein clusters. This finding is of particular interest in assay technologies where BSA is used as a blocking or stabilization agent.

Protein aggregation on the surface has been found for α-Syn at neutral pH on a hydrophilic surface as well as on a model membrane. The crucial stage of this process is the very beginning where the nucleation step takes place. It has been found that in the long term protein aggregation almost exclusively proceeds at those positions which were populated through a common adsorption event within the first few minutes. New nucleation sites, by

contrast, were usually not observed to occur after the initial stage. Interestingly, even at the low bulk concentrations applied in this study (1 nM) the aggregates evolve into amyloid fibrils after long exposure times. This could be proven by a clear enhancement of fluorescence emission upon binding of ThT to the α-Syn fibrils. Using epifluorescence microscopy some of the elongated fibril structures formed after long exposure times were found to protrude into the bulk solution with one of their endings and being tethered to the surface with the other ending. This suggests that the growth of the fibrils starts at the initially determined positions which in the end remain the surface anchoring sites and proceeds in a certain direction not necessarily along the surface.

Given the vast effort of research in the field of protein aggregation including the formation and pathological effects of amyloid fibrils it must be considered essential to clarify the underlying mechanistic aspects. Misconceptions in this field can easily occur due to incomplete or improper experimental investigation. At some point, for instance, surface bound protein aggregates that form in the solution and afterwards deposit onto the surface may have very similar characteristics compared to those that grow directly on the surface. Thus, without knowing the exact aggregation mechanisms and the surface behavior one can easily be misled when the further evolution of protein aggregates is concluded from a certain state. Evaluating the effects of the discussed mechanism on the biological activity and cytotoxicity of the proteins and designing interfaces that allow for a certain control over aggregation processes will be important topics for future research.

9 Summary and Outlook

Studying protein adsorption phenomena on solid surfaces is a complex and also fascinating endeavor. Its scientific relevance is manifested in various problems encountered in research areas such as designing biocompatible materials, tracing biological events that trigger or prevent diseases, improving analytical devices, or control fouling processes to name a few. Ever since the 1970s, when Leo Vroman had observed exchange mechanisms between adsorbed plasma proteins, researchers are aware of the great complexity inherent to protein adsorption events.[81, 83] Although continuous effort in this field has been advancing our understanding considerably over the past decades we are still far from a complete and unique view on how do proteins behave upon contact with solid interfaces. The objective of this dissertation was to mechanistically explain some of the complex and controversially discussed effects related to protein adsorption on the basis of substantial experimental observations. Simplistically expressed, the most important achievements can be outlined with a clearer and deeper understanding of the three phenomena cooperative protein adsorption, overshooting adsorption kinetics, and protein aggregation. Naturally, the practical realization of such a research ambition is tightly connected with the choice of the used experimental techniques. Herein, the main focus was put on fluorescence methods whose primary benefit is the high sensitivity that enables adsorption experiments at low bulk protein concentrations. In particular the use of super critical angle fluorescence (SAF) detection has proven advantageous due to the possibility of selectively investigating processes on the surface and thereby neglecting interferences from the bulk solution. Other techniques frequently applied in the field of protein adsorption, especially label-free detection techniques are typically by orders of magnitude less sensitive and are therefore more suitable at higher bulk protein concentrations. Most of the phenomena studied in this work, however, would have been screened by high adsorption rates which are a natural consequence of increased bulk concentrations.

The main drawback of fluorescence techniques is the need of a fluorescent marker which has to be attached to the protein. To consolidate the validity of the conclusions based on the experimental observations performed in this work, it had to be clarified that the marker molecule does not noticeably affect the behavior of the protein. Certainty on this issue was provided by a set of experiments which allowed to compare the adsorption behaviors of labeled and native proteins. Fortunately, only a minor influence of the marker on the protein adsorption behavior was noticed. Also, different applied buffer conditions in terms of their pH and ionic strength appeared not to markedly alter the fluorescence intensity justifying the reliability of the experimental methods. Apart from the fluorescent marker there was another potential risk that may discredit the reliability of experimental data, namely the influence of transport processes to the measured adsorption kinetics. However, with the help of model calculations it was shown that although transport processes probably do influence kinetic parameters the mechanistic conclusions are not affected within the estimated frame of the transport rates.

The strategy to study protein adsorption phenomena defined in this work is best outlined in the following steps. First, suitable experiments that can provide mechanistic information had to be found. From experience it was already known that one promising possibility consists of acquiring adsorption kinetics, i.e., the protein uptake on the surface as a function of time. In particular the systematic study of the adsorption of labeled and unlabeled proteins as well as the desorption of proteins through buffer rinsing gave access to valuable mechanistic details. A further successful experimental approach was to record time-resolved surface scan images during the course of protein adsorption which revealed the protein density distribution on the surface and even the existence of adsorbed protein aggregates. In the second step, the chosen methods were applied to generate comprehensive data sets at defined experimental conditions. Within one data set only the bulk protein concentration was varied which was pivotal for reliantly interpreting the adsorption behavior. Different data sets were obtained by individually varying the pH, the ionic strength conditions, the surface chemistry, or even the used model protein. In the final step the experimental data served for the development of a mechanistic model description either through a system of rate equations or through an algorithm that represents a Monte-Carlo simulation, or, as was done in the case of protein aggregation, through an illustrative explanation. The validity of such a description was tested by comparing the predicted adsorption behavior with the experimental data. Finding a sufficiently accurate model description without exceeding the number of included

terms and parameters beyond necessity was the major challenge in this step.[*] Every additional term in the rate equations certainly improves the overlap between model and experiment. However, care was taken that only those terms were included whose importance could be justified from a mechanistic point of view.

Proceeding along the described route the frequently reported effect that protein adsorption occurs in a cooperative manner was explained with a model that suggests two independent adsorption pathways, Langmuir-type and cooperative adsorption pathway, depending on the local conditions in which a protein approaches the surface. The pivotal element is found in the cooperative adsorption pathway which contains the possibility of a lateral tracking or guidance of a protein that approaches an occupied surface site to an available site close to one or a few pre-adsorbed proteins. The decisive step forward made with this model was that the whole adsorption kinetics could be described with one single model. Earlier studies had also proposed the mathematical formalism for increasing adsorption rates but failed to consistently include a term leading to surface saturation. Consequently, the adsorption mechanism standing behind the model presented herein which points to the described tracking effect has not been formulated in such a concise fashion before.

For the sake of simplicity the rate equations which represent the model contain some crude approximations especially when it comes to the point where the increasing surface coverage causes the break-down of the tracking mechanism. This limitation was overcome by a Monte-Carlo simulation handling the proposed adsorption mechanism at the microscopic level by considering each protein individually. One important benefit of the simulation was a connection between the macroscopically amenable shape of the adsorption kinetics and the microscopic events behind the adsorption mechanism mainly manifested by an exact length of the maximum lateral tracking distance r_{coop}. Additionally, experimentally obtained protein density distributions on the surface could be accurately reproduced. Thus, the accordance of experimental data with two different model descriptions highlights the validity of the proposed cooperative adsorption model. With the help of rate equations protein adsorption kinetics can be phenomenologically explained and also fitted to obtain the involved parameters. The Monte-Carlo simulation, by contrast, is inappropriate to perform a curve fit but allows a more precise treatment of the adsorption mechanism at the microscopic scale and can even be exploited to simulate surface scan images.

[*] The idea behind this is a rather general heuristic principle in science often referred to as Occam's razor.

A second mechanistic model was developed in this work to explain several phenomena encountered during the adsorption of the model protein β-Lactoglobulin. Apart from cooperative effects, overshooting adsorption kinetics were experimentally observed which turned out to be connected with changing desorption characteristics. To account for these phenomena the model contains three different states of adsorbed proteins, an initial, a reversible, and an irreversible state. It was found that the transition of the irreversibly bound initial state into the less tightly bound reversible state occurs suddenly at a critical coverage level which consequently leads to the observed overshoot. In analogy to the rate equations that represent the cooperative model, the transition of the preferred adsorption state from the initial into the reversible state is approximated by a step-like process. As proteins bound to the surface in the reversible state tend to relax into the final irreversible state, the adsorption kinetics still exhibit an increasing behavior after the overshoot albeit at a much slower rate. The cooperative effects during β-Lg adsorption are most prominent in the early adsorption process. Therefore, the adsorption of proteins in the initial state is described in analogy to the model that treats cooperativity. Referring to the current state of research in the field of protein adsorption, the proposed model largely reduces the mystery of the overshooting effect by providing a consistent and comprehensible explanation. In contrast to previous works on this topic the model is based on a strong experimental fundament that provides certainty on the transition of a tightly bound first state of the protein into a loosely bound second state in that moment when a critical surface density is exceeded.

A somewhat different experimental approach was applied to study protein aggregation or clustering as a further effect related to protein adsorption. Although there are suggestions that cluster formation can be revealed by kinetic analyses, this way was disregarded as it leads to inconclusive results. In particular it was shown in this work that cooperativity is not necessarily a result of protein aggregation in the sense of a real protein-protein contact as is assumed in some works.[65, 67] The successful method in this study was the use of fluorescence microscopy combined with FRET imaging. Using the model protein BSA at acidic pH conditions protein clusters were noticed to form inside the buffer solution and subsequently deposit onto the surface. Low bulk protein concentrations had to be used because cluster deposition is in competition to monomer adsorption and is therefore screened at higher concentrations. Due to the FRET technique changes in the average inter protein distance of cluster proteins in time were revealed and explained by a spreading process. Since the spreading rate turned out to strongly depend on the chosen surface chemistry conclusions

about the underlying mechanism were possible. Surfaces on which protein monomers show a fast surface diffusion induce fast spreading rates as was found in the case of the OTS coated, hydrophobic surface. In the case of a reduced surface diffusion, as was found on the hydrophilic glass surface, cluster spreading rates were slow. It is therefore a consistent mechanistic concept to assume a continuous spreading of those cluster proteins which are in contact with the surface which in turn open gaps for proteins located above to come in contact with the surface. Within a sufficiently long time scale such a behavior may lead to surface aggregates which equal two-dimensional surface crystals.

Inversely to the behavior of BSA clusters, the protein α-Syn was proven to exclusively aggregate on the surface. During long exposure times these aggregates grow considerably and finally form surface tethered amyloid fibrils even though the bulk protein concentration was kept as low as 1 nM. Protein aggregates on surfaces can thus have completely different histories including in-solution and on-surface growth. The on-surface growth mechanism is the typically proposed one when protein aggregates are detected on a surface. However, the discovery that protein aggregates can also come from the solution and spread on the surface opens a new perspective on this topic which has not been reported before.

To this end the study highlights the need for a careful interpretation of experimental data. The simple appearance or the shape of protein aggregates gives little information about their growth mechanism. If, for instance, time-resolved surface scan images are impossible as is the case in most AFM studies the detection of a flat surface cluster can potentially lead to the misinterpretation of a crystal growth mechanism on the surface. FRET imaging is therefore considered to constitute a powerful tool for acquiring comprehensive time-resolved experimental data on protein clusters which is essential to unravel their behavior at the surface.

With the results presented in this dissertation some interesting phenomena observed during protein adsorption processes can be mechanistically understood. Future work should include investigations on the influence of these phenomena on the protein's functionality. Many effects such as the transitions between different adsorption states necessarily induce conformational re-orientations which most likely affect the biochemical activity of the individual proteins. Further, there is little information on how important ensemble effects like cooperativity are for the control of biological processes connected to protein adsorption. Naturally, these questions imply a considerable increase in experimental complexity as suitable model systems have to be designed with buffer and surface properties that are in

accordance with real biological systems. Furthermore, the continuous investigation of the protein's functionality adds a new dimension to the applied analytical techniques.

The results obtained on protein aggregates and their behavior on surfaces give rise to further exciting research targets. Is there a link between the different protein aggregation mechanisms observed in vitro with biological events, for instance diseases, in vivo? What are the opportunities of manipulating the surface characteristics to achieve a control over on-surface aggregation or protein cluster deposition and spreading? The first results on α-Syn aggregation are already a step forward towards decoding the biophysical processes behind plaque formation in neural tissue leading to Parkinson's disease. Since α-Syn amyloid fibrils are not observed to form in solution in vitro under physiological bulk protein concentrations it can be concluded that the surface plays a crucial role in this process. Further investigations on this topic are subject of our current research.

Abbreviations

AFM	atomic force microscopy
α-Syn	α-Synuclein
ATR-IR	attenuated total internal reflectance – infrared spectroscopy
β-Lg	β-Lactoglobulin
BSA	Bovine serum albumin
CD	circular dichroism
DLVO	Derjaguin, Landau, Verwey, Overbeek
DOPC	1,2-dioleoyl-*sn*-glycero-3-phosphocholine
DOPS	1,2-dioleoyl-*sn*-glycero-3-phospho-L-serine
EM	electron microscopy
ET	energy transfer
FCS	fluorescence correlation spectroscopy
Fib	Fibrinogen
FITC	fluorescein isothiocyanate
FRET	Förster resonance energy transfer
HMWK	High molecular weight kininogen
IgG	Immunoglobulin G
Lys	Lysozyme
MC	Monte-Carlo
MD	molecular dynamics
MLV	multilamellar vesicle
NHS	N-hydroxysuccinimide
OD	optical density
ODE	ordinary differential equation
OTS	octadecyltrichlorosilane
OWLS	optical waveguide lightmode spectroscopy

PBS	phosphate buffered saline
QCM	quartz crystal microbalance
RSA	random sequential adsorption
SAF	supercritical angle fluorescence
SAM	self-assembled monolayer
SLB	supported lipid bilayer
SPR	surface plasmon resonance
STED	stimulated emission depletion
ThT	thioflavin T
TIRF	total internal reflection fluorescence
Tris	tris(hydroxymethyl) aminomethane
ULV	unilamellar vesicle
VDW	van der Waals

Bibliography

1. K. Nakanishi, T. Sakiyama and K. Imamura, *J. Biosci. Bioeng.*, 2001, **91**, 233-244.

2. A. Hinderliter, P. F. F. Almeida, C. E. Creutz and R. L. Biltonen, *Biochemistry*, 2001, **40**, 4181-4191.

3. A. Hinderliter, R. L. Biltonen and P. F. F. Almeida, *Biochemistry*, 2004, **43**, 7102-7110.

4. A. Hinderliter and S. May, *J. Phys.: Condens. Matter*, 2006, **18**, 1257-1270.

5. T. A. Horbett and J. L. Brash, *Proteins at Interfaces II. Fundamentals and Applications*, American Chemical Society: Washington, DC, 1995.

6. V. Vogel and G. Baneyx, *Annu. Rev. Biomed. Eng.*, 2003, **5**, 441-463.

7. R. K. Walker and S. Krishnawamy, *J. Biol. Chem.*, 1994, **269**, 27441-27450.

8. M. Malmsten, D. Muller and B. Lassen, *J. Colloid Interface Sci.*, 1997, **193**, 88-95.

9. C. Janiak, *Chemie in Unserer Zeit*, 2001, **35**, 348-354.

10. U. M. Elofsson, M. A. Paulsson and T. Arnebrant, *Colloids Surf., B*, 1997, **8**, 163-169.

11. U. M. Elofsson, M. A. Paulsson and T. Arnebrant, *Langmuir*, 1997, **13**, 1695-1700.

12. P. A. Dimilla, S. M. Albelda and J. A. Quinn, *J. Colloid Interface Sci.*, 1992, **153**, 212-225.

13. J. J. Gray, *Curr. Opin. Struct. Biol.*, 2004, **14**, 110-115.

14. C. A. Haynes and W. Norde, *Colloids Surf., B*, 1994, **2**, 517-566.

15. C. A. Haynes and W. Norde, *J. Colloid Interface Sci.*, 1995, **169**, 313-328.

16. V. Hlady and J. Buijs, *Curr. Opin. Biotechnol.*, 1996, **7**, 72-77.

17. M. Malmsten, *J. Colloid Interface Sci.*, 1998, **207**, 186-199.

18. W. Norde, *Colloids Surf., B*, 2008, **61**, 1-9.

19. C. Czeslik, *Chem. Unserer Zeit*, 2006, **40**, 238-245.

20. R. Heuberger, G. Sukhorukov, J. Vörös, M. Textor and H. Mohwald, *Adv. Funct. Mater.*, 2005, **15**, 357-366.

21. N. P. Huang, et al., *Langmuir*, 2001, **17**, 489-498.

22. S. Zürcher, et al., *J. Am. Chem. Soc.*, 2006, **128**, 1064-1065.

23. P. Billsten, M. Wahlgren, T. Arnebrant, J. Mcguire and H. Elwing, *J. Colloid Interface Sci.*, 1995, **175**, 77-82.

24. C. E. Giacomelli and W. Norde, *J. Colloid Interface Sci.*, 2001, **233**, 234-240.

25. J. McGuire, M. C. Wahlgren and T. Arnebrant, *J. Colloid Interface Sci.*, 1995, **170**, 182-192.

26. A. Sethuraman and G. Belfort, *Biophys. J.*, 2005, **88**, 1322-1333.

27. C. M. Dobson, *Philos. Trans. R. Soc. London, B*, 2001, **356**, 133-145.

28. M. Sunde and C. Blake, *Adv. Protein Chem.*, 1997, **50**, 123-159.

29. J. Israelachvili, *Intermolecular and Surface Forces*, 2nd Ed. edn., Academic Press, London, 1991.

30. F. Carlsson, E. Hyltner, T. Arnebrant, M. Malmsten and P. Linse, *J. Phys. Chem. B*, 2004, **108**, 9871-9881.

31. F. Fang and I. Szleifer, *J. Chem. Phys.*, 2003, **119**, 1053-1065.

32. M. G. E. G. Bremer, J. Duval, W. Norde and J. Lyklema, *Colloids Surf., A*, 2004, **250**, 29-42.

33. M. Bellion, et al., *J. Phys.: Condens. Matter*, 2008, **20**, 404226.

34. A. Quinn, H. Mantz, K. Jacobs, M. Bellion and L. Santen, *Epl*, 2008, **81**, 56003.

35. M. Skepö, *J. Chem. Phys.*, 2008, **129**, 185101.

36. F. Fang and I. Szleifer, *Biophys. J.*, 2001, **80**, 2568-2589.

37. I. Langmuir, *J. Am. Chem. Soc.*, 1932, **54**, 2798-2832.

38. M. Karlsson and U. Carlsson, *Biophys. J.*, 2005, **88**, 3536-3544.

39. S. Noinville, F. Bruston, C. El Amri, D. Baron and P. Nicolas, *Biophys. J.*, 2003, **85**, 1196-1206.

40. T. J. Su, J. R. Lu, R. K. Thomas, Z. F. Cui and J. Penfold, *Langmuir*, 1998, **14**, 438-445.

41. C. F. Wertz and M. M. Santore, *Langmuir*, 2002, **18**, 1190-1199.

42. T. J. Su, J. R. Lu, R. K. Thomas, Z. F. Cui and J. Penfold, *J. Phys. Chem. B*, 1998, **102**, 8100-8108.

43. C. Czeslik, C. Royer, T. Hazlett and W. Mantulin, *Biophys. J.*, 2003, **84**, 2533-2541.

44. W. Norde and C. E. Giacomelli, *J. Biotechnol.*, 2000, **79**, 259-268.

45. S. Koutsopoulos, A. M. Tjeerdsma, J. F. T. Lieshout, J. van der Oost and W. Norde, *Biomacromolecules*, 2005, **6**, 1176-1184.

46. T. Zoungrana, G. H. Findenegg and W. Norde, *J. Colloid Interface Sci.*, 1997, **190**, 437-448.

47. A. N. Asanov, L. J. DeLucas, P. B. Oldham and W. W. Wilson, *J. Colloid Interface Sci.*, 1997, **196**, 62-73.

48. F. Höök, M. Rodahl, B. Kasemo and P. Brzezinski, *Proc. Natl. Acad. Sci. U. S. A.*, 1998, **95**, 12271-12276.

49. P. Facci, D. Alliata, L. Andolfi, B. Schnyder and R. Kotz, *Surf. Sci.*, 2002, **504**, 282-292.

50. T. J. Su, J. R. Lu, R. K. Thomas and Z. F. Cui, *J. Phys. Chem. B*, 1999, **103**, 3727-3736.

51. E. Brynda, V. Hlady and J. D. Andrade, *J. Colloid Interface Sci.*, 1990, **139**, 374-380.

52. B. D. Fair and A. M. Jamieson, *J. Colloid Interface Sci.*, 1980, **77**, 525-534.

53. J. J. Ramsden, *Chem. Soc. Rev.*, 1995, **24**, 73-78.

54. J. J. Ramsden, *Phys. Rev. Lett.*, 1993, **71**, 295-298.

55. P. Schaaf and J. Talbot, *J. Chem. Phys.*, 1989, **91**, 4401-4409.

56. E. L. Hinrichsen, J. Feder and T. Jossang, *J. Stat. Phys.*, 1986, **44**, 793-827.

57. J. Talbot, G. Tarjus, P. R. Van Tassel and P. Viot, *Colloids Surf., A*, 2000, **165**, 287-324.

58. P. Lavalle, C. Gergely, A. Lustig and V. Ball, *J. Chem. Phys.*, 2000, **113**, 8212-8224.

59. P. Schaaf, J. C. Voegel and B. Senger, *J. Phys. Chem. B*, 2000, **104**, 2204-2214.

60. J. Talbot, X. Jin and N. H. L. Wang, *Langmuir*, 1994, **10**, 1663-1666.

61. A. N. Asanov, L. J. DeLucas, P. B. Oldham and W. W. Wilson, *J. Colloid Interface Sci.*, 1997, **191**, 222-235.

62. V. Ball, A. Lustig and J. J. Ramsden, *Phys. Chem. Chem. Phys.*, 1999, **1**, 3667-3671.

63. H. Nygren, S. Alaeddin, I. Lundström and K. E. Magnusson, *Biophys. Chem.*, 1994, **49**, 263-272.

64. A. Herrig, M. Janke, J. Austermann, V. Gerke, A. Janshoff and C. Steinem, *Biochemistry*, 2006, **45**, 13025-13034.

65. A. P. Minton, *Biophys. Chem.*, 2000, **86**, 239-247.

66. A. P. Minton, *Biophys. J.*, 1999, **76**, 176-187.

67. A. P. Minton, *Biophys. J.*, 2001, **80**, 1641-1648.

68. R. P. Richter, J. L. K. Him, B. Tessier, C. Tessier and A. R. Brisson, *Biophys. J.*, 2005, **89**, 3372-3385.

69. M. Van der Veen, M. C. Stuart and W. Norde, *Colloids Surf., B*, 2007, **54**, 136-142.

70. V. Ball and J. Ramsden, *J. Phys. Chem. B*, 1997, **101**, 5465-5469.

71. V. Ball and J. Ramsden, *Colloids Surf., B*, 2000, **17**, 81-94.

72. E. N. Vasina and P. Dejardin, *Langmuir*, 2004, **20**, 8699-8706.

73. R. Kurrat, J. E. Prenosil and J. J. Ramsden, *J. Colloid Interface Sci.*, 1997, **185**, 1-8.

74. M. Wahlgren and U. Elofsson, *J. Colloid Interface Sci.*, 1997, **188**, 121-129.

75. P. A. Cuypers, G. M. Willems, H. C. Hemker and W. T. Hermens, *Ann. N. Y. Acad. Sci.*, 1987, **516**, 244-252.

76. E. N. Vasina and P. Dejardin, *Biomacromolecules*, 2003, **4**, 304-313.

77. S. M. Daly, T. M. Przybycien and R. D. Tilton, *Langmuir*, 2003, **19**, 3848-3857.

78. L. K. Filippov and N. L. Filippova, *J. Colloid Interface Sci.*, 1996, **178**, 571-580.

79. H. Ohshima, N. Fujita and T. Kondo, *Colloid Polym. Sci.*, 1992, **270**, 707-710.

80. H. Ohshima, H. Sato, H. Matsubara, A. Hyono and M. Okubo, *Colloid Polym. Sci.*, 2004, **282**, 1174-1178.

81. L. Vroman and A. L. Adams, *Surf. Sci.*, 1969, **16**, 438-446.

82. L. Vroman, A. L. Adams, G. C. Fischer and P. C. Munoz, *Blood*, 1980, **55**, 156-159.

83. L. Vroman, A. L. Adams and M. Klings, *Fed. Proc.*, 1971, **30**, 1494-1502.

84. S. M. Slack and T. A. Horbett in, *Proteins at Interfaces. II. Fundamentals and Applications (Eds. T.A. Horbett, J. L. Brash), ACS, Washington*, 1995, 112-128.

85. J. L. Brash and P. Tenhove, *Thromb. Haemostasis*, 1984, **51**, 326-330.

86. T. A. Horbett, *Thromb. Haemostasis*, 1984, **51**, 174-181.

87. J. L. Robeson and R. D. Tilton, *Langmuir*, 1996, **12**, 6104-6113.

88. P. A. Mulheran, D. Pellenc, R. A. Bennett, R. J. Green and M. Sperrin, *Phys. Rev. Lett.*, 2008, **100**, 068102.

89. J. L. Ortega-Vinuesa, P. Tengvall and I. Lundstrom, *J. Colloid Interface Sci.*, 1998, **207**, 228-239.

90. R. Ishiguro, Y. Yokoyama, H. Maeda, A. Shimamura, K. Kameyama and K. Hiramatsu, *J. Colloid Interface Sci.*, 2005, **290**, 91-101.

91. J. Zhang and X. Y. Liu, *J. Chem. Phys.*, 2003, **119**, 10972-10976.

92. M. R. H. Krebs, G. L. Devlin and A. M. Donald, *Biophys. J.*, 2007, **92**, 1336-1342.

93. E. van der Linden and P. Venema, *Curr. Opin. Colloid Interface Sci.*, 2007, **12**, 158-165.

94. S. M. Chen, F. A. Ferrone and R. Wetzel, *Proc. Natl. Acad. Sci. U. S. A.*, 2002, **99**, 11884-11889.

95. C. C. Lee, R. H. Walters and R. M. Murphy, *Biochemistry*, 2007, **46**, 12810-12820.

96. Z. Ignatova, A. K. Thakur, R. Wetzel and L. M. Gierasch, *J. Biol. Chem.*, 2007, **282**, 36736-36743.

97. A. K. Menon, D. Holowka, W. W. Webb and B. Baird, *J. Cell Biol.*, 1986, **102**, 534-540.

98. T. Cellmer, R. Douma, A. Huebner, J. Prausnitz and H. Blanch, *Biophys. Chem.*, 2007, **125**, 350-359.

99. J. M. Andrews, W. F. Weiss and C. J. Roberts, *Biochemistry*, 2008, **47**, 2397-2403.

100. A. M. Morris, M. A. Watzky, J. N. Agar and R. G. Finke, *Biochemistry*, 2008, **47**, 2413-2427.

101. R. V. Pappu, X. Wang, A. Vitalis and S. L. Crick, *Arch. Biochem. Biophys.*, 2008, **469**, 132-141.

102. A. M. Donald, *Soft Matter*, 2008, **4**, 1147-1150.

103. D. El Moustaine, V. Perrier, L. Smeller, R. Lange and J. Torrent, *FEBS J.*, 2008, **275**, 2021-2031.

104. J. Khandogin and C. L. Brooks, *Proc. Natl. Acad. Sci. U. S. A.*, 2007, **104**, 16880-16885.

105. M. Stefani and C. M. Dobson, *J. Mol. Med.-JMM*, 2003, **81**, 678-699.

106. J. W. Corsel, G. M. Willems, J. M. M. Kop, P. A. Cuypers and W. T. Hermens, *J. Colloid Interface Sci.*, 1986, **111**, 544-554.

107. A. Puerta, A. Jaulmes, M. De Frutos, J. C. Diez-Masa and C. Vidal-Madjar, *J. Chromatogr. A*, 2002, **953**, 17-30.

108. V. Krisdhasima, J. McGuire and R. Sproull, *J. Colloid Interface Sci.*, 1992, **154**, 337-350.

109. C. A. Leduc, L. Vroman and E. F. Leonard, *Ind. Eng. Chem. Res.*, 1995, **34**, 3488-3495.

110. G. J. Szölősi, I. Derényi and J. Vörös, *Physica A*, 2004, **343**, 359-375.

111. M. Nonella and S. Seeger, *ChemPhysChem*, 2008, **9**, 414-421.

112. G. L. Gambino, A. Grassi and G. Marletta, *J. Phys. Chem. B*, 2006, **110**, 4836-4845.

113. T. Hagiwara, T. Sakiyama and H. Watanabe, *Langmuir*, 2009, **25**, 226-234.

114. G. Raffaini and F. Ganazzoli, *Langmuir*, 2004, **20**, 3371-3378.

115. G. Raffaini and F. Ganazzoli, *J. Phys. Chem. B*, 2004, **108**, 13850-13854.

116. G. Raffaini and F. Ganazzoli, *Phys. Chem. Chem. Phys.*, 2006, **8**, 2765-2772.

117. G. L. Gambino, G. M. Lombardo, A. Grassi and G. Marletta, *J. Phys. Chem. B*, 2004, **108**, 2600-2607.

118. V. Tozzini, *Curr. Opin. Struct. Biol.*, 2005, **15**, 144-150.

119. S. Ravichandran and J. Talbot, *Biophys. J.*, 2000, **78**, 110-120.

120. D. Pellenc, R. A. Bennett, R. J. Green, M. Sperrin and P. A. Mulheran, *Langmuir*, 2008, **24**, 9648-9655.

121. D. Pellenc, O. Gallet and H. Berry, *Phys. Rev. E*, 2005, **72**, 051904.

122. P. A. Mulheran, D. Pellenc, R. A. Bennett, R. J. Green and M. Sperrin, *Phys. Rev. Lett.*, 2008, **1**, 068102.

123. V. P. Zhdanov and B. Kasemo, *Proteins: Struct., Funct., Genet.*, 2000, **40**, 539-542.

124. B. Lassen and M. Malmsten, *J. Colloid Interface Sci.*, 1996, **180**, 339-349.

125. S. H. Mollmann, U. Elofsson, J. T. Bukrinsky and S. Frokjaer, *Pharm. Res.*, 2005, **22**, 1931-1941.

126. Y. W. Huang and V. K. Gupta, *J. Chem. Phys.*, 2004, **121**, 2264-2271.

127. C. Calonder, Y. Tie and P. R. Van Tassel, *Proc. Natl. Acad. Sci. U. S. A.*, 2001, **98**, 10664-10669.

128. C. Calonder and P. R. Van Tassel, *Langmuir*, 2001, **17**, 4392-4395.

129. Y. Tie, C. Calonder and P. R. Van Tassel, *J. Colloid Interface Sci.*, 2003, **268**, 1-11.

130. J. S. Sharp, J. A. Forrest and R. A. L. Jones, *Biochemistry*, 2002, **41**, 15810-15819.

131. F. Höök, et al., *Colloids Surf., B*, 2002, **24**, 155-170.

132. K. L. Marchin and C. L. Berrie, *Langmuir*, 2003, **19**, 9883-9888.

133. R. T. T. Gettens, Z. J. Bai and J. L. Gilbert, *J. Biomed. Mater. Res. A*, 2005, **72A**, 246-257.

134. A. Toscano and M. M. Santore, *Langmuir*, 2006, **22**, 2588-2597.

135. C. C. Dupont-Gillain, C. M. J. Fauroux, D. C. J. Gardner and G. J. Leggett, *J. Biomed. Mater. Res. A.*, 2003, **67A**, 548-558.

136. S. Kidoaki and T. Matsuda, *Langmuir*, 1999, **15**, 7639-7646.

137. J. J. Davis, C. M. Halliwell, H. A. O. Hill, G. W. Canters, M. C. van Amsterdam and M. P. Verbeet, *New J. Chem.*, 1998, **22**, 1119-1123.

138. I. I. Rzeznicka, et al., *Chem. Phys. Lett.*, 2009, **472**, 113-117.

139. H. Nygren, *Biophys. J.*, 1993, **65**, 1508-1512.

140. H. Nygren and M. Stenberg, *Biophys. Chem.*, 1990, **38**, 77-85.

141. T. Funatsu, Y. Harada, M. Tokunaga, K. Saito and T. Yanagida, *Nature*, 1995, **374**, 555-559.

142. M. Tokunaga, K. Kitamura, K. Saito, A. H. Iwane and T. Yanagida, *Biochem. Biophys. Res. Commun.*, 1997, **235**, 47-53.

143. A. Yildiz, J. N. Forkey, S. A. McKinney, T. Ha, Y. E. Goldman and P. R. Selvin, *Science*, 2003, **300**, 2061-2065.

144. J. Enderlein, T. Ruckstuhl and S. Seeger, *Appl. Opt.*, 1999, **38**, 724-732.

145. T. Ruckstuhl, J. Enderlein, S. Jung and S. Seeger, *Anal. Chem.*, 2000, **72**, 2117-2123.

146. T. Ruckstuhl, M. Rankl and S. Seeger, *Biosens. Bioelectron.*, 2003, **18**, 1193-1199.

147. D. Verdes, T. Ruckstuhl and S. Seeger, *J. Biomed. Opt.*, 2007, **12**, 034012.

148. M. Rankl, T. Ruckstuhl, M. Rabe, G. R. J. Artus, A. Walser and S. Seeger, *ChemPhysChem*, 2006, **7**, 837-846.

149. J. Ries, T. Ruckstuhl, D. Verdes and P. Schwille, *Biophys. J.*, 2008, **94**, 221-229.

150. H. Qian and E. L. Elson, *Proc. Natl. Acad. Sci. U. S. A.*, 1990, **87**, 5479-5483.

151. N. L. Thompson, A. W. Drake, L. X. Chen and W. Vanden Broek, *Photochem. Photobiol.*, 1997, **65**, 39-46.

152. F. Hillger, D. Nettels, S. Dorsch and B. Schuler, *J. Fluoresc.*, 2007, **17**, 759-765.

153. B. Schuler, E. A. Lipman and W. A. Eaton, *Nature*, 2002, **419**, 743-747.

154. A. K. Kenworthy, *Methods*, 2001, **24**, 289-296.

155. K. Truong and M. Ikura, *Curr. Opin. Struct. Biol.*, 2001, **11**, 573-578.

156. S. W. Hell and J. Wichmann, *Opt. Lett.*, 1994, **19**, 780-782.

157. E. N. Vasina, P. Dejardin, H. Rezaei, J. Grosclaude and H. Quiquampoix, *Biomacromolecules*, 2005, **6**, 3425-3432.

158. M. D. Gouda, M. A. Kumar, M. S. Thakur and N. G. Karanth, *Biosens. Bioelectron.*, 2002, **17**, 503-507.

159. M. Malmsten, B. Lassen, K. Holmberg, V. Thomas and G. Quash, *J. Colloid Interface Sci.*, 1996, **177**, 70-78.

160. A. R. Mackie, F. A. Husband, C. Holt and P. J. Wilde, *Int. J. Food Sci. Technol.*, 1999, **34**, 509-516.

161. A. A. Bhattacharya, T. Grune and S. Curry, *J. Mol. Biol.*, 2000, **303**, 721-732.

162. B. Y. Qin, M. C. Bewley, L. K. Creamer, H. M. Baker, E. N. Baker and G. B. Jameson, *Biochemistry*, 1998, **37**, 14014-14023.

163. Z. Yang, I. Mochalkin, L. Veerapandian, M. Riley and R. F. Doolittle, *Proc. Natl. Acad. Sci. U. S. A.*, 2000, **97**, 3907-3912.

164. T. S. Ulmer, A. Bax, N. B. Cole and R. L. Nussbaum, *J. Biol. Chem.*, 2005, **280**, 9595-9603.

165. T. J. Peters, *All about albumin: biochemistry, genetics and medical applications*, Academic Press, San Diego, CA, 1996.

166. W. E. Fowler and H. P. Erickson, *J. Mol. Biol.*, 1979, **134**, 241-249.

167. M. Verheul, J. S. Pedersen, S. P. F. M. Roefs and K. G. de Kruif, *Biopolymers*, 1999, **49**, 11-20.

168. J. Kim and G. A. Somorjai, *J. Am. Chem. Soc.*, 2003, **125**, 3150-3158.

169. K. Sakurai, M. Oobatake and Y. Goto, *Protein Sci.*, 2001, **10**, 2325-2335.

170. H. J. Gruber, et al., *Bioconjugate. Chem.*, 2000, **11**, 696-704.

171. M. J. Roberti, C. W. Bertoncini, R. Klement, E. A. Jares-Erijman and T. M. Jovin, *Nature Methods*, 2007, **4**, 345-351.

172. M. E. Mcgovern, K. M. R. Kallury and M. Thompson, *Langmuir*, 1994, **10**, 3607-3614.

173. R. Tero, H. Watanabe and T. Urisu, *Phys. Chem. Chem. Phys.*, 2006, **8**, 3885-3894.

174. I. Reviakine and A. Brisson, *Langmuir*, 2000, **16**, 1806-1815.

175. T. Ruckstuhl and D. Verdes, *Opt. express*, 2004, **12**, 4246-4254.

176. P. Reichert, *Water Sci. Technol.*, 1994, **30**, 21-30.

177. A. Gajraj and R. Y. Ofoli, *Langmuir*, 2000, **16**, 8085-8094.

178. S. H. Mollmann, L. Jorgensen, J. T. Bukrinsky, U. Elofsson, W. Norde and S. Frokjaer, *Eur. J. Pharm. Sci.*, 2006, **27**, 194-204.

179. K. E. Sapsford and F. S. Ligler, *Biosens. Bioelectron.*, 2004, **19**, 1045-1055.

180. V. Buschmann, K. D. Weston and M. Sauer, *Bioconjugate Chem.*, 2003, **14**, 195-204.

181. V. Krisdhasima, P. Vinaraphong and J. Mcguire, *J. Colloid Interface Sci.*, 1993, **161**, 325-334.

182. J. Yguerabide, E. Talavera, J. M. Alvarez and B. Quintero, *Photochem. Photobiol.*, 1994, **60**, 435-441.

183. J. E. Berlier, et al., *J. Histochem. Cytochem.*, 2003, **51**, 1699-1712.

184. Y. Lüthi, J. Ricka and M. Borkovec, *J. Colloid Interface Sci.*, 1998, **206**, 314-321.

185. W. T. Hermens, M. Benes, R. Richter and H. Speijer, *Biotechnol. Appl. Biochem.*, 2004, **39**, 277-284.

186. B. Levich, *Discuss. Faraday Soc.*, 1947, **1**, 37-49.

187. Z. Adamczyk, B. Siwek, P. Warszynski and E. Musial, *J. Colloid Interface Sci.*, 2001, **242**, 14-24.

188. J. M. M. Kop, J. W. Corsel, M. P. Janssen, P. A. Cuypers and W. T. Hermens, *Journal de Physique*, 1983, **44**, C10_491-C410_494.

189. A. Nadarajah, C. F. Lu and K. K. Chittur, in *Protein at Interfaces II*, ed. T. A. Horbett, Brash, J. L., ACS Symposium series 602, ACS, Washington, 1995, vol. 602, pp. 181-194.

190. V. B. Fainerman, et al., *Colloids Surf., A*, 2006, **282**, 217-221.

191. K. Rezwan, L. P. Meier and L. J. Gauckler, *Biomaterials*, 2005, **26**, 4351-4357.

192. J. H. Santos, N. Matsuda, Z. M. Qi, T. Yoshida, A. Takatsu and K. Kato, *Surf. Interface Anal.*, 2003, **35**, 432-436.

193. L. Shi and K. D. Caldwell, *J. Colloid Interface Sci.*, 2000, **224**, 372-381.

194. B. Singla, V. Krisdhasima and J. McGuire, *J. Colloid Interface Sci.*, 1996, **182**, 292-296.

195. J. R. Lu, X. B. Zhao and M. Yaseen, *Curr. Opin. Colloid Interface Sci.*, 2007, **12**, 9-16.

196. A. Minton, *Biophys. Chem.*, 2000, **86**, 239-247.

197. R. D. Tilton, C. R. Robertson and A. P. Gast, *J. Colloid Interface Sci.*, 1990, **137**, 192-203.

198. Y. Luthi, J. Ricka and M. Borkovec, *J. Colloid Interface Sci.*, 1998, **206**, 314-321.

199. V. Ball, *Colloids Surf., B*, 2004, **33**, 129-142.

200. O. Hollmann, T. Gutberlet and C. Czeslik, *Langmuir*, 2007, **23**, 1347-1353.

201. O. Hollmann, C. Reichhart and C. Czeslik, *Z. Phys. Chemie-Int. J. Res. Phys. Chem. Chem. Phys.*, 2008, **222**, 205-215.

202. O. Hollmann, R. Steitz and C. Czeslik, *Phys. Chem. Chem. Phys.*, 2008, **10**, 1448-1456.

203. C. Haynes and W. Norde, *Colloids Surf., B*, 1994, **2**, 517-566.

204. P. Schaaf and J. Talbot, *Phys. Rev. Lett.*, 1989, **62**, 175-178.

205. J. Talbot and P. Schaaf, *Phys. Rev. A*, 1989, **40**, 422-427.

206. R. J. Marsh, R. A. L. Jones and M. Sferrazza, *Colloids Surf., B*, 2002, **23**, 31-42.

207. M. Gottschalk, H. Nilsson, H. Roos and B. Halle, *Protein Sci.*, 2003, **12**, 2404-2411.

208. P. R. Van Tassel, *Materialwiss. Werkstofftech.*, 2003, **34**, 1129-1132.

209. S. R. Euston, *Curr. Opin. Colloid Interface Sci.*, 2004, **9**, 321-327.

210. O. Hollmann, C. Reichhart and C. Czeslik, *Z. Phys. Chem.*, 2008, **222**, 205-215.

211. N. El Kadi, et al., *Biophys. J.*, 2006, **91**, 3397-3404.

212. J. M. Andrews and C. J. Roberts, *Biochemistry*, 2007, **46**, 7558-7571.

213. S. Mehalebi, T. Nicolai and D. Durand, *Soft Matter*, 2008, **4**, 893-900.

214. M. Vendruscolo and C. M. Dobson, *Nature*, 2007, **449**, 555-555.

215. R. C. Liu, D. H. Hu, X. Tan and H. P. Lu, *J. Am. Chem. Soc.*, 2006, **128**, 10034-10042.

216. D. Chandler, *Nature*, 2005, **437**, 640-647.

217. S. Chandra, G. Gallardo, R. Fernández-Chacón, O. M. Schlüter and T. C. Südhof, *Cell*, 2005, **123**, 383-396.

218. T. Ban, D. Hamada, K. Hasegawa, H. Naiki and Y. Goto, *J. Biol. Chem.*, 2003, **278**, 16462-16465.

219. N. Bonini and B. Giasson, *Cell*, 2005, **123**, 359-373.

220. R. J. Perrin, W. S. Woods, D. F. Clayton and J. M. George, *J. Biol. Chem.*, 2000, **275**, 34393-34398.

221. Q.-L. Ma, P. Chan, M. Yoshiia and K. Ueda, *J. Alzheimers Dis.*, 2003, **5**, 193-148.

222. H. Naiki, K. Higuchi, M. Hosokawa and T. Takeda, *Anal. Biochem.*, 1989, **177**, 244-249.

Acknowledgements

Many people supported me during the work on my dissertation and I would like to take this opportunity to express my gratitude to them.

Firstly, I would like to thank Prof. Dr. Stefan Seeger for giving me the opportunity to carry out my dissertation in his research group and for giving me the freedom to explore the fascinating world of protein adsorption.

Further I like to thank Prof. Dr. Peter Hamm and Prof. Dr. John A. Robinson for agreeing on supervising me as members of the Promotionskomitee.

For the collaboration on the α-Synuclein project I thank Prof. Dr. Roland Riek and Alice Soragni from the ETH Zurich.

I wish to express my gratitude to all present and former group members of the Seeger group for a stimulating and encouraging working atmosphere. In particular I am indebted to Dr. Dorinel Verdes for his constant and reliable support throughout the whole dissertation. Special thanks go to Dr. Jan Zimmermann with whom I had the pleasure to work on several projects and who was always an encouraging and cooperative office mate to me. I thank Dr. Georg Artus for his competent advice on several sub-projects of the dissertation as well as Dr. Thomas Ruckstuhl and Christian Winterflood for valuable discussions.

Many thanks go to the staff of the PCI Institute for providing an excellent infrastructure with a particular emphasis on the workshop members Armin Kühne, Roland Zehnder, and Horst Blasi and the institute secretary Chantal Henningsen-Conus.

Finally, I would like to thank my family and Kathrin for their constant love and support.

Curriculum vitae

Name: Rabe
First name: Michael
Date of Birth: May 8, 1980
Nationality: German

Education:

2005 – 2009	*PhD Program in Physical Chemistry* University of Zurich, Switzerland
2005	*Diploma in Physical Chemistry* University of Zurich, Switzerland
2004 - 2005	*Diploma Studies in Physical Chemistry* University of Zurich, Switzerland
2003	*Diploma in Analytical Chemistry* University of Applied Sciences Magdeburg-Stendal (FH), Germany Title of Diploma Thesis: 'Metalloprotein Characterisation Studies'
1999 - 2003	*Diploma Studies in Analytical Chemistry* University of Applied Sciences Magdeburg-Stendal (FH), Germany
1998 - 1999	*Civil Service* Sozialstation Stendal, Germany
1998	*Abitur* Diesterweg-Gymnasium Tangermünde, Germany